CITY UNIVERSITY LONDON

City Research Online

The generation and classification of small leaks in a high pressure water system

By Robert Shepherd

This thesis is submitted for the Degree
of Doctor of Philosophy at the Department
of Computing, City University, London

NDTM 1060

August 2011

Contents

Table of Figures

Chapter 5 Candidate Sensor Systems

Chapter 6 Data Acquisition

Chapter 8 Operator Advisory System (GUI)

List of Tables

Abbreviations

ANN – Artificial Neural Network

ATU – Air treatment unit

FPGA – Fully Programmable Gate Array

FFT – Fast Fourier Transform

LOCA – Loss Of Coolant Accident

LOFT- Loss Of Flow Test

Matlab™- Matrix Laboratory

OAS – Operator Advisory System

PWR – Pressurised Water Reactor

RC – Reactor Compartment

SNR – Signal to Noise Ratio

Acknowledgements

Declaration

I grant the powers of discretion to the University Librarian to allow this thesis to be copied in whole or part without further reference to me. This permission covers only single copies made for study purposes, subject to normal conditions of acknowledgement.

Abstract

This report investigates the detection of small leaks from the primary system of a Nuclear Pressurised Water Reactor. Leak rates of 12 g/s are invariably difficult to detect and locate. The typical leak indicators in a nuclear reactor control room are a drop in pressure and level from the pressuriser, and the air sampler detecting particulate matter. However, in both cases the leak is normally quite substantial by the time any parameters or values are obviously outside the normal operating conditions. Therefore, a small leak could go undetected for a significant amount of time. As part of the reactor safety studies, it is important to have more information about small leaks.

Due to the lack of small leak data, the solution was to construct a high pressure water rig producing temperatures and pressures close to those experienced in the primary circuit, these being 200ºC and 100 bar respectively. Pressure is maintained by a vane water pump and heating is achieved by passing a high current through a small diameter, thin walled pipe. To reproduce different size cracks, various size carburettor jets are used. The water on exiting this crack, flashes to steam and immediately meets metallic pipe lagging, which is typical of most primary systems.

With the typical crack scenario recreated it is now important to add sensors that will detect conditions associated with a small leak. These sensors are either mounted on or around the lagging material. The parameters that are monitored include vibrations, acoustics, thermal variations, moisture change, air flow and pressure adjustment leaving a predetermined outlet. The sensor outputs are pre-processed and the non-linear data are applied to an artificial neural network, whereas the other data are applied to a digital logic system. The results showed that with 13 different leak rates, separated by only 1.4 g/s the ANN was able to correctly differentiate and identify different leak sizes with a certainty of over 97%. The results from all the analysis are further presented graphically through an Operator Advisory System. This informs the operator of the predicted leak size and location. All of the available sensor data relevant to the leak can be viewed and location of the leak is presented by a three dimensional model of the reactor system.

Chapter 1
Introduction

1.1   Background

Reactor safety will always be of upmost importance, even more so when a reactor is working within the close confines of a submarine. Companies such as Rolls Royce who design and manufacture the reactor components for the submarines, strive to reduce the likelihood of component failure. However, there are many factors that can cause pipes to leak and studies in stress corrosion cracking examine these contributors. In addition being a combat vehicle it is possible that the submarine could become damaged while in service.

Consequently, being able to detect a small leak from the primary circuit at the earliest possible opportunity avoids a potentially dangerous situation arising. Currently the primary means of detecting leaks is by monitoring the level of the pressuriser. However, due to the enormous volume of this vessel a very small leak will result in a minute drop in level. Unfortunately, the level of the pressuriser also varies with power level. Other sensors monitoring the reactor include: an air particulate detector, bilge alarm, humidity detector, as well as pressure and temperature in the reactor compartment. In addition, when a leak is confirmed, locating the leak area is very difficult as the steam flows along the inside of the metallic lagging.

Therefore, for all of the above reasons it is clear that a system is required to detect very small leaks. However, the reactor system has not been configured to detect and locate leaks and therefore no data are available for analysis. Consequently, a large part of this report describes the design and construction of a high temperature and pressure water rig. This is a unique approach to leak detection, as the solution will undoubtedly reveal characteristics of a leak that could not have been accounted for in a simulation.

There are many applications when leak detection is required ranging from oil rigs, vehicle coolant systems to home central heating systems and in each case there are different degrees of leak detection. Test rigs have been built for many different leak situations but the combination of pressure, temperature and environment make the test rig very specific to this application.

The array of sensor technology today is enormous and every year more advanced sensors become available. Therefore, this research tries to apply the most suitable sensors for this application. However, the sensor is meaningless without the ability to interpret its data. Therefore, the study will show that the data are either capable of merely determining the existence of a leak or they can be further analysed using complex non-linear algorithms found in artificial neural networks. Using this technique it is proposed that the size of the leak can be established.

Being able to present the mathematical results in a clear and logical manner would enable this system to be implemented in a real situation. This report discusses an operator advisory system that would enable the plant state to be monitored at all times and relay any warning messages to the operator. Such a system would clearly identify the leak location, size, time at which it started and offer assistance in isolating the leak area.

This report is the culmination of a three year research project, sponsored by the Ministry of Defence in collaboration with City University London. For the duration of the project, the work was carried out in the Nuclear Department at HMS Sultan, a Naval training base in Gosport.

1.2   Aims and Objectives of Current Work

The aim of this project is to detect and characterise very small leaks from a high temperature and pressure water system, as typified by a nuclear reactor.

The following objectives will be addressed in order to achieve this goal:
- Research the literature from other authors on leak detection techniques

- Design and build a high temperature and pressure water rig to replicate those found in the RC primary system
- Review sensors suitable for this application
- Configure and program a data acquisition device to acquire sensor data at the correct sampling rate and in a format suitable for pre-processing
- Pre-process data to establish whether the sensor input can determine the leak size or just that a leak exists
- Apply complex non-linear data to an artificial neural network with the intention of classifying all 13 different leak sizes
- Design and produce an operator advisory system to present the results.

Currently there is very little data available on small leaks in the magnitude of 12 g/s (40 litres/hour). The motivation behind this study is to characterise a leak to within a tolerance of 1.4 g/s (5 litres/hour), on a system operating at 100 bar, 200 ˚C nominally. The method of characterising the leak will be achieved using an Artificial Neural Network (ANN). In previous leak detection systems, it is typical to only use a single sensor; this report will use a number of different sensors that in combination will confirm and provide undisputable evidence that a small leak exists.

The study will also show measurements taken of a leak in an open environment, to compare with a pipe encased in lagging. For this report, only measurements taken with a lagged pipe will be used, as this represents the typical scenario in the primary circuit. However, other industries use high pressure pipes that are not lagged, and therefore, the data may have some relevance to these fields. Finally the data will be presented to an operator through the use of an Operator Advisory System (OAS). The intention is to supply this system with leak data and allow the software to determine the leak size using an ANN. A confidence level will be associated with the prediction and data from other sensors will be available to corroborate the existence of a leak.

1.3 Thesis Structure

The remainder of this thesis is composed as follows:

Chapter 2 reviews the literature on leak detection both in the nuclear field and the commercial sector. This includes the use of Artificial Neural Networks (ANN) for measuring transient responses from the primary system, and suggestions for building a successful operator advisory system.

Chapter 3 describes the methodology of the project, identifying the procedures that will be necessary to building a rig, measuring the leak characteristics, analysing the input data and presenting the output data through an OAS. Special attention is made to hard and soft computing techniques and in particular ANNs.

Chapter 4 comprehensively describes the design of the high temperature and pressure water rig. Details include; the design concept, schematics, components, safety features and operation.

Chapter 5 discusses a possible array of sensors that could be applied to small leak detection. Initially, a significant number of sensors are proposed, but through experimentation or feasibility of use, this list is condensed to only the most appropriate for this application. The results from the final set of sensors are examined and their suitability as an input to an ANN is assessed.

Chapter 6 examines the data acquisition device. It explores the physical hardware, the programming of the Fully Programmable Gate Array (FPGA) and onboard software to record the sensor data, and produces a test procedure for carrying out a single experiment at one leak size.

Chapter 7 evaluates the data, and determines whether they are suitable for an ANN or digital logic system. Illustrations are made showing the background (no leak) data levels for each sensor represented against their new level, when a leak is present. However, this chapter focuses very heavily on the application of ANNs, the success of various networks and their resilience when noise is added to the input data.

Chapter 8 discusses the Operator Advisory System, and the typical screen shots expected during a leak situation. In addition, this chapter investigates implementing this system in a real reactor compartment, and how the work to date could be scaled up.

Chapter 9 draws a conclusion on all the work carried out and makes suggestions for further work, both in terms of the rig and possible trial implementation into a Reactor Compartment (RC).

Chapter 2
Literature Review

In order to understand and appreciate the work that has been studied to date, a literature review has been performed. Due to the diversity of this project, the search criteria include: operator advisory systems, leak detection methods, nuclear loss of coolant accidents (LOCA), Artificial Neural Networks and combinations of all these areas. The intention is to use the knowledge gained by others and build a system that exploits and extends the work done to date. Where possible, papers that had a nuclear influence were selected over other industrial papers. The library at HMS Sultan provided the majority of the nuclear material, and other journals were found either through searching on the internet or through accessing technical journals, via the Athens system.

2.1   Nuclear Leak Detection

During this section, some of the text is highlighted in **bold** to signify the sensors that were used during the respective experiments. It also gives some validity for the inclusion of similar sensors used in this report.

Bausch (1989) carried out very extensive research into small leak detection in nuclear power plants which they named 'leak-before-break'. Their assumption was that a pipe will fail slowly and predictably, firstly as a small crack/flaw and then developing into a detectable leak well before the pipe fails. Their research aimed to calculate three phenomena: crack stability, crack length and flow rate of steam leaving a crack. The tests were initially carried using a circumferential groove for the crack and later a small hole of diameter 0.78mm. The sensors used during their tests were: **video camera, IR camera, sound level meter, flow meter** and general observation by the operator. It is somewhat surprising, but their test showed the IR camera to be ineffective and no increase in audible level was detected 9 metres away. From the sensors outlined in this report, a video and thermal camera are intended to be used in this project, but only as a means of recording the activity for documentary evidence.

Videoing the rig while steam is exiting the orifice provides a means of permanent evidence of how the steam exits the orifice and how the steam escapes through the lagging material. The video and IR camera will not be carried forward into the final group of sensors, as they would firstly require the operator to visually assess the sensor input on a periodic basis, which is time consuming, and secondly because the harsh neutron environment within the reactor compartment would damage the p-n junction within the transistor electronics. A sound level monitoring device and steam flow meter are anticipated in the final set of sensors.

Gopal (1977) investigated failure analysis of the nuclear steam supply system by applying online diagnostic instrumentation for acquiring and analysing data from critical plant equipment and systems. The areas they have identified are: *"any changes in the vibrational characteristics of the system, acoustic monitoring to detect and locate leaks, metal impact examination in order to detect loose debris in the reactor vessel and steam generators, core barrel vibration, sensor response time delay and change in coolant flow rate"*. It was found that the combination of the diagnostic systems and analytical laboratory work improved the likelihood of detecting faults.

Lee (2001) examined the use of ceramic **humidity sensors** for leak detection on water reactors. The detector worked by the absorption of water vapour onto the sensor surface increasing its electrical conductivity. The sensor was positioned between the piping and surrounding insulation. The sensors were then spaced 1.5 metres apart and ganged together in series. A clever method of leak detection was accomplished by using sensors with different combinations of capacitance and conductance and measuring the AC impedance characteristics. This allowed detection and position very simply, and minimised the number of wires between sensors. However, rather disappointingly, it took one hour to locate a leak, when the leak rate was one litre/hour, and the sensors were spaced one metre apart. The intention is to use humidity sensors for this project, and this paper demonstrates that the technique works, but the detection time was rather poor.

Siemens (1994) developed a system called FLUS to detect small leaks from power stations. The method adopted used a measurement tube mounted adjacent to the high temperature and pressure pipe being measured. Lagging material then surrounds the

two pipes. The measurement pipe, by comparison to the main pipe has only 6mm internal diameter. The method works by allowing escaping moisture to enter the measurement tube at regular 0.5 m intervals along its length. At the start of the measurement pipe, which could potentially be 2 km long, is a pump that blows compressed air every 5 to 10 minutes at a velocity of 1 m/s. At the measurement end, a PC monitors the increase in dewpoint and by knowing the flow velocity, tube length and cycle rate the position of the leak can be identified. Depending upon the pipe length and duty cycle, detection times down to 15 minutes have been achieved with a detection accuracy of 1 to 2 metres. This system has been trialled on the Bohunice VVER-440 for over two years, and has produced good results. Humidity sensors are going to be used for this project, but rather than using a measurement tube, discrete devices will be mounted at predetermined distances external to the lagging, with the intention of detecting leaks in seconds rather than minutes.

Hayashi (1996) investigated a sodium water leak detection system in the steam generator unit (SGU) of a liquid fast breeder reactor. Various test scenarios were created by either using piezoelectric transducers as leak simulators inside a test vessel, or digitally synthesising the leak. The leak is then monitored by attaching an **accelerometer** to the outside of the vessel. Typical background noise was acquired from a SGU of a prototype fast reactor in the UK. In all cases the leak signal recorded was lower than the typical background noise. Therefore, a sequence of digital band-pass filters, twice squaring (multiply the input signal with itself) and integration yields a signal in the frequency domain. Further enhancements were made by tuning into the most prominent frequency components and thus improve the signal to noise ratio. The intention of this study is to also tune into the dominant frequency components and use an accelerometer for leak detection. In addition, if a real background noise source can be acquired from a PWR primary circuit, then that will be mixed with the leak data acquired from the text rig.

2.2   Current Methods of Detecting a Loss of Coolant Accident

At present, the primary system instrumentation on a PWR is not configured to detect very small leaks rapidly. The sensors installed to detect LOCA predominantly respond to large leaks, and the monitoring equipment gives the operator a gauge for the severity of the break once it has happened. Shimanskii (2004b) also reported that

using these current methods resulted in slow detection of leaks and gave no information regarding its location. The sensors illustrated below, are the primary means of identifying a leak:

- Drop in pressuriser level and pressure
- Detection of radiation matter
- Reactor compartment change in temperature and pressure
- Reactor Compartment bilge alarm
- Increase in reactor power.

See Appendix A for a more detailed explanation of the reactor system. The majority of the above sensors need no explanation, but an interesting phenomenon has been observed in relation to an increase in reactor power during a LOCA. There are two possible reasons for this: firstly, because the pressuriser is being topped up with cold water, and this cold water entering the primary circuit causes an increase in reactivity, and hence an increase in power and secondly, because any boiling within the pipe would cause latent heat of evaporation thus causing removal of heat from the surrounding water and consequently an increase in power.

However, all of the above indicators are typically only present during a large pipe break, and to detect a small dripping pipe would not be obvious with the present measuring devices. To put into context, the primary circuit contains several tonnes of water, and a tiny drip is not going to have any bearing on the water temperature, pressure or pressuriser level. Consequently, it is clear that improved methods are needed to detect small pipe cracks, before they become are large scale problem.

2.3   Operator Advisory System

The following papers suggest different approaches to an Operator Advisory System (OAS). Some advise the operator of the best course of action to take in the event of a reactor incident, while others merely try and identify the existence of an unknown transient.

Alty (1995) specialised in interface technologies, i.e. methods of presenting information to operators more clearly and concisely. Alty has spent years researching

multimedia techniques, and has found that operators are dissatisfied with existing interfaces, primarily due to the extra complexity of modern systems. It was found that operators struggled to understand what the information was telling them, and therefore any new multimedia system should be clear and concise. It was found the following methods yielded the best comprehension for operators: representing information in a variety of ways, verbally announcing the problem (but only in extreme cases) and combining visual and spoken messages. Unsatisfactory methods included: using different sound levels as a method of warning severity of incident, too many warning messages and the frequent use of sound. The approach adopted for the visual representation of data was to underline critical parameters, add vertical lines for time outstanding, use colour to represent severity and allow these parameters to be double clicked to gain further information. This information will be incorporated in the OAS intended for this project, in terms of what needs to be displayed and how it should be represented to the operator.

Kun (2007) developed a system that regulates and supervises the actions of an operator in the event of an abnormal event occurring in the nuclear power plant. The system monitors the users' response to irregular situations and validates their response both qualitatively and quantitatively using an ANN. The suggestions and warnings should hopefully lead to fewer human errors when emergencies occur.

Folds (1997) researched whether a computer could accurately give road traffic advisory messages without operator intervention. This paper is not concerned with the nuclear domain but it shows that an advanced computer system in a control centre is able to interpret input data and relay an output message to multiple users without any operator intervention. It does in fact have remarkable similarities to the control room of a nuclear reactor, because it was found that operators occasionally failed to notice a dial slowly changing or a new value on a display. This system was designed to alert road users to an incident, but also offer advisory information of alternative routes and expected waiting times. The system had to ensure the wording was accurate to avoid misinterpretation, and timely to enable road users to take evasive action. If allowed, the system had the capability to take control of the entire operation away from the operator. If compared to the nuclear system, it almost resembles interpreting the results and controlling the reactor system without operator intervention. This would

be an unrealistic expectation of this project and represents a level of automation that many nuclear operators would have difficulty accepting. It would however, take advisory systems to a new level. The conclusions from this report were that offering drivers' advice without an operator was more productive than waiting for the operator to accept the message.

2.4   Acoustics

This section will show that acoustics are a very important means of identifying leaks. A steam leak from an RC would typically be composed of two main sound sources: firstly the steam leak, but also the background noise derived from pumps, valves, motors, and ventilation systems for example. The key is to extract the frequencies that are significant to the leak and effectively filter out everything else. However, there are two fundamental problems that acoustic monitoring suffers from: when the background is significantly louder than the leak, and when a piece of machinery resonates at the same frequency as the leak.

Holland (1995) investigated the noise correlation between predicted and measured noise on a luxury yacht and containership. This paper was concerned with the background noise that people living on board may experience. The conclusion was that the principal noise sources were generated by: the main propulsion machinery, the auxiliary engines, the propeller and transverse propulsion unit.

This project requires a background noise measurement to be taken, and the positioning of these microphones will undoubtedly be affected by their relative position to these reported noise sources. Because these sources are the most dominant, it is important that during the noise signature measurement, all of the above devices are measured at different loads and speeds, as their resonant frequencies might coincide with resonances from potential cracks. This paper has demonstrated the key background noise sources and the importance of measuring their contribution at different engine loads. The background noise measurement is further examined in section 5.1.

Y. Gao (2005) researched different acoustic/vibration sensors for leak detection in plastic pipes. This principle is primarily designed to detect leaks from buried water

pipes by attaching sensors capable of measuring the pressure, velocity and acceleration on either side of the leak. It was shown through theoretical prediction that hydrophones measuring pressure responses are more suited for low signal to noise environments, whereas for a sharp peak correlation coefficient, accelerometers are better. The results obtained during tests were carried out using plastic pipes which heavily attenuate the high frequency signals, whereas metal pipes do not. The method of leak detection is obtained simply by measuring the vibration or acoustic signals either side of the leak. These signals were then processed to correlate the two signals, thus producing a cross correlation function for the two signals. The exact location of the leak could then be calculated by entering the time delay between the detection of the signal at both sensors and having a record of the distance between the sensors. This method could be applied to the current project, but its application is typically for very long pipes, and in this paper, sensor separation is 102.6 metres. Therefore, it is felt that the mere presence of new acoustics and vibrations will be adequate for the proposed system, as the sensor separation will be small, typically 1 to 2 metres.

D'Souza (2006) investigated whether a relationship existed between sound pressure level and steam leak size. An experiment was performed by opening a valve on a boiler plant by set increments. A sound level meter was used to firstly determine the background noise and then measure the steam leak at distances of 2 and 4 metres. The results although not conclusive showed that there was possibly a linear relationship between sound intensity and leak rate. The sound level meter also yielded the best results when set to measure the third octave audio signal. Through spectral analysis, it was found that most energy from the steam leak existed between 4 and 12 kHz.

2.4.1   Nuclear Acoustics

Proskuryakov (2007) examined the conditions for resonance interaction between flow pressure oscillations and mechanical vibrations on a VVER-1000 reactor, (*Vodo-Vodyanoi Energetichesky Reactor*, which translates as *Water-Water Energetic Reactor*). In order to measure these effects pressure pulsation sensors, vibration sensors, dynamic tension sensors and mechanical motion sensors were all attached to pipe work and main plant equipment. It was found that under certain conditions the

frequency of the main coolant pump and Eigen (natural) coolant pressure oscillations could overlap. This mutual resonance has the potential to damage the reactor vessel head. As a consequence of these findings, it has been advised that the operator is given advance warning of a potential mutual resonance occurrence, and thus make adjustments to the operating conditions to reduce the potential for dynamic metal fatigue.

Brunet (2003) studied the acoustics of water leaks inside steam generators using acoustic detectors. This was the third sensor used for this application, with the other two being hydrogen detectors and rupture disks. The intention was for early detection of a steam leak in order to prevent neighbouring pipe work from getting damaged by the high velocity and pressure of the escaping steam. It was anticipated that the flow rate of steam would vary from tens of g/s to hundreds of g/s. The authors identified three frequency bands for investigation: 0-20kHz, 20-100kHz and 50-300kHz. The simulation using the steam generator for steam leaks has shown promising results at half power, but the background noise at full power prove to make detection more difficult.

Kunze (1999) developed an acoustic leakage monitoring system for a nuclear power plant, which attempted to detect cracks before they materialised. It was an early warning system aimed to be implemented on reactor coolant and surge lines, such that corrective action can be carried before the failure manifests itself. Kunze and Streicher (1990) are both members of the Siemens power generation group and heavily engaged in the acoustic monitoring of the primary system. Streichers work involves monitoring of loose parts and leakage monitoring. The net result being a PC based system that provides: "*information to the operator on plant status, early warning of problems and their effect on the system leading to suggested remedial action, preventative measures to safeguard the personnel and system and finally maintaining efficient running of the system beyond its specified operating life*", taken from Streicher (1990).

Shimanskii (2005) has developed a method of acoustic leak detection using high temperature resistant microphones. Their work has been concentrating on determining the position and size of the leak, with typical leak rate of 0.23m^3/h (230l/h). This

target sensitivity was chosen due to guidelines determined by the International Electrical Engineering Commission Standard No. 1250. They have referred to their concept as 'leak before rupture', and concluded that at least three independent leak methods are required in order to meet their objectives. These being:

- **Detection,** and this condition was satisfied when the sound pressure waves exceed a predetermined threshold level. This threshold level is calculated by taking an average of the background noise and fluctuations;
- **Location,** and this was achieved by triangulation using two microphones and measuring their relative delays;
- **Leak size,** and this was empirically calculated as the relationship between coolant flow and acoustic power.

It was further found that "*the integrated acoustic power level is proportional to the logarithm of the leak size*" Shimanskii (2005), and this is in agreement with Morishita (1995) and Mochizuki (2000). It was also found that the main sources of low frequency background noise are due to the circulation pumps and cooling ventilation. These noises are derived from the hydrodynamic noise of the coolant and vibrations from the rotating equipment. These positions could be ideal points for microphone positioning in a reactor, in order to have a good background noise measurement. Shimanskii (2004) also found that during testing on the Fugen power plant, that the optimal distance for detection was 3.5-5 metres for a leak rate of 46 litres/hour, at a frequency range of 16-20kHz. The RBMK (high-power channel reactor - *reactor bolshoy moshchnosty kanalny)* reactor, differed slightly with optimal detection distance at 4 metres, for a leak rate of 230 litres/hour with frequency range 8 - 12.5 kHz. Therefore, using this information, during acoustic tests on the rig (described later), the best compromise is to position the microphone 4 metres from the rig and have a microphone capable of working in the 8-20 kHz range. D'Souza (2006) performed some very similar work, but concentrated on the 4-12 kHz range.

2.5   Artificial Neural Networks

Weller (1997) developed ANNs to diagnose a range of PWR conditions including large leak detection, and from this analysis predict future plant conditions. The ANN was able to successfully predict PWR conditions for both one and many time steps ahead. Interestingly, although networks with multiple hierarchical layers were developed, it was found that simple ANNs with only one or two layers of hidden nodes were sufficient to model the complexity. The investigations found that using a large set of PWR variables was preferential to a smaller set and when applied to an ANN was able to identify six main PWR transient conditions.

Antonio (2006) studied two methods of identifying transients in the nuclear power plant, as well as a 'don't know' response. The first used a genetic algorithm that comprised natural and consistent classification rules based on the cluster size. This method showed good capabilities for classifying unlabelled transient reactor signals, but also provided the 'don't know' response. In some cases, the latter response was actually more desirable than an incorrect diagnosis. The second approach used ANNs trained using the backpropagation algorithm. Two ANNs were used: the first performed a preliminary transient identification while the second ANN validated the first ANN by using an associative neural simulator that estimated the value of each state variable. Validation of both methods was achieved by applying a hypothetical reactor incident and noisy data.

Fantoni (1995) studied data from the OECD Halden Reactor Project with the intention of firstly identifying the state of the plant and secondly monitoring for faults. The system used a comprehensive real time data monitoring system, thereby checking whether each sensor value was in line with expectations. If not, it had to establish whether a fault truly existed or whether the sensor was malfunctioning. If a sensor was occasionally producing erroneous data, the system entered more realistic data for that period. All this processing was carried out before the data went to the control system. This report was concerned with signal validation, and although many analytical methods exist the emphasis was on the application of ANNs for pattern recognition in steady state and transient conditions. The idea was to train an ANN on

a very specific plant operating range, and consequently in this case use nine unique ANNs. These ANNs were all trained independently, received different plant parameters and had potentially dissimilar architectures. Through the combination of clustering and applying a back propagation algorithm, signal validation was achieved for all plant states. The system was then validated based upon irregular plant conditions and multiple sensor failures and was found to yield a successful classification rate of 97%.

Basu (1994) designed a fault diagnostic system that examined transients to identify faulty components or systems in the reactor system. A difficulty was encountered when using ANNs, and Basu found this was "*as the number of variables n in the problem increases, the complexity increases faster than a polynomial of order n*". This problem was addressed by using a modular hierarchy and splitting one back propagation algorithm into two. During testing the system was able to successfully classify 27 unique transients and detect the four normal operating conditions. The main conclusion from this paper was that using a dynamic node architecture and modular design, dramatically increased the capability of the ANN system.

Wainwright (1995) wrote an interesting paper about how the regulators view the use of artificial intelligence (AI) in the nuclear industry. Obviously, any new technology that can ensure the safe working of a nuclear power plant should be seen as an asset. However, concerns have been raised regarding the use of ANNs because of the importance of selecting an appropriate topology for the task, and finding good training data. Issues with weights not converging, inconsistent network performance and overall instability are worries associated with this technology. The nuclear industry requires a high level of safety, and using a software based system with potential numerical inadequacies causes enormous concern. If an operator takes action, based upon incorrect information, it could in fact exacerbate a situation. The system presented in this report hoped to overcome these shortcomings and worries by fusing hard and soft computing methods, as well as giving the operator full capability to interrogate all the input data.

Becraft (1993) designed an operator advisory system for a chemical process plant using AI to diagnose faults. The detection of the fault was achieved through the use of

a hierarchical use of an ANN and expert system. By analysing the sensor and alarm inputs the ANN was able to diagnose a fault, the expert system then chose whether to accept the result or suggest an alternative solution. The advantage of using an ANN at the preliminary stage was that it can accept a mixture of faults at once, analyse faults previously not encountered, learn from experience and extrapolate information from noisy data. Whereas the expert system was knowledge based, and as such was based on stored words and phrases, but the great advantage was that they are able to provide an explanation of their reasoning and methodology. Therefore, combining these two quite unique systems yields a solution that can not only diagnose a fault, explain the reason behind its diagnosis but also provide a suggested course of action. Although, this system has been trialled on a chemical plant, the methodology could very easily be transferred across to a PWR.

Seker (2003) was able to implement an elman recurrent network for condition monitoring of the nuclear power plant system and detecting motor bearing damage. The elman network was chosen over other multi-layer networks because of its suitablility for solving problems in dynamic systems. This paper fully explains the Elman structure and gives a mathematical derivation for the network. It also transforms the sensor data from the time to frequency domain using an FFT, before applying this data to an ANN. This is one of the intentions of this report. This paper was able to successfully use the Elman network to monitor the reactor system and detect anomalies, in addition to detecting bearing damage. These conclusions are significant, because they add strength to the use of ANNs in a nuclear application.

Adah (1997) used a Jordan recurrent ANN to simulate the core neutron environment in a nuclear power plant. Due to the non-linearity of the input data, the recurrent network was chosen because it captures the complex dynamics of the system, and therefore can more accurately predict the system response. In-order to assess the performance of the ANN, different forms of input data are applied to evaluate the ANNs ability to interpolate, extrapolate, handle missing data in addition to noisy data. The transient conditions evaluated by the ANN were during: core trip, and tripping of the pumps. The results showed the significant advantages compared to conventional methods, and the ANN was more tolerant to noisy and incomplete data. It is the

intention to use a recurrent ANN in addition to introduce noisy data to validate the performance of the network, in this report.

Evsukoffa (2005) investigated neuro-fuzzy systems for nuclear reactor fault detection and isolation. The approach taken was to: obtain sensor data from the reactor system, apply it to a fuzzification module, then supply an ANN with fuzzified attributes. Two different ANN topologies where assessed: feedforward and recurrent. The later method was able to generalize better during the detection and isolation of serious faults. The results obtained from the ANN were then presented to an operator using a graphical interface, which used evolving coloured shades to represent symptoms and diagnostic results. This report will culminate with a graphical operator advisory system, and it will also attempt to convey the diagnostic information in a friendly and communicative manner.

2.6 Summary

This chapter has reviewed literature from acoustic leak detection, both nuclear and commercial, artificial neural networks, operator advisory systems and the current techniques used to detect leaks from a nuclear reactor. However, one factor that becomes apparent is the lack of available small leak data, also noted by D'Souza (2006). In addition, nearly all of the authors have produced leak detection methods through the use of a single sensor as opposed to using a collection of different sensors types. Even though the authors discuss different leak sizes, having detected the leak, very little information is given regarding the accuracy, size and location of the leak. Some of the papers examine larger leaks of about 200 litres/hour, but through discussions with reactor operators at HMS Sultan, a leak of about 100 litres/hour can be detected by conventional instrumentation, used to monitor the reactor system. Leaks smaller than 100 litres/hour can also be detected, by only through observing the drop in pressuriser level and this could be over several days.

ANNs are discussed in the nuclear domain, but in all cases relate to transient analysis of the reactor system. It is only through learning the typical dynamics of the PWR can anomalies be detected. The recurrent ANN is exploited by a number of the authors due to its ability to converge to a solution for a dynamic system application, and therefore it will also be evaluated in this study.

There is no mention of any type of lagging material when the acoustic leak systems were being tested, and therefore it must be assumed that tests where carried out on a bare pipe. The primary pipe from a nuclear reactor is insulated by a thick metallic lagging material and therefore the acoustic levels maybe significantly attenuated by this. Therefore, by taking into account everything that has been read in the literature and through discussions with nuclear reactor operators, a suitable area for investigation would be to devise a system that had:

- Leaks smaller than 100 litres/hour
- Multiple different sensor inputs
- Data applied to an ANN or logic system, to characterise the leak size
- A graphical data output, namely an operator advisory system.

However, given the above set of requirements, a set of leak data is needed. As none is available it will be necessary to design and build a rig that can replicate the conditions experienced at the time of a small primary circuit leak.

Chapter 3
Research Methods

3.1 Introduction

This report details the work that will be undertaken in the detection of small leaks
from the primary circuit of a Pressurised Water reactor (PWR). Details regarding the
architecture of the PWR are provided in Appendix A. This study is necessary because
during normal operation of the PWR, the sensors that monitor the reactor system do
not have the sensitivity to detect very small leaks quickly from the primary system.
The literature review carried out subsequently, has demonstrated that small leaks can
be detected, but in nearly all the systems evaluated, only one sensor type is used and
the time to identify the leak with confidence can be nearly an hour. Claytor (1986)
said "*no currently available single leak-detection method combines optimal leakage
detection sensitivity, leak location ability, and leakage measurement accuracy*". This
project will attempt to amalgamate a number of different sensors types and combine
hard and soft computing techniques as discussed by Ovaska (2004).
As no leak data is available for a naval nuclear reactor, the first task will be to create
leak data that can accurately represent the typical characteristics of a leaking primary
system. This will involve building a high temperature and high pressure rig capable of
heating water to 200˚C and pressurising it to 100bar, with a variety of different leak
rates.

3.2 Methodology

The two most important components for the test rig will be a high pressure pump and
heating device. The intention is to have a pump capable of achieving and exceeding
the typical pressure in the primary circuit of a PWR, but in order to avoid this
document becoming confidential, run the pump at a nominal 100 bar. When
considering the pump itself, this should produce a non pulsing output, and therefore a
three vane reciprocal pump will be required. As the chosen running pressure has been
set at 100 bar, in order to have the facility to run at PWR pressures but also maintain a

good overhead, a 200 bar pump should be acquired, with flow in excess of the largest orifice selected.

The water heating can be accomplished in a variety of ways. An immersion heater could heat a reservoir of water prior to being pumped. However, the input specification of the pump, will determine this temperature. In addition, larger leaks will require higher flow rates and therefore this reservoir of water could become depleted very quickly in some cases. As this option already has many limiting factors, more suitable methods include direct resistive heating and cartridge heaters. Direct resistive heating would involve applying high voltage and current levels to a hollow metallic pipe, while water is flowing through it. As the hot metallic pipe is in direct contact with the water, there is a very good heat transfer to the water. The second option could use cartridge heaters. These come in a variety of sizes, power outputs and temperature ranges. This method of heating would require a holder being constructed to retain the cartridge and through being in close proximity to the water pipe transfer the heat by conduction through the surrounding metal. This is less efficient than resistive heating but because the cartridge can run at temperatures approaching 600°C, there is sufficient overhead to heat the water. The requirement for the water temperature is: being capable of reaching the typical PWR temperature, but for typical running conditions run a nominal 200°C.

The two elements required by the pump and heaters are water and electricity respectively. In the nuclear laboratory at HMS Sultan, there is mains water available and two three phase sockets, capable of supply over 10kW's each.

The water pressure will need to be controlled and restricted through the use of valve(s) for altering the pressure and a pressure relief valve for limiting the pressure to a predetermined maximum level. The pressure adjustment could be accomplished using either one or two valves. One valve could make large pressure adjustments while another could fine tune the pressure. The actual variation could be achieved either using a motorised valve or manually. A pressure relief valve is required to avoid the pressure reaching a dangerous level, and therefore this will be set at 150 bar. To monitor the pressure in the system, there should be sufficient gauges to cross reference each other. Therefore, having two analogue and one digital should be adequate.

It is anticipated that the pump will vibrate and operate at high noise levels; therefore to enable silent monitoring of the leak, an accumulator will be needed in the system.

This should have sufficient capacity to ensure the pressure is maintained for a satisfactory period of time to capture data. The capacity can be calculated based upon the flow rates of the orifices.

The pipes connecting all of the above components should ideally be of a small internal diameter, to reduce the volume of water for heating. This pipe should ideally be made from stainless steel, because it does not rust, and is capable of withstanding high pressure. Through observation and calculation a suitable pipe should be acquired. The pipe outside diameter should be of an industry standard size, to ensure fittings, couplings and other components can attach to it. In addition to metal pipes, rubber hoses should also be fitted on the exit from the water pump and on tight radiuses. Due to the vibrations produced by the pump, pump manufacturers recommend flexible pipes into and out of the pump.

To ensure the water used in the test rig does not contain contaminants and limescale, which could potentially fur the pipes and block the orifice, a de-ionising tank should be fitted with sufficient capacity to flow at the level specified by the water pump.

The final component in the test rig is the leak element. The various options range from bending a pipe, to create a crack, to drilling a hole in a pipe with a diameter chosen to correlate to a flow rate at 100 bar. The other considerations that need accounting for are:

- Maintaining the ability to fit the metallic lagging over the leak area
- Ensuring that the metallic lagging will be able to clamp around a pipe with a surface temperature of 200˚C, as per the typical primary pipe.

The plan is to use orifices of varying flow rates that can easily be inserted and removed, at leak rates significantly smaller than can be measured at present in the PWR. In addition, having orifices that vary by minimal flow rates would be preferential as it would provide a higher level of leak analysis. At present, levels of 100 litres/hour can be detected, and therefore this should be the maximum leak rate. The lowest leak rate will be determined by the technology available to produce the smallest aperture.

All of the above components should then be housed in a strong and moveable shell with protective shields around the high temperature areas.

Control and data monitoring should be carried out at a safe distance from the test rig, although it would be advisable to attach the data acquisition device as close to the

orifice as possible to minimise cable lengths from the sensors. HMS Sultan, Nuclear Department, does not currently have a data acquisition device, therefore one would be required. The specification of such a device should ensure that sensors such as microphones and accelerometers, which high bandwidths, are capable of being fully utilised. Shannons theorem (Beaty (2004)) requires the sampling frequency to be twice the required frequency bandwidth. Therefore, to measure up to 26kHz would require a sampling frequency of at least 52kS/s. Most other sensors can be run at lower sampling speeds. Therefore, the preliminary specification for this device, is to have the capability to run at 52kS/s but adjustable for sensors that only require sampling speeds in the order of 1kS/s. The data acquisition device must also be adaptable, and have the provision to accept a variety of sensor types. This requirement is not only applicable for this project but for other future academics to use this piece of equipment.

Through a combination of the literature review and an understanding of different sensor types, a set of sensors will be evaluated for this project. This set will then be further refined through a thorough selection process, resulting in only the most significant, in terms of data output, being used in the final setup.

The collected data will then need pre-processing to determine whether each specific sensor will be capable of diagnosing the presence of a leak, and further whether it will be able to verify the leak size. After examination of this data, it is anticipated that some sensors will be applied to a digital logic system that merely indicates the detection of a leak, whereas, other data of a more complex nature will require non-linear analysis. This data will also need further processing to extract the most significant parameters/features from the data set, and apply these to an artificial neural network. ANNs have been selected for a number of reasons: prior experience of using artificial intelligence for predicting stock market movement, Shepherd (2004), the results of which were very good, the suitability of ANNs for classification problems and the project supervisors' speciality being in this area.

The final deliverable will be an Operator Advisory System (OAS). This system will enable the numeric results from Matlab™ to be shown graphically. It will enable the presentation of different sensor data at different leak rates to be displayed in a comprehendible manner. The aspiration is that this OAS will become the precursor to a graphical user interface within in a naval nuclear command centre. The requirements of the OAS are that validation for the results will be achieved by allowing the operator

to interrogate the input data, hence providing clarification for the leak size suggested. Recommendations will be made to isolate the leak, and the leak location will be illustrated with a 3 dimensional model of the reactor system.

This report builds on the first and second year report Shepherd (2008 and 2009 respectively), and therefore contains common material. There have been two predecessors to this work, namely Weller (1997) and D'Souza (2006). The former investigated the use of ANNs and Evolutionary Computation for the monitoring of small transients in complex non-linear system, of a Pressurised Water Reactor (PWR). The latter investigated the use of ANNs for intelligent monitoring of small transients in a complex system represented by a PWR. Both projects were working toward an Operator Advisory System, and even though their results would be invaluable to an operator, the format adopted would need skilled interpretation. Consequently, this work will attempt to merge the knowledge gained in the application of the ANNs for the primary system in a PWR, but also deliver a graphical OAS.

The following sections will describe the two approaches to analysing the data from the various sensors.

3.3   Introduction to Hard Computing

People have been using hard computing techniques since the advent of the computer, creating precise analytical models using logical and mathematical reasoning, unlike soft computing which has a degree of uncertainty and imprecision, but tends towards using tools for pattern recognition and prediction. Some of the hard computing systems include:

- Logical systems
- Sentential logic
- Predicate logic.

The principles of hard computing rely on ideal cases, whereas most real world problems exist in non-ideal environments. This report will use the simplest and most common hard computing technique, namely logic gates, such as AND, NOT, OR, XOR. However, logic gates rely on data being binary form. To achieve this, a threshold level is determined and values above this threshold are denoted by a 1 and below a 0. Consequently, in the no leak scenario, all the data appears at logic 0, then when a leak occurs the temperature or humidity rises above a predetermined threshold

level and it becomes logic 1. By applying multiple sensor outputs into an AND logic gate, the output will only be at logic level 1, when all inputs are in agreement, and when this occurs the probability is high that a leak exists. The OR gate could be used to take account of sensor redundancy.

3.4 Introduction to Soft Computing

Soft computing is typically used for analysing complex systems where conventional analytical solutions have failed. A soft computing system can tolerate imprecision, partial truth and uncertainty. They can be trained to recognise handwriting, images and speech in addition to making forecasts on the weather and the stock market. This is therefore branching into the area of Artificial Intelligence and Machine Learning. Some of these areas include:

- Artificial Neural Networks (ANN)
- Fuzzy Logic
- Evolutionary Computation
- Genetic Algorithms
- Chaos Theory.

This report will concentrate on using ANNs as the primary technique for predicting the leak size. If this technique is not successful other techniques listed above will be applied to the data, and their results analysed. At this stage no soft computing techniques should be dismissed as the data have not previously been applied to an ANN and so the level of success is unknown. The expectation is that the combination of ANNs and logical systems will be sufficient to provide the operator with enough information to make an informed judgement for his proceeding actions. This is in agreement with the conclusion from Wainwright (1995).

For the last 20 years ANNs have been used to solve numerical problems in the nuclear industry, as demonstrated in Chapter 2. Their applications have been as diverse as predicting the two phase mixture density of the coolant around the reactor (Lombardi, 1997) to plasma shape recognition in a Tokamak Machine, (Greco, 2005). However, this project draws its ANN research from previous work such as PWR monitoring (Weller, 1997) and fault diagnosis (Basu, 1994).

3.5   ANN Background

ANNs are inspired by neural networks found in the human brain, but rather than using neurons and synapses, signals are propagated through the use of artificial neurons and weighted connections. An ANN is an adaptive non-linear system, able to learn to perform a function, having been subject to input data, and possibly target data. It is an adaptive system because during the training phase it is able to modify its system parameters. Having trained the network, it is important to further verify the network through two further stages called validation and test. During the validation phase a small percentage of the input data validates that the network is generalising well and stops training before overfitting starts. Overfitting is a situation where the network has been trained too much and therefore becomes very good at classifying the training set but poor at classifying data it has not encountered before. The last phase uses the remaining unseen data and performs a completely independent test of the network generalisation. By achieving good generalisation means that the ANN can approximate a target value on data it has not previously trained on or seen before. These phases are known as training, validation and test and the entire set of input data is typically split 70%, 15%, 15% to each of these respective areas.

When the ANN is presented with a set of input data and a corresponding set of target data, this is called a supervised network. This type of system learns by calculating the difference between the system output and target output, this is output error, and by adjusting the system parameters on subsequent iterations tries to reduce the output error to an acceptable level.

Conversely in an unsupervised network no target data are available and therefore the network produces its own classification based on the input data.

3.5.1   Topologies and development of an ANN

Figure 3.1 represents a mathematical model of an ANN, showing the data flow from input to output. The representation between the biological and artificial neural network is:

- Synapses of the neurons are represented by weights
- The strength of the connection between an input (χ_j) and a neuron is the value of the weight (w_{kj})

- - A negative weight infers an inhibitory connection
  - A positive weight reflects an excitatory connection
- The activity in the neuron cell is denoted by the summing junction which adds all the inputs modified by their respective weights together
- The last stage is known as the activation function and Figure 3.1 uses the threshold function, whereby through comparison of v_k and a threshold value θ_k, the output is either 1 if the neuron fires or 0. Other activation functions include the piecewise-linear function and sigmoid function, and these can have values between 0 and 1 (or in some cases -1 to 1).
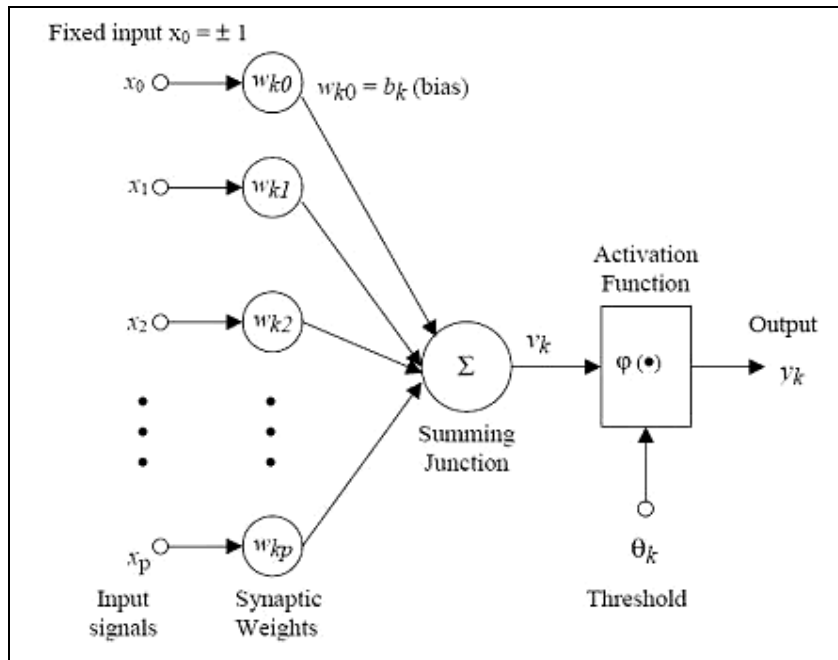
Figure 3.1 Mathematical model of an ANN (Courtesy of NeuroAl (2010))

The activity from the neuron is given by:

$$v_k = \sum_{j=0}^{p} w_{kj} x_j$$

where x_j and w_{kj} are the input and weight of the jth synapse.

Therefore, the final output of the neuron (y_k) is the value of the interval activity (v_k) multiplied by the activation scale factor.

In order to achieve a successful outcome from an ANN, there are a number of steps that need to be adhered to. Figure 3.2 shows a typical ANN iteration cycle.

41

```
                    ┌─────────────┐
                    │    START    │
                    └──────┬──────┘
                           │
                           ▼
              ┌──────────────────────────┐
              │      COLLECT DATA         │
              │   - scale if necessary    │
              └────────────┬─────────────┘
                           │
                           ▼
              ┌──────────────────────────┐
              │  CONSTRUCT THE NETWORK    │
              │      - Topology           │
              │      - Size               │
              │      - Functionality      │
              └────────────┬─────────────┘
                           │
                           ▼
              ┌──────────────────────────┐
              │    TRAIN THE NETWORK      │
              └────────────┬─────────────┘
                           │
                           ▼
              ┌──────────────────────────┐
              │    VALIDATE AND TEST      │
              │        NETWORK            │
              │    - On unseen data       │
              │ - Achieve good generalisation │
              └────────────┬─────────────┘
                           │
                           ▼
              ┌──────────────────────────┐
              │  EVALUATE PERFORMANCE     │
              │      - % Error            │
              │      - Regression         │
              └────────────┬─────────────┘
                 Poor      │   Good
                           ▼
                    ┌─────────────┐
                    │    STOP     │
                    └─────────────┘
```
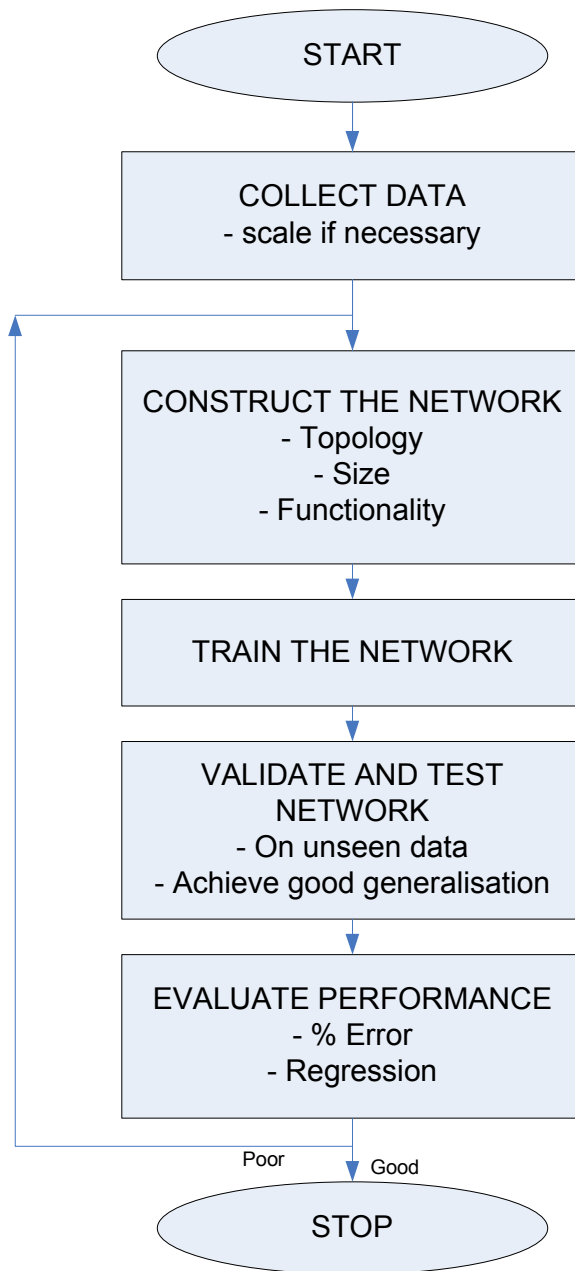
Figure 3.2 ANN Iteration Cycle

3.5.2   ANN Architecture

The architecture of an ANN is determined by:

- The connections made between neurons
- Processing elements
- Number of layers
- Flow of the signal through the ANN.

42

Figure 3.3 shows two ANN topologies, these being the feed-forward and recurrent neural network. Figure 3.1 showed a typical example of a feed-forward network, where the data enters the network through the input layer. They then proceed to the summing junction and onto the activation junction to produce an output. This output will then become an input for the artificial neurons in the next layer. This process of feeding the subsequent layer is how the ANN has become known as feed-forward, and this cycle continues until the last layer is reached.
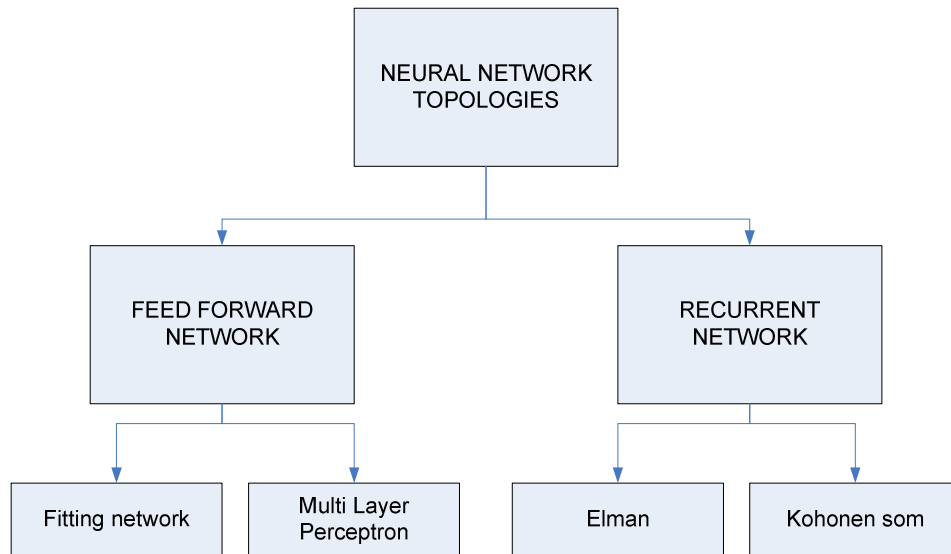
Figure 3.3 Feed forward versus recurrent neural network topologies

The architecture of a recurrent network is shown in Figure 3.4. This differs from Figure 3.1 because at each time step a copy of the hidden layer units is made, in a new area, called the context layer. This copy is then presented back to the hidden layer denoted by z^{-1}. Therefore, the error computation of the hidden layer is improved during training because the error function is determined by both the previous and present time steps.

Recurrent network with hidden neurons
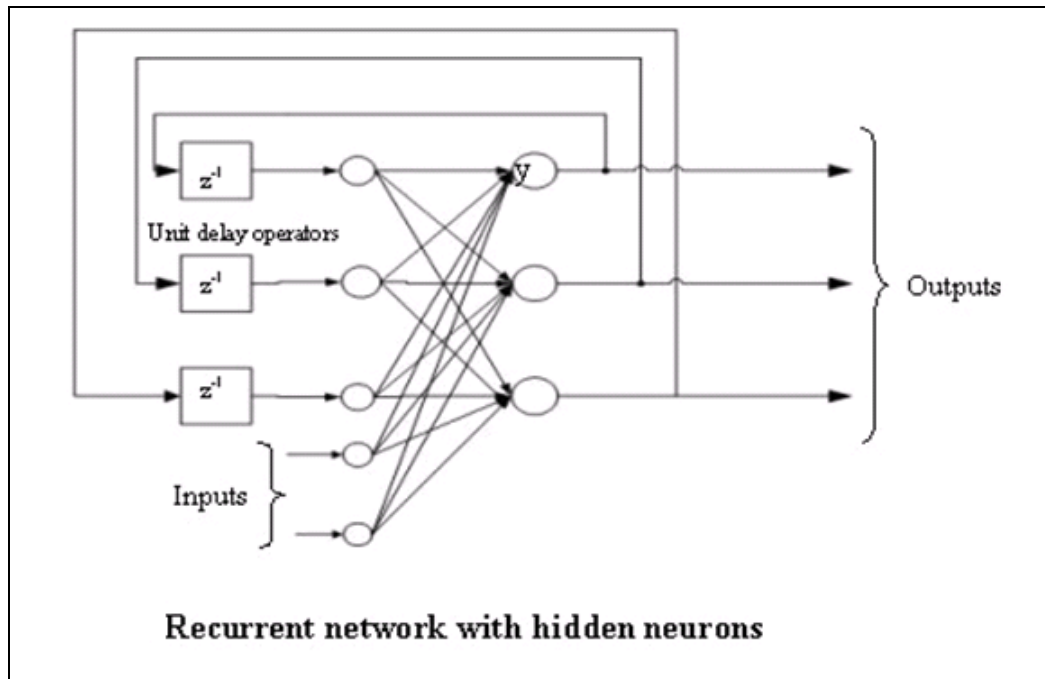
Figure 3.4 Recurrent ANN

3.5.3 Multi-Layer Perceptron (MLP)

The multi-layer perceptron (MLP) is one of the fundamental ANNs used to solve non-linear problems. This type of network typically consists of three layers of units, namely the input, hidden and output, as shown in Figure 3.5. The input layer represents the input data to the network, i.e. each unit denotes a separate input parameter. These input units are then attached via weighted links to the hidden layer. The hidden layer is further attached to the output layer through fully connected bi-directional weighted links. It is only through the modification of the weights from repetitive training that learning occurs. In other words, learning is achieved in a similar way to humans, i.e. by performing small changes to the input data and observing the effect on the output data, eventually a condition is met when the desired output reaches a satisfactory agreement with the input conditions. The system is initially trained on a known set of input and output data, known as training data. If the ANN is able to converge to a pre-determined level of agreement, new data can be analysed.
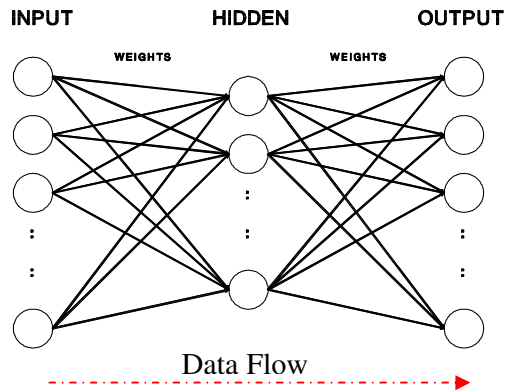
Figure 3.5 Multi-Layer Perceptron (MLP), Brown (2004)

3.5.4 Elman Network

The Elman network is a type of recurrent network (as shown in Figure 3.4) because it has a closed loop feedback path from the hidden layer to the input layer. It memorises past events in order to influence the current time step. Due to this feedback, the network is far more fault tolerant to missing data than a standard MLP would be. This loop also enables it to distinguish between identical pieces of data that may have appeared during the training cycle, as it is capable of storing temporal and spatial patterns. "*The most important advantage of Elman's network is a robust feature extraction ability*", Seker (2003).

3.5.5 Self Organising Map

The Self Organising Map (SOM) is another type of recurrent network, but uses data visualisation techniques. This type of network uses unsupervised learning, in other words the training is purely data driven, and no previous knowledge of the input data is known. This kind of network learns to detect correlations in the input vectors and adapt the future output to take account of the input. Neurons in the competitive layer identify groups containing familiar input vectors for classification onto the output map. Therefore, artificial neurons that are adjacent to each other learn to respond to similar input vectors. Figure 3.6 shows a simple two dimensional lattice containing 16 nodes and two inputs. Each node has an effective x and y coordinate containing a

vector of weights of the same dimension as the input vectors. Therefore, if the training data consists of vectors V, with n dimensions:

$$V_1, V_2, V_3 \ldots\ldots V_n$$

then correspondingly, each node would contain a weight vector W, of n dimensions:

$$W_1, W_2, W_3 \ldots\ldots W_n$$

The SOM architecture differs from the conventional ANN, because the lines connecting the nodes in Figure 3.6 only represent adjacency and do not signify a connection, as might be expected.
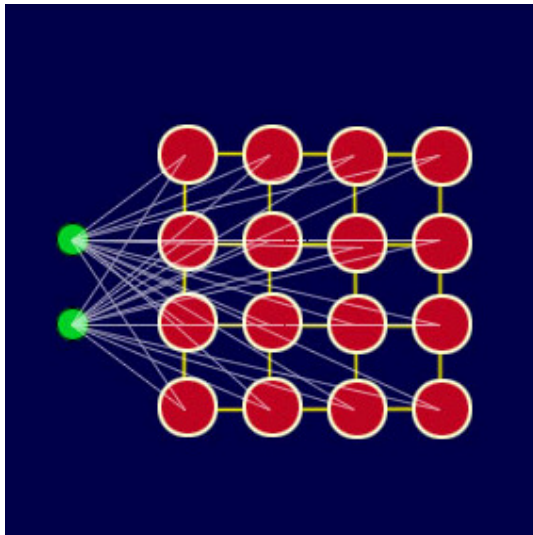
Figure 3.6 SOM Architecture

Consequently, SOMs are ideally suited for pattern recognition and clustering of data. In the commercial world, credit card companies use this technology to detect fraudulent activity and digital paper scanners use this concept to identify characters on a page.

3.6 Summary

This chapter reviewed the research methods of this study. Initially, the concept of a rig to replicate the high temperatures and high pressures within the primary circuit of a PWR was presented, and then a description of every potential component in the rig was described. Different methods of analysing the data were offered, ranging from using digital logic to ANNs. Different ANN topologies and architectures were explored including ANN networks such as Elman and SOM.

Chapter 4

Design and Implementation of High Pressure and High Temperature Test Rig

The biggest hurdle with the project is acquiring data, as none are freely available. Therefore, the only solution is to re-create the primary circuit conditions. A diagram of a simplified reactor is shown in Figure 4.1, and the primary circuit is shown in red. The reactor typically runs at pressures and temperatures exceeding 100 bar and 200˚C respectively. Consequently, a rig would have to be developed that could pressurise and heat the water to these high levels.
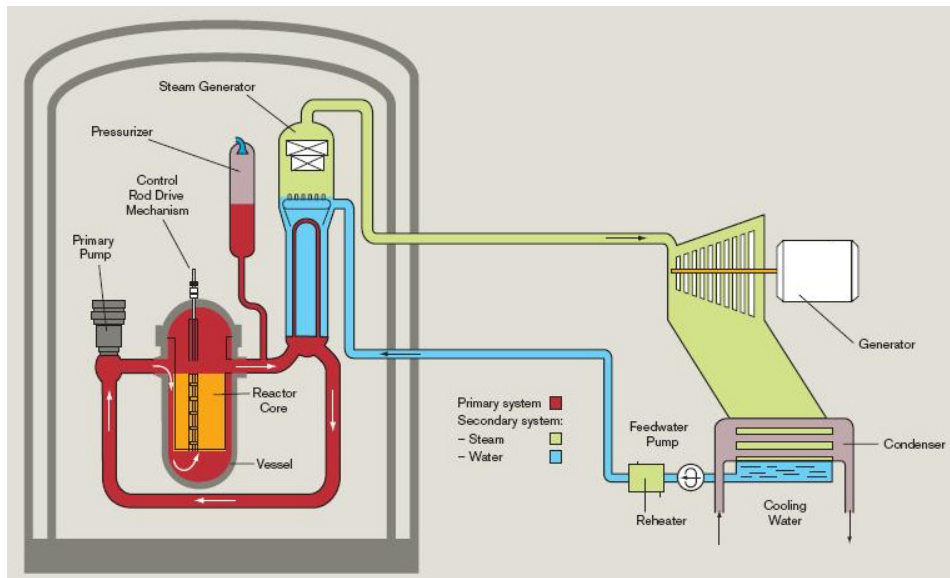
Figure 4.1 Architecture of a Pressurised Water Reactor (PWR), Areva (2005)

Therefore, the challenge is to independently build a rig capable of these temperatures and pressures, have it certified for use, devise sensors to record the leak data, analyse and apply the data to an ANN and finally build an OAS.

The research carried out in this report and D'Souza (2006) has illustrated the lack of available small leak data. Consequently, it was decided that building a suitable rig to replicate the effects during a small leak from a primary circuit of a nuclear reactor,

and measure as comprehensively as possible all conceivable signals that emanate from the leak, was the best approach.

Therefore, this section describes the design thoughts behind the rig, the manufacture and construction as well as the calculated pressures and forces the steam release will develop. The following chapter describes the sensors chosen and preliminary results.

4.1 Requirements

During the early conception of the design, it was decided that the temperatures and pressures should be representative of the real primary circuit. Therefore, the temperatures and pressures have been simplified to 200˚C and 100 bar respectively. If required, the rig could be run at higher temperatures and pressures but for Health and Safety reasons any increase should only be minimal, and only if there is a strong belief of discovering significantly different results.

The requirements for the rig are:

- High pressure, nominally 100 bar
- High temperature, nominally 200ºC
- Variable leak size (flow rate 40 – 100 litres/hour)
- Water pump, options:
    - high pressure 200 bar and low flow 1-7 litre/min
    - low pressure 2 bar and very low flow 1 litre/min
- Adaptable for other applications (low pressure)
- Stainless steel construction (as per primary circuit)
- Leak area has provision for metallic lagging to be fitted
- Stands and clamps available to hold sensors
- Low cost (less than £3000) and adaptable (each section is removable)
- Moveable, robust and safe.

4.2 Rig Components

In order to produce a rig that could satisfy the requirements in section 4.1, the design must have a:

- High pressure pump (up to 200 bar)

- Method of heating water (up to and beyond 200°C)

- An orifice to replicate a crack, with the potential to be varied in size

- A means to alter the pressure in the system (typically 100 bar)

- A constant flow of water, pulsation damper fitted if required

- A safety device to limit pressure to 150 bar

- A control system to vary the water temperature

- A source of ionised water

- Mounting for sensors and lagging.

The following sections fully describe how each design component was selected, either through measurement or calculation, and its suitability to the task. Some of the early design concepts failed and information regarding those items can be found in appendix B and C.

4.3 An Orifice of Varying Size

One of the hardest parts of the design was deciding how to create a measurable crack. In order to quickly crack a pipe, a bending or crushing moment can be applied, taking it past its elastic limit. The normal route to pipe fatigue and cracking is by a phenomenon called stress corrosion cracking (SCC). SCC is composed of three major contributing factors; tensile stress, corrosive environment and susceptible alloy. When all three are evident, pipe failure is possible.

However, for the purpose of this project multiple size cracks were required. In bending/crushing a pipe, the difficulty is relating a specific pressure or angle to a pipe to a specific size of crack. Another problem is its ease of adaptation, i.e. how easily could the crack size be changed, and then how simply could the cracked section of pipe be inserted in and out of the rig? The dilemma is does one create multiple cracked pieces of pipe, or a single piece of pipe that is given an ever increasing crack size? The issue with the latter approach is returning to an old test at a later stage, if additional sensors are used or the test parameters are changed. Consequently, it was decided that the most repeatable and accurate way to represent a crack is with a round hole. It could be considered an idealised crack, with the advantages of it being easily reproduced, mathematically derivable in terms of volume flow but most importantly a known measurable and repeatable quantity. This in turn creates another predicament,

would different hole sizes have to be drilled in various sections of pipe, and is a drill bit available that can produce a hole 0.1mm? With these questions in mind, the idea of cutting a fine groove into a bolt was conceived. The idea being, different bolts with different depths of grove could be inserted into the water pipe and easily changed from test to test. The concept was to use an Electro Discharge Machine (EDM), and very accurately cut a fine groove into the length of a bolt. The foreseen issues with this are: the minimum channel width, limited to 0.25mm due to the width of the EDM wires. However, it would be preferential to go as small as possible in order to observe the first signs of a leak. Also, cutting a narrow groove through bolts treads is not producing a true channel due to the reciprocating thread, therefore this idea was rejected. The requirement was to obtain a bolt that already had a pre-cut hole in the centre with ranges from 0.1mm to 1mm.

4.4   Variable Hole Sizes

The solution was to use a carburettor jet from a car. A make of jet (Mikuni) was found that had increasing flow rates from 10cc/min to 100cc/min in 2.5cc/min increments. A table showing the conversion from cc/min to g/s and litre/hour is in Appendix D. Therefore, the set chosen was 10, 12.5, 15 up to 40cc/min (13 jets). The carburettor jet is shown in Figure 4.2. This system is an improvement on the work carried out by Bausch (1989), who was limited to a 0.78mm fixed hole which would equate to roughly 100cc/min. The small side holes are unnecessary in the design for this application and were not anticipated to cause too much turbulence to the flow. The small 1.5mm opening at the foot of the jet narrows to the determined size around the threaded area, internally. A flat head screw driver slot at the top of the jet, allows them to be easily inserted and removed.
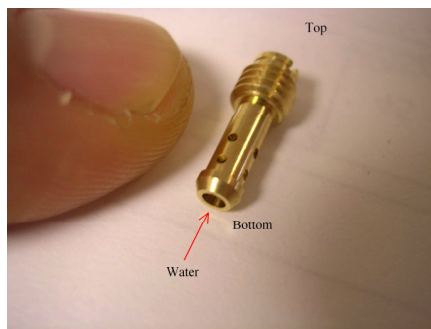
Figure 4.2 Carburettor jet

The carburettor jet is inserted into the M5 threaded hole shown in Figure 4.3.
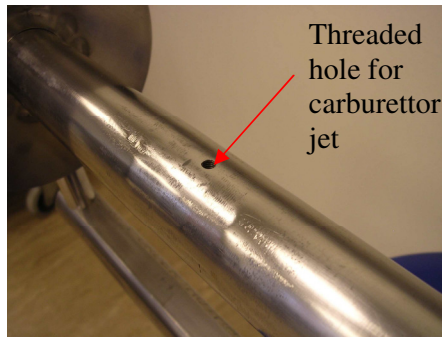
Figure 4.3 Threaded orifice for jet

4.4.1 Calculating Exit Velocity from Jet

Understanding the exit velocity of the water from the orifice enables the mass flow rate to be calculated. It is also important to understand the effect of exit velocity, as it is conceivable that the water could have cut through the lagging, if its exit velocity was high enough.

In order to apply the continuity equation, the carburettor jet can be assumed to be a sharp edged orifice. Consequently the flow of water is restricted through it. The level of restriction is determined by the D_1 to D_2 ratio, illustrated in Figure 4.4. In the case of the carburettor jets, the D_1 size within the jet is always 1.5 mm, whereas the orifice diameter D_2 varies from 0.25 mm to 0.575 mm. Therefore, the ratio varies from 0.166 to 0.38. Taking a rough average of the two and referring to Appendix E, a flow coefficient of 0.6 can be assumed.
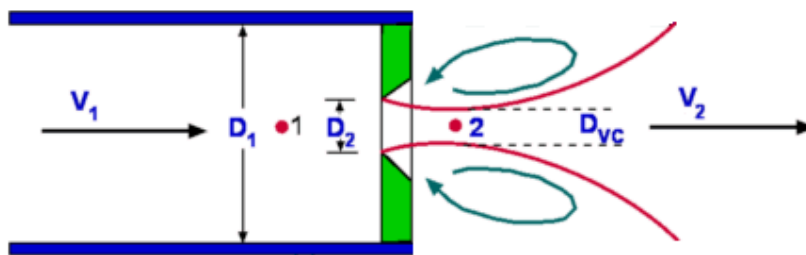
Figure 4.4 Flow through an orifice, Auld (1995)

The label D_{VC} is called the Vena Contracta, and is the minimum diameter of the jet of water that emerges from the orifice. Due to the ratio of the orifice to pipe diameter, there is an acceleration of the water flow, and consequently the water exits at a faster

velocity. This can be demonstrated using the continuity equation Auld (1995), shown below:

$$\rho_1 A_1 V_1 = \rho_2 A_2 V_2 = \dot{m}$$ **Equation 1 Continuity equation**

(ρ) density of water 1000 kg/m^3 @ 20˚C, and 850 kg/m^3 @ 200˚C

(A) Area is m^2 (A = π r^2 = π (d/2)^2), d can be either D_1 or D_2

(V) Velocity is m/s

It can be deduced from Equation 1 that by decreasing the orifice size D_2, leads to an increase in velocity V2.

The Reynolds number enables one to determine whether the flow through a pipe and orifice is laminar, transient or turbulent. The flow is:

Laminar if R_e < 2300

Transitional 2300 < R_e < 4000

Turbulent if R_e > 4000

The majority of the pipes used in the rig have a 5 mm internal diameter, and the following Reynolds (equation 2) calculates whether the conditions in the pipe are laminar, transitional or turbulent.

(V) The viscosity of water is 1.0x10^{-4} N.s/m^2

(D) Diameter of pipe 5 mm (0.005 m)

(U_{in}) Velocity entering small diameter pipe (see equation 4),

when flow is 11.6 g/s (smallest jet) U_{in}=0.69 m/s

flow at 29 g/s (largest jet) U_{in}=1.68 m/s

The Reynolds equation is shown below, Crane (1979)

$$R_e = \frac{\rho U_{in} D}{V}$$ **Equation 2 Reynolds equation**

Therefore, R_e varies between 29,590 and 71,428 depending on the flow rate in the pipe. The calculation shows the flow is turbulent, and consequently Bernoulli's equations can be used. Bernoulli's principle states that, increasing the speed of a fluid will cause a corresponding decrease in pressure or a decrease in the fluid's gravitational potential energy simultaneously. Figure 4.5 shows how the flow varies depending upon the Reynolds number.

Flow profile with laminar flow   Flow profile with turbulent flow
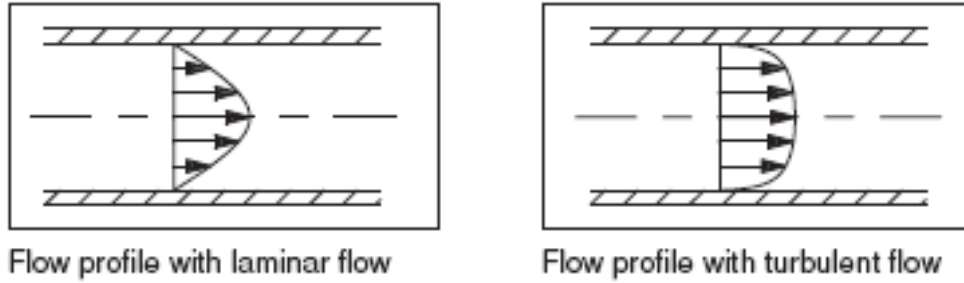
Figure 4.5 Laminar and Turbulent flow profiles, Parker (2005)

It is useful to know the Reynolds number, as this will determine whether the Bernoulli equation can be applied to calculate the pressure difference across at the orifice. Therefore:

(D) Pipe diameter 0.005 m

(D_2) Orifice diameter 2.5×10^{-4} m

(G_2) The mass velocity leaving the orifice is:

$$G_2 = G\left(\frac{D}{D_2}\right)^2 = 633\left(\frac{0.005}{2.5 \times 10^{-4}}\right)^2 = 2.53 \times 10^5 \text{ kg/m}^2\text{s}$$

Therefore, the Reynolds number at the orifice is:

$$R_e = G_2 \frac{D_2}{V} = 2.53 \times 10^5 \frac{2.5 \times 10^{-4}}{1.0 \times 10^{-4}} = 6.32 \times 10^5 \quad \text{(flow condition at orifice)}$$

Using Bernoulli's equation (Equation 2), enables the exit velocity to be calculated using the pressures known in the system.

$$P_1 - P_2 = \frac{\rho}{2}\left(V_2^2 - V_1^2\right) \qquad \textbf{Equation 3 Bernoulli equation}$$

Therefore, by combining Equations 1 & 2, and the flow coefficient from Appendix E, it can be deduced that:

$$D_{VC} = 0.6D_2$$

$$A_{VC} = \frac{\pi D_{VC}^2}{4}$$

$$\dot{m} = \rho A_{VC} V_{VC}$$

Therefore, using equation 2, ignoring V_1, as it is negligible compared to V_2, and re-arranging for V_2 yields:

$$V_2 = \sqrt{\frac{2}{\rho}\left(P_1 - P_2\right)}$$

$$V_2 = \sqrt{\frac{2}{850}\left(100 * 10^5\right)} = 153.4 \text{ m/s}$$

153.4 m/s is the exit velocity from the orifice, and will remain a constant, as long as the internal pressure remains constant. It must, however, be noted that the mass flow rate will vary with jet size.

4.4.2 Shear Strength of Carburettor Jet

An important consideration into the safe working of the rig is that the carburettor jet does not become a projectile, with the large pressure of water at the base of the jet, shown in Figure 4.2. As part of the final commissioning of the rig, the entire system will be pressurised to 210 bar, this was to ensure the rig components had an adequate level of safety margin. Consequently, it is important to calculate the shear strength of the threaded part of the jet, otherwise the jet may become a bullet under pressure if the threads are not strong enough. Determination of this is as follows.

The maximum test pressure will be 210 bar this equals 3045.84 lbs/in^2
The area occupied by the 5 mm threaded jet is ($A_1 = \pi r^2$) = 19.635 mm^2 or 0.0304 inch^2

Known values:
N_{th} = number of threads engaged = 4
p = pitch of thread = 0.8 mm
D_{core} = diameter of core = 4.0184 mm

A = (Nth.p). π .Dcore   **Equation 4 Area of failure surface**
 = 40.21 mm^2

τ = failure shear stress = worst case 77 N/mm^2
Failure force = A.τ = 40.21 x 77   **Equation 5 Failure force**
= 3096.17 N

A_1 = Area of 5 mm threaded jet = 19.635 mm^2
P = water pressure = 210 bar
The pressure force is = P.A_1 **Equation 6 Pressure force**

$= (210 \times 10^5).(19.6 \times 10^{-6}) = 411.6$ N

By dividing equation 5 by equation 6 gives the amount of overhead preventing the jet breaking away from its threaded area. The result shows that even when using the worst case scenario, the threaded section of brass component is more than seven times stronger than required. It should also be noted that the likelihood of the jet ever becoming a projectile was unlikely because the jet was always enclosed by the lagging. Figure 4.6 shows the water flashing to steam as it exits the jet. The left half of this picture is taken with a normal camera, whereas the right side is taken with a thermal camera. The images have been superimposed on each other. The metallic object at the top of the picture is a pitot static probe.
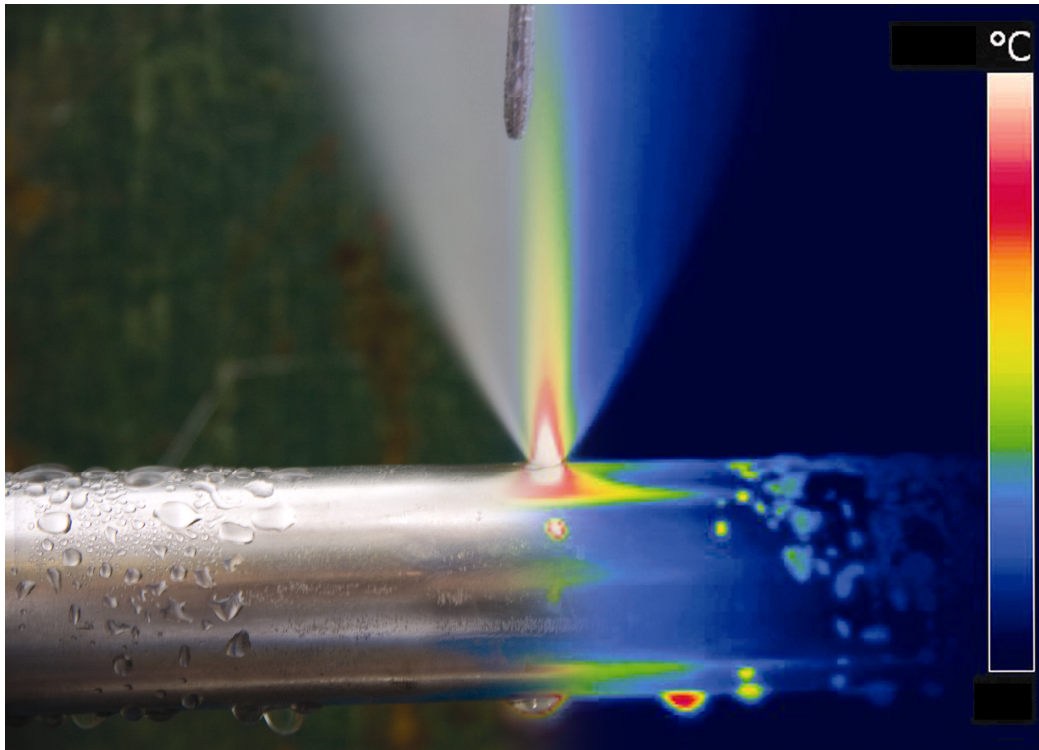
Figure 4.6 Steam exiting orifice, picture composed of real and thermal image

The temperature scale on the right hand side of Figure 4.6 has been removed because the thermal camera is uncalibrated and may cause confusion.

4.5   DC Power Supply

In order to heat water to 200°C, a large amount of power is required. The DC power supply shown in Figure 4.7, is capable of providing 45 volts and 280 amps, up to a theoretical maximum power of 12.6 kW, but 10 kW continuous.

Through experimentation, current was passed through several different lengths and side wall thicknesses of stainless steel pipe. When the correct resistance of pipe was obtained the full power of the DC supply could be released. By passing water through the pipe when the supply is running the water is very quickly heated, this is known as direct resistance heating. This is exactly the same principle used to illuminate a light bulb. In fact, during tests with a section of pipe and mains water, the pipe glowed red hot and steam was measured leaving the pipe at over 500°C.

Figure 4.7 DC Power Supply

The DC supply shown in Figure 4.7 is a Delta Elektronika, SM45-70D (45 volts and 70 amps maximum per unit), and consists of four DC supplies coupled together in parallel, with the top unit being the master and the other three being slaves. There is also a facility to disable the output when the unit is used in a controlled system.

In order to get maximum transfer of power from the DC power supply to the pipe, the optimum resistance for the pipe needs to be calculated. Using the measures known:

Continuous usable Power is 10,000 Watts

Maximum voltage is 45 volts

Therefore, using the power equation $P = V^2/R$

The resistance required for a maximum power is 0.2025 ohms.

In real terms this means if the resistance is above 0.2025 ohms the maximum power will be reduced and if the resistance is lower then this value the power supply will be unable to supply enough current and may cause the power supply to start tripping.

It was further found by experimentation (results shown in Figure 4.8), that using a 4 m length of pipe, 5 mm internal diameter, 0.7 mm wall thickness and with a resistance of 0.24 ohms, water at mains pressure could be boiled using a power of 3.5 kW. Using this pipe, the maximum power has been calculated to be 8.437 kW. The results from the laboratory experiment are shown in Figure 4.8, together with a possible temperature gradient. This experiment was conducted with water from the mains tap and therefore the pressure was probably less than 1 bar, even though the flow was 7.5 g/s. This experiment was necessary purely to confirm that direct resistance heating was a feasible method of quickly and easily heating water.
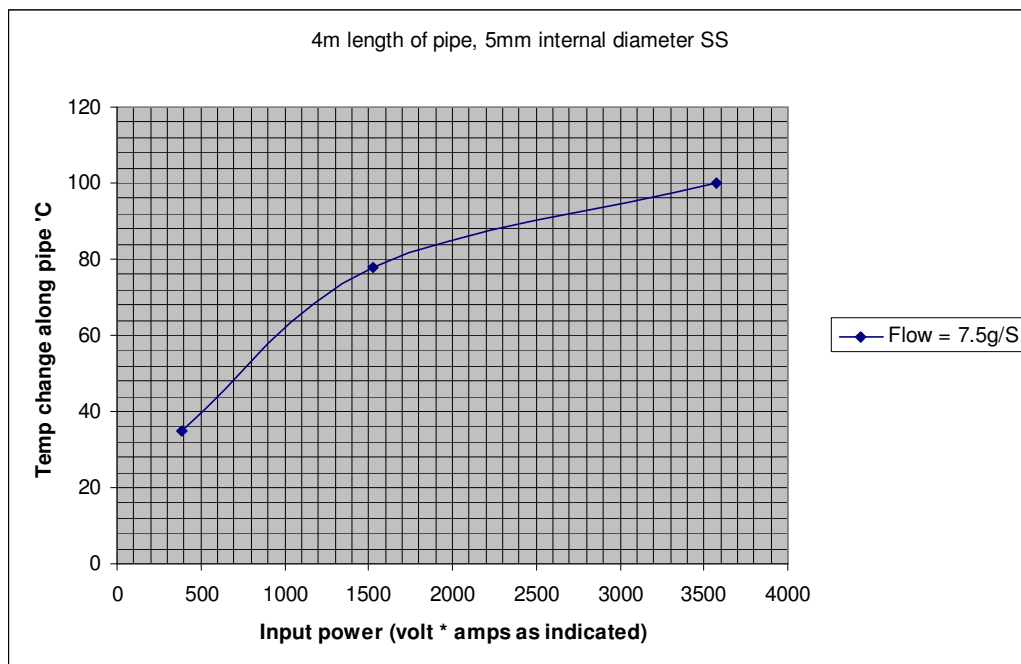
Figure 4.8 Power required to heat water from 12.6ºC to boiling and beyond

Other pipe lengths and diameters were tested, but it was found that their resistance was too low, resulting in a low current, and hence a low power, incapable of heating the water to 100ºC. For these reasons the final pipe needed to be 4 metres in length and have a small wall diameter to increase the resistance.

4.6   Heated Coil Section

In order to make the 4 metre thin walled stainless steel pipe more functional it was coiled up, as shown in Figure 4.9. The DC supply was then attached at the points highlighted in the diagram.

To prevent the current taking an alternative route through the rig, the coil supports were rubberised between the connection point for the DC supply and support bracket.
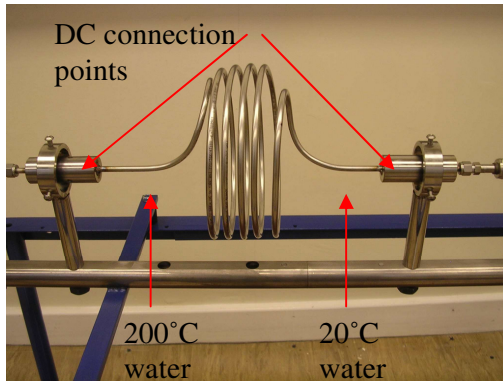
Figure 4.9 Heated coil section

Establishing that the heated coil could heat the water by this principle was the first step in the overall system design Once the mass flow rate and heating capacity of the coil were known other components such as the water pump could be sourced.

The Steady State Energy equation (equation 7) will determine the highest flow rate attainable given the power available and the specific heat capacity of water.

Given that:

(C_P) Specific heat capacity of water is 4200 J/kg˚C

(T_{in}) The temperature entering the heated section of pipe is 20˚C

(T_{out}) The temperature exiting the heated section of pipe is 200˚C

(Q) The DC power applied to heat the water up is 10 kW

($\dot{m}$) Mass flow rate

Therefore, using the Steady flow energy equation

$$Q = \dot{m} C_p \Delta T$$ **Equation 7, Steady State Energy Equation**

$$\dot{m} = \frac{Q}{C_p \left(T_{out} - T_{in} \right)} = 13.23 \text{ g/s} \quad \text{(when the power supply is running at 10 KW)}$$

Therefore, 13.23 g/s is the maximum flow achievable through the rig, in order to maintain the water temperature at 200°C using only a 10 kW power supply. Using the carburettor jets, the smallest five have flow capacities between 11.6 and 15.6 g/s, and it has been found that the DC power supply can heat the final jet to 200°C when it is running at the maximum 12KW. When running at 15 g/s (0.015 Kg/s), by multiplying this figure by 60, the volume flow rate is calculated to be 0.936 l/min (56.2 l/h), which would enable the first four jets to be used.

Consequently the rig is shown to be limited by its heating capacity. In order to reach the required temperature and pressure using the larger jets pre-heating of the water would be required. The following section illustrates the approach adopted.
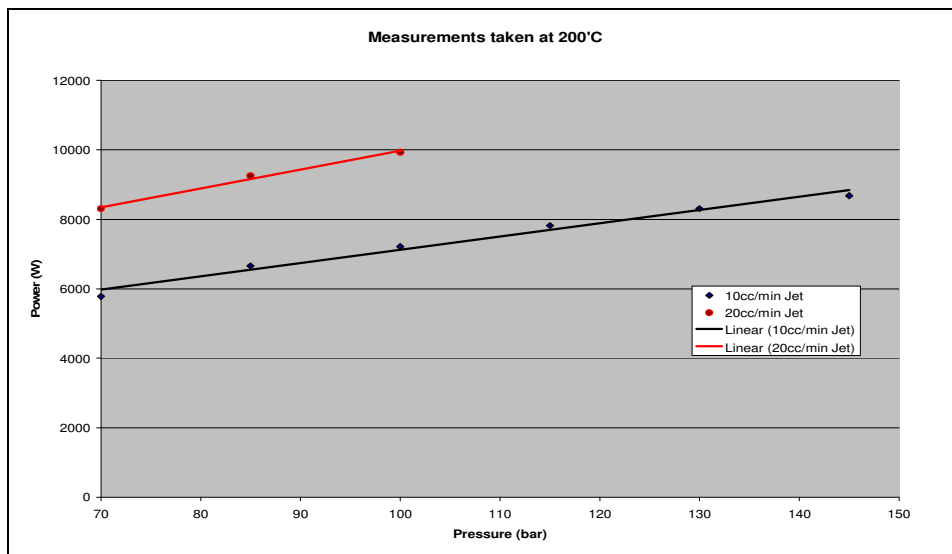
Figure 4.10 Power versus pressure

An important aspect of the design is understanding the velocity of water flowing through the heated section of pipe. This is significant because if the water flow is too fast the contact time between the heated pipe and water will be insufficient to heat the water to the required temperature. This can be calculated knowing:

(A) Area of 5 mm diameter pipe is 1.96×10^{-5} m^2

(ρ) Density of water is 1000 kg/m^3 @ 20°C, however the density at the orifice output falls to 850 kg/m^3 @ 200°C

(G) The mass velocity is the mass flow (28 g/s, largest jet) divided by the area, hence 1428 kg/m^{2}s

Consequently, the velocity entering the heated section of pipe is:

$$U_{in} = \frac{G}{\rho} = 1.68\,\text{m/s}$$ **Equation 8, Velocity entering small diameter pipe**

Jet flow	40 l/h (smallest jet)	100 l/h (largest jet capable of being heated to 200˚C)	217 l/h (largest jet in range)
Velocity in heated pipe	0.69 m/s	1.68 m/s	3.6 m/s

Table 4.1 Relationship between flow and pipe velocity

Referring to Table 4.1, it can be observed that the velocity change between the smallest and largest usable jet is about 1 m/s. Also, because the pipe is heated and the density has reduced this results in the 100 l/h jet velocity increasing by 0.26 m/s.

4.7   Cartridge Heaters

In order to achieve a greater range of leak rates more power is needed to heat the water. Various methods were considered such as kettle element heaters or gas torches, however they were dismissed because integrating them into the rig would have been difficult and in the latter case dangerous.

Another dilemma was at what part of the water system to heat the water. An initial consideration was to place the heating element before the pump. An immersion type system could heat the water up to 80˚C then the coiled heater would have an easier task of heating the water. The problem with this approach is that the water pump is not rated for receiving water above 40˚C. Therefore for logistical reasons the only area available to heat the water was immediately before the coiled heater. This is also a logical choice as there would be minimal heat loss from that section of the system to the next.

The final solution was to use cartridge heaters inserted into a brass holders as shown in Figure 4.11. This holder can contain four 1.5 kW cartridge heaters situated around the periphery with the water pipe inserted through the central hole. Using two of these assemblies (Figure 4.12) placed in series allows for an extra potential of 12 KW to be

used. Each one of these assemblies has its power controlled and monitored at all times, see section 4.16.2. By combining these heaters with the coiled heaters gives the system a 22 kW capacity.

Using equation 3, the new maximum flow rate is 29 g/s. This means that 13 unique jets can be used to deliver 13 sets of data.
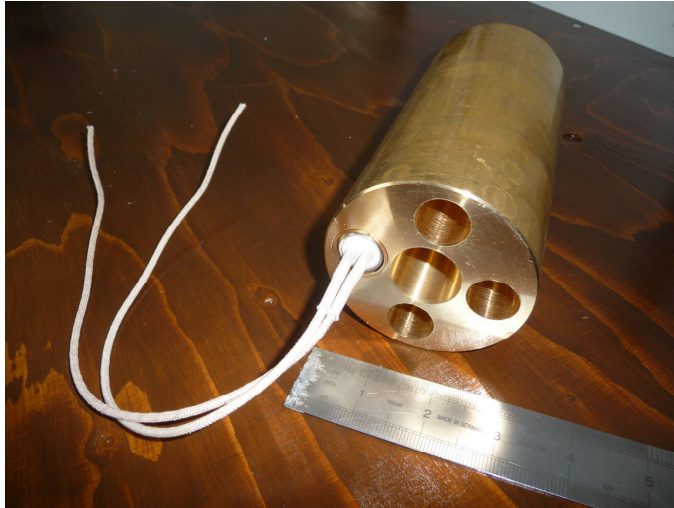
Figure 4.11 Brass holder for cartridge heaters
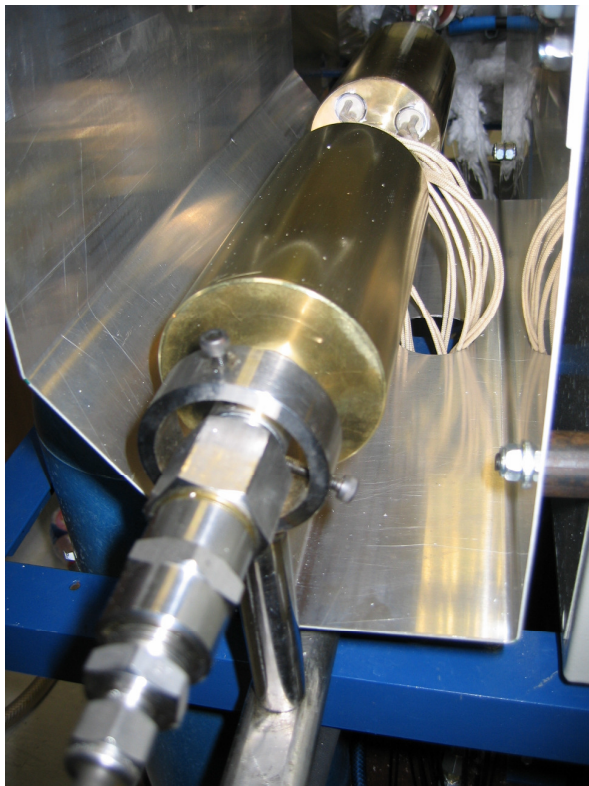
Figure 4.12 Water Pre-heaters

4.8   Water Pump

The water pump has two fundamental requirements, to deliver the required pressure and the required flow. The requirement is for the pressure to be 100 bar, but in order to offer a safe working margin a 200 bar pump was used.

From Figure 4.13, it can be seen the chosen range of jets varies from a measured 11.66 g/s to 28 g/s. This would equate to a requirement of 40 to 100 litres/hour from the water pump. However since it has been calculated that the total heating capacity available is 22 kW, the maximum jet size to fulfil the pressure and temperature criteria is 28 g/s (100 litre/hour), as shown in Figure 4.13. Consequently, it could be deduced that any pump that can supply in excess of 100 litres/hour, would be adequate.
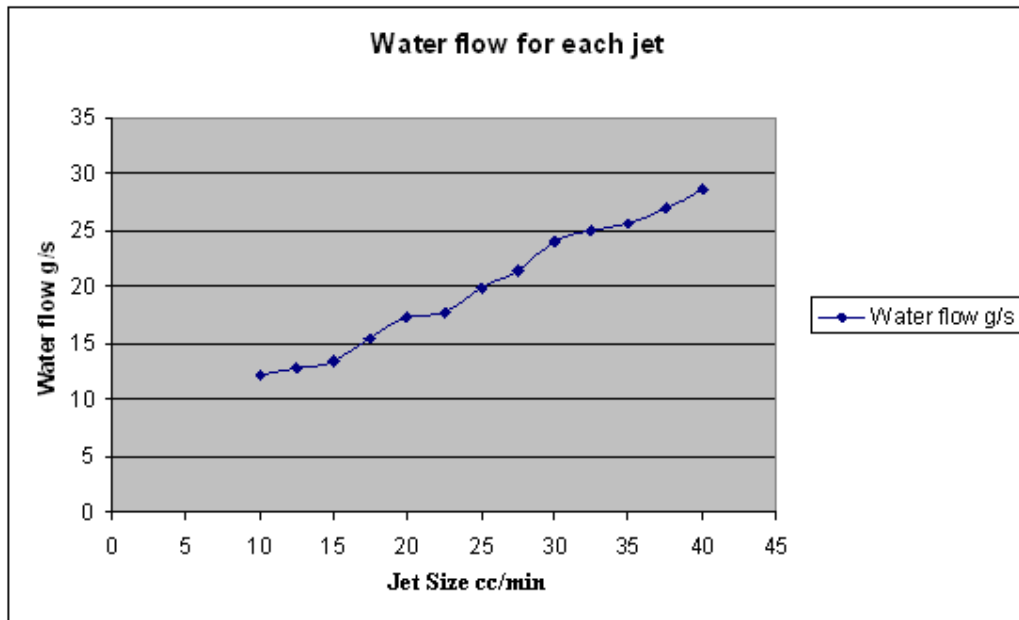
Figure 4.13 Measured water flow for rig jets

With regard to Figure 4.13, the x-axis indicates the value of the jet stamped onto its body. A 10 cc/min carburettor was originally intended to flow 10 cubic centimetres per minute of petrol at 0.25 bar. For the purpose of this report the same jet has been measured as emitting 12 g/s of water at 100bar of water pressure.

When the rig has the largest jet fitted, 100 litres/hour of water exits through the orifice, this hot water under pressure then immediately flashes to steam as it enters the atmosphere, resulting in 100800 litres/hour or 28 litres/second of steam.

In conclusion, the requirement for the pump is: a maximum pressure of 200 bar and a flow of 120 litres per hour. The other requirement is to use a 3 piston reciprocating pump. During early conception of this project, a single piston pump had been tested, but it produced a pulsed output. Therefore, at that stage it was essential to have a reservoir and accumulator as a pulsation damper. The initial mathematics for this pump are in Appendix C. However, another pump was subsequently sourced that delivered 200 bar and 360 litres per hour, using three reciprocating pistons. The flow was higher than required by the system, but a needle valve (as described in section 4.17), was able to compensate for that.

4.9 Accumulator

An accumulator was first considered when the only pump available was a single piston pump that delivered a pulsed flow of water. The intention was to use the accumulator to remove any pulsed flow. However, a 3 piston reciprocating pump was sourced and so this requirement was no longer needed. Having run the rig and experienced the degree of noise and vibration the pump creates, the accumulator has a new function of maintaining water pressure after the pump has been switched off. As the accumulator stores water at pressure, when this vessel has received its predetermined pressure of 100 bar and its pumping source has been removed, the orifice becomes the natural route of discharging this stored pressure. The size of the orifice will directly affect the length of time the accumulator will take to discharge. Typically, with a small jet of 40 litres/hour, it can take 45 seconds to drop in pressure from 100 bar to 90 bar. This time reduces with increasing jet size, and with the largest jet fitted this time can be reduced to only 15 seconds. However, during this period the only measurable parameter is from the water/steam exiting the orifice. Therefore, there is no interference from other sources on the leak data.

The accumulator sourced is a standard bladder type, with a physical size of 10 litres and for this application the nitrogen bladder is charged to 70% of its working pressure, i.e. 70 bar when the application is to run at 100 bar.

4.10 De-ionising tank

An ion exchange tank was required because it was found that the local water supply had a high chalk content, and during the heating process the pipes were starting to get lined with a layer of this deposit, causing the jet orifice to decrease in size. Consequently, a de-ionising tank was introduced. The tank contains H-OH IX resin resulting in water that has the purity of distilled water. A problem was discovered with the first de-ionising tank, where the water pressure exiting the orifice would fluctuate in its intensity. On further investigation it was deduced that the flow through that tank was insufficient for the 6 litres/minute required by the pump. Therefore, a higher flow tank was procured.

4.11 Lagging

The point at which the water leaves the orifice is encased by a layer of lagging material. The purpose of the lagging in the PWR is to maintain the high temperature in the pipe. The lagging material used in this rig was provided by Darchem, which is the company that supplies all the lagging material for the submarines. The Navy refer to this lagging as Metlag, as shown in Figure 4.14.
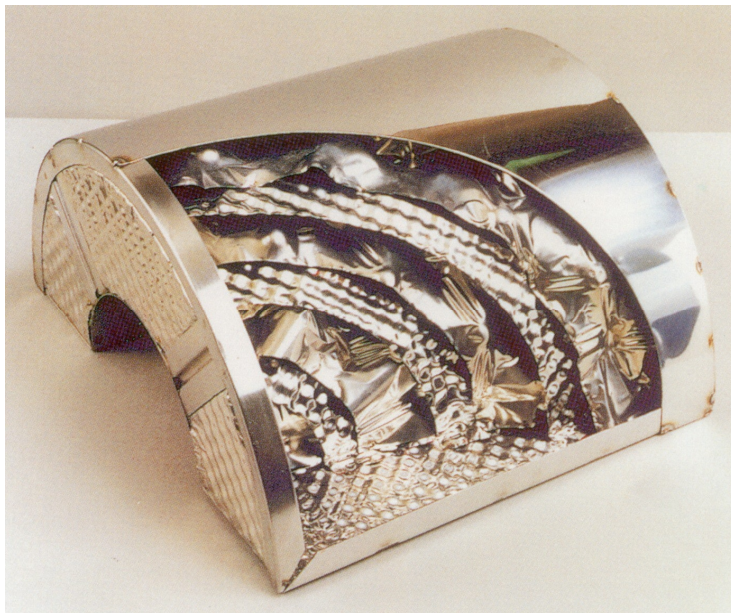
Figure 4.14 Internals of Metlag, picture courtesy of Darchem

Figure 4.15 below, shows the pipe with orifice in centre, before the lagging is applied and Figure 4.16 shows the section with lagging.
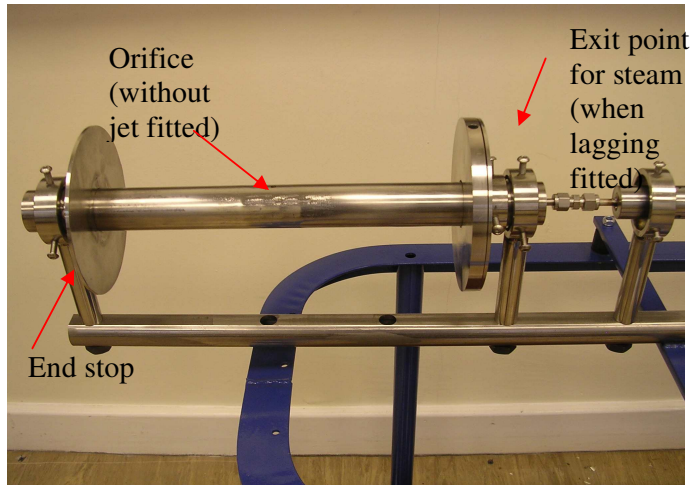
Figure 4.15 Orifice visible and end stops for lagging
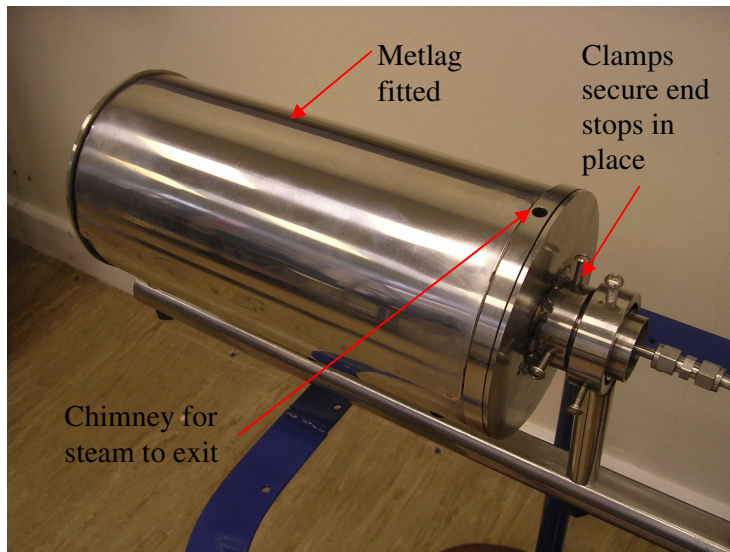
Figure 4.16 Lagging attached over orifice

It has been reported that should a steam leak occur under the lagging it can propagate inside the lagging for several metres, thereby making the exit leak position very difficult to determine. Therefore, a chimney was introduced where the steam can be vented, this allows sensors to monitor that area. In the normal running of the plant without leaks, no steam would be expected to exit from the chimney

The known measurable parameters from the orifice area and lagging material ($\dot{m}$) Mass flow rate is $5.00e^{-3}$ kg/s

(D$_1$) Pipe outside diameter 0.038 m

(b) Gap between pipe and lagging 0.0015 m

(D$_2$) Lagging outside diameter 0.15 m

(L) Lagging length 0.3m

(w) Gap between lagging sections 0.001 m

(x) Vapour fraction of flow 0.5

(P$_0$) Atmospheric pressure at ground level 1 bar

(P$_1$) Pressure under lagging 2 bar (this value was chosen as an example to illustrate what the force might be, if the pressure inside the lagging is 1 bar higher than the outside)

(V$_g$) Specific volume from steam tables 1.694 m^3/kg

The forces exerted on the lagging from the leak have been calculated to be:

$$F_1 = (P_1 - P_0).D_1.L = 10^5 \times 0.038 \times 0.3 = 1140\text{N}$$

This equation negates the value of π, because it is the projected area of the cylinder of lagging which is relevant. The value of 1140N is equivalent to the weight of 1.5 people sitting on the lagging opposing the internal forces, assuming the pressure under the lagging is 2 bar. In reality this would not be the case as the lagging sections do not form a perfect seal.

The following equations enable the escape velocity to be calculated.

(A) Flow area, $A = \pi.D.b = 1.7907e^{-4}$ m^2

($\dot{V}$) Volume flowrate = x. $\dot{m}$ .V$_g$ = 4.235e^{-3} m^3/s

(U$_1$) Velocity of steam at pipe surface = $\dot{V}$ /A = 23.65 m/s

(L$_2$) Length of gap on lagging surface = 2.π.D$_2$ + 2.L = 1.5425 m

(A$_2$) Escape area = L$_2$.w = 1.5425x10^{-3} m^2

(V2) Escape velocity of steam = $\dot{V}$ /A$_2$ = 2.7456 m/s

The escape velocity refers to the speed of the steam that will exit the lagging at all the joints.

4.12 Orifice and Pipe Heater

Figure 4.15 shows the orifice, the pipe and the Metlag ends. It has been demonstrated that the rig is capable of heating the water to 200ºC, at 100 bar, as can be seen in Figure 4.17. However, even though the jet is at the correct temperature and pressure, it is clear that the pipe itself resides at a much lower temperature. This creates a number of problems, namely:

- The steam will condense quickly when it comes into contact with the cold pipe and lagging
- Its is not representative of the real primary leak under the lagging
- The rig incorporates a chimney design as a steam exit, but is unlikely to work correctly if the steam has all condensed.
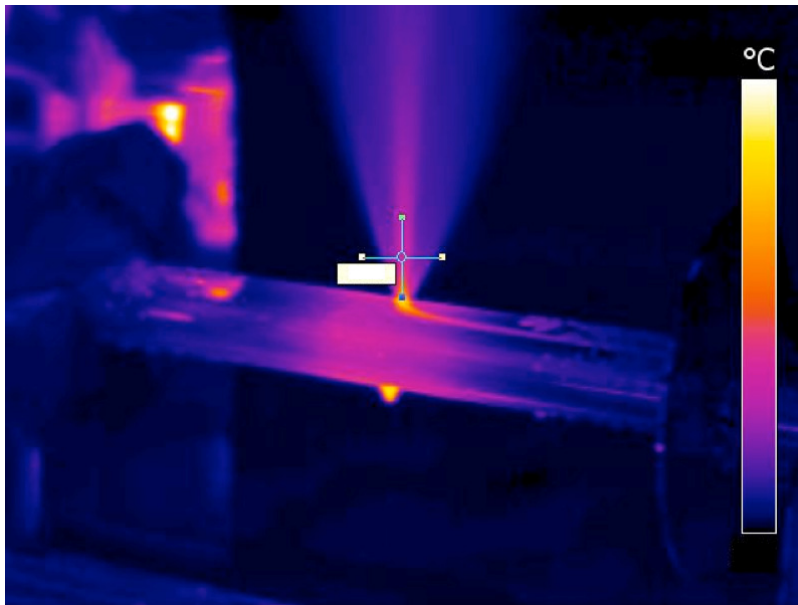
Figure 4.17 Thermal image of jet without pre-heated pipe

The solution to the problem is to use a cartridge heater, inserted into the hollow pipe, and heat the pipe up to 200ºC, as shown in Figure 4.18.

Figure 4.18 Cartridge heater components

Figure 4.18 shows the components before the cartridge heater was fitted into the pipe. A brass collar was machined to fit inside the stainless steel pipe and drilled out to accept the cartridge heater. A slot was also machined into the brass collar to allow a thermocouple to monitor the temperature on the outside of the brass. This thermocouple is used in a control loop to maintain the temperature at 200°C.

4.13 Pipe Selection

Pipe work connects all the components together and consequently the pipe wall thickness must be sufficient for the desired operating pressure. To add a degree of safety, the pipe work has been designed to withstand 1.5 times the maximum operating pressure, i.e. 210 bar. With this in mind, the entire construction is in stainless steel, as it is strong, anti-corrosive and used in the PWR.

When selecting a pipe for use in a high pressure system, it is essential that the pipe is correctly specified for the application. Consequently Equation 9, the hoop stress equation, is used to ensure the pipe wall thickness is adequate for the applied pressure. During the early phase of pipe selection, the hoop stress equation gives an approximate guide to the pipes applicability to the task. However, this equation is only designed for thin wall pipes. This criteria is met only if the internal diameter is

greater than 10 times the wall thickness (d > 10t), or can be re-written as radius divided by wall thickness (r / t) must be at least 5.

The calculations for the wall thickness were carried out using the hoop stress equation, Menon (2004). Whereby:

$$\sigma_h = \frac{P.D}{2t} = \sigma_m.E.F \quad \textbf{Equation 9, Barlows equation for Hoop Stress}$$

The known values are:

(P) Typical operating Pressure 10 MPa (100 bar)

(d) Internal diameter 5 mm (used in coiled pipe)

(E) Seam joint factor, 1.0 for seamless

(F) Design factor, 0.72 for water

(σ_m) Minimum design stress of material 210 MPa

(t) Wall thickness, to be calculated

(D) Outside diameter mm

Therefore, the hoop stress of the material is:

$$\sigma_{h(m)} = 210*1*0.72 = 151.5 \, \text{MPa}$$

Applying this value to equation 5, and re-arranging for t yields:

$$t = \frac{P.D}{2\sigma_h}$$

t = 0.211 mm @ 100 bar (for pipe 1)

Assuming a linear relationship between pressure and wall thickness, the wall would need to be greater then 0.43 mm to withstand the test certification pressure of 210 bar.

The final pipe selection consisted of the small 5 mm diameter pipe (used as the heated coil) having a wall thickness of 0.7 mm ($\sigma_{h(m)} = 342$ Mpa).

However, on closer inspection of the final pipe chosen, the ratio of radius to pipe wall thickness does not comply with the required diameter to thickness ratio. As mentioned earlier, the hoop stress equation is designed for thin walled pipes and consequently computes an average value of hoop stress through the wall. Whereas, using thick wall

theory, which is computed with Lamés equations, takes into account that the hoop and radial stresses are not constant through the wall. In contrast the highest levels are found on the inner and outer surfaces. Lamés equations (labelled as 10, 11, 12 and 13) are specifically designed for thick walled pipes. Figure 4.19, shows the three principal stresses on a section of pipe. The primary stresses in the design are the radial and hoop stress, the axial stress is normally applied to a cylinder that is closed at both ends, but because the carburetor jet is a large restrictor, the axial stress will also be calculated.
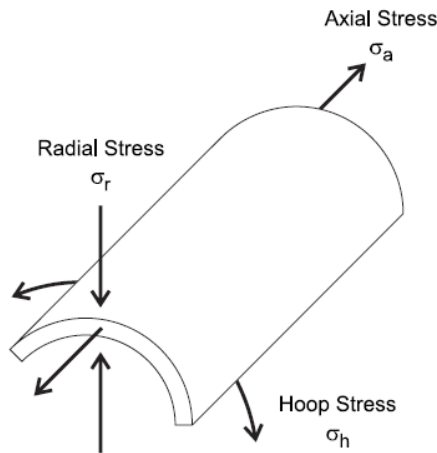
Figure 4.19 Three principal pipe stresses, Newman (2002)

Lamés equations are:

$$\sigma_r = A - \frac{B}{r^2} = -P_r \qquad\qquad \textbf{Equation 10, Radial Stress}$$

$$\sigma_h = A + \frac{B}{r^2} \qquad\qquad \textbf{Equation 11, Hoop Stress}$$

A and B are constants, and can be derived from

$$A = \sigma_a = \frac{P_{in} r_{in}^2 - P_{out} r_{out}^2}{r_{out}^2 - r_{in}^2} \qquad\qquad \textbf{Equation 12, Lamés constant A and Axial Stress}$$

$$B = \frac{r_{in}^2 r_{out}^2 (P_{in} - P_{out})}{r_{out}^2 - r_{in}^2} \qquad\qquad \textbf{Equation 13, Lamés constant B}$$

σ_a is the Axial stress, but is only used if the pipe has closed ends

r_{in} is the inner radius at pressure P_{in} and

r_{out} is the outer radius of the pipe at pressure P_{out}

r is the distance from the pipe centre line

Therefore, inserting the known values for the 5 mm diameter pipe into the equations, yields:

$$A = \frac{21*(2.5^2) - 0.1*(3.2^2)}{3.2^2 - 2.5^2} = 32.64 \text{ (the radius is shown in mm for simplification)}$$

$$B = \frac{2.5^2 * 3.2^2 (21 - 0.1)}{3.2^2 - 2.5^2} = 335.24$$

$$\sigma_h = 32.64 + \frac{335.24}{2.5^2} = 86.28 \text{ MPa is the Maximum hoop stress at 210 bar}$$

$$\sigma_r = 32.64 - \frac{335.24}{2.5^2} = -21 \text{MPa} \quad \text{therefore } P_r = 210 \text{ bar}$$

$$\sigma_a = A = 32.64 \text{ MPa}$$

The hoop stress is a positive figure because it is a tensile force, and the value decreases from the inside of the pipe to the outside. The radial stress is a negative figure because the force on the inside of the pipe is compressive and the value decays to zero as it reaches the outside surface. In summary, the calculated values for hoop stress using the two different techniques for the pipe are:

Pipe internal diameter	Using Hoop stress	Using Lamés for hoop stress	Maximum hoop stress for pipe
5 mm	75 MPa	86.28 MPa	342 MPa

Table 4.2 Hoop Stress for stainless steel pipes

Table 4.2, containing the calculated values for the 5mm diameter pipe can now be compared with the certified measured values from the manufacturer, which are:

Tensile strength 688 MPa

Elastic limit 322 MPa

A5, Ag Elongational fracture 45%

Hydrostatic test 340 bar

Distention test 520 bar

Now that the three pipe stresses have been calculated, Von Mises equation can be used to determine the yield point of steel, shown in Equation 14.

Using Von Mises equation, Newman (2002)

$$\sigma_{vm} = \left\{ \frac{1}{2}\left[(\sigma_h - \sigma_a)^2 + (\sigma_h - \sigma_r)^2 + (\sigma_a - \sigma_r)^2 \right] \right\}^{\frac{1}{2}} \qquad \textbf{Equation 14 Von Mises}$$

Now applying the 3 stress values calculated previously for the 5 mm pipe at 210 bar:

$$\sigma_{vm} = \left\{ \frac{1}{2}\left[(53.64)^2 + (107.28)^2 + (53.64)^2 \right] \right\}^{\frac{1}{2}} = 92.9 \text{ MPa}$$

The value for the elastic limit from the manufacturer was 322 Mpa, therefore this pipe is more than adequate for the range of pressures used.

It has now been proven that the pipe can withstand the pressure in the system, the next criteria is to determine whether it will impede the maximum flow from the pump.

The chosen pump is capable of flowing 6 l/m (0.1 l/s) at a pressure of 100 bar. Therefore, equating gives:

A flow of 0.1 l/s = 100×10^{-6} m^3/s

The pipe area = $(2.5 \times 10^{-3})^2 * \pi = 19.63 \times 10^{-6}$ m^2

Therefore, **velocity in pipe leaving pump** = $100 \times 10^{-6} / 19.63 \times 10^{-6} = 5.09$ m/s

The most important safety consideration is that the pressure relief valve can flow all the available water in the event of a problem in the system. Therefore, this small system is analysed below.

From the equation $P_1 = P_2 + \Delta Pf$

P_1 is the amount of pressure required by the pump to push the water through the pipe

P_2 is the pressure as the water returns to the reservoir, (atmospheric pressure is 1 bar)

ΔPf is the pressure due to friction in the pipe, this is calculated by:

$$\Delta Pf = f \frac{L}{D} \rho \frac{u^2}{2}$$

f = friction factor = 0.01

L = length of pipe = 1 m

D = Diameter of pipe = 0.005 m

ρ = Density of water = 10^3 kg/m^3

u = Velocity of water in pipe = 6.77 m/s

Therefore, computing yields a ΔPf of 0.5 bar.

Consequently, provided the pump can deliver more than 1.5 bar of pressure the pipe work will be capable of maintaining the flow.

4.14 Pressure Control

The pressure to the jet is controlled by a motorised needle valve, shown in Figure 4.20. This in turn has its control from the control centre, described in section 4.16.2, via a switch that allows the user to increase or decrease the pressure. During normal operation of the rig, the needle valve can pass up to 318 litres per hour. In order to avoid the user damaging the needle valve by driving it hard closed/open, an optical transistor circuit limits the maximum closure of the valve. This is achieved by a swing arm on the back of the valve moving inward and outward as the valve opens and closes. The optical switches are set to stop the valve one turn from its maximum open or closed position to avoid damaging the valve. This switch is also vitally important as the motor does not stop immediately when the user depresses the switch, but continues for another quarter of a turn.
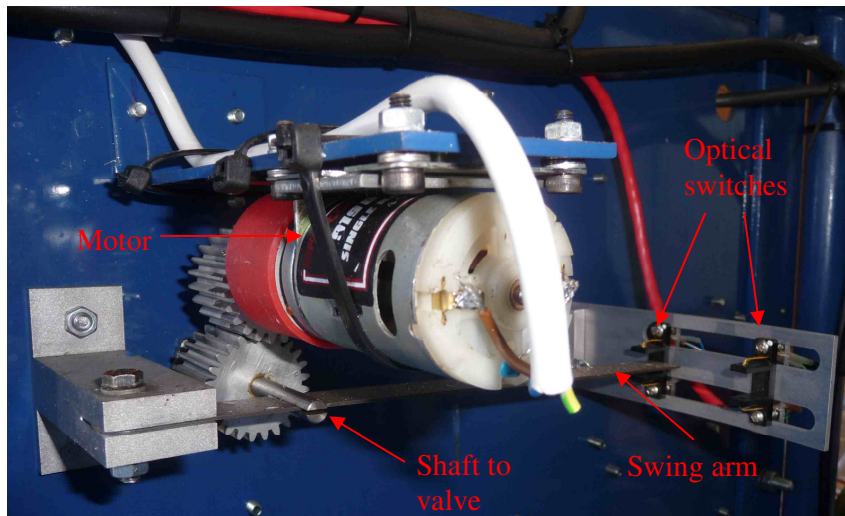
Figure 4.20 Motorised needle valve and optical transistor

4.15 Electrical Safety

Due to the fact that there is potentially 280 Amps (at a maximum of 45 Volts) passing through certain parts of the rig, it is very important that other parts are isolated to prevent any chance of electrocution should an individual touch the rig.

Figure 4.21, shows some of the electrical isolating devices. The water pipe supports are mounted on a support rail and attached to the water pipe via a high temperature rubber. There is also a dielectric isolator that prevents any of the DC current passing back along the water pipe. These two electrical isolation devices prevent the current finding another route to ground, which could result in very little current flowing through the coiled section of tube. As the diagram also shows, there is a metal shield around the coil to stop individuals touching the coil, as it reaches 200˚C, but also to minimise any danger should the coiled pipe break. After this picture was taken the coiled pipe was lagged to minimise heat loss.
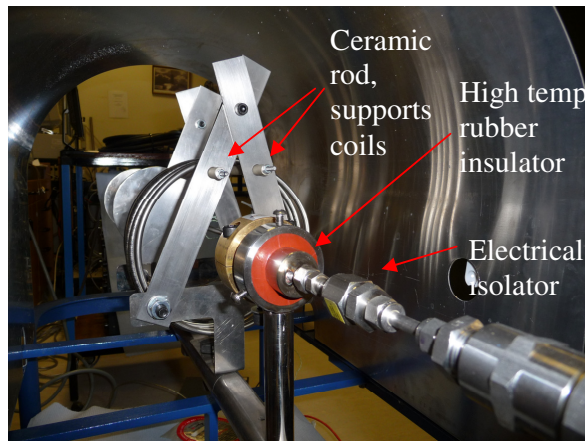
Figure 4.21 High temperature rubber insulator supporting water pipe

To further maintain a level of safety, rubber supports have been added between the upper half of the rig and the rig frame, as shown in Figure 4.22.
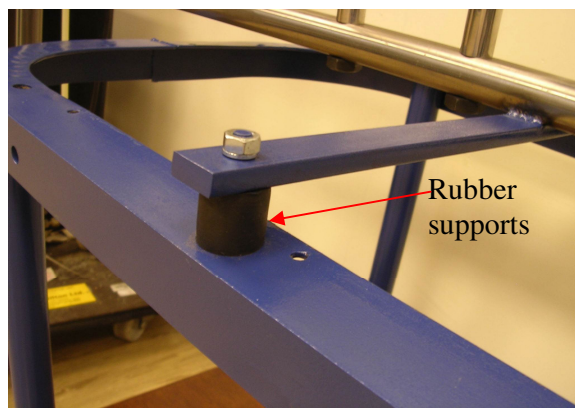
Figure 4.22 Rubber supports

4.16 Instrumentation and Control

Due to the dangerously high temperatures and pressures on the rig, being able to control and monitor these parameters is extremely important. The following two sections describe the mechanical and electrical system.

4.16.1 Mechanical System

With reference to Figure 4.23 and Figure 4.24, it can be seen that the rig is fitted with a number of pressure gauges and a pressure relief valve. The pressure gauge on the accumulator informs any users of the pressure being maintained. An isolation valve can also be used to isolate the accumulator should other users wish to use the rig for a low pressure application. The pressure gauge will indicate to the user that the accumulator is still at pressure, but the valve will keep it out of circuit.

The pressure relief valve is a safety device designed to open in the event of over pressurisation of the rig. It has a screw that has been professionally set at 150 bar, to potentially allow pressures up to this value, but release any pressure above this value, should a fault occur in the system. The analogue and digital pressure gauges must agree, so that the operator is confident of the rig's operating pressure.
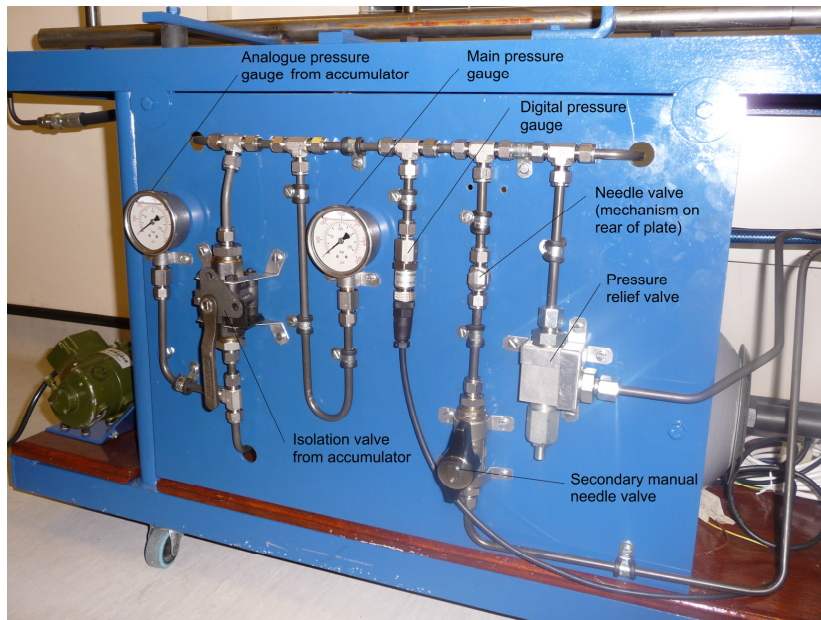
Figure 4.23 Analogue display panel

4.16.2 Electrical System

The control centre allows the user to set the following operating conditions:

- Pressure
- Water temperature
    - Temperature on heated coil
    - Temperature on cartridge heaters
- Maintain correct temperature on orifice pipe heater.

It also has safety switches to turn off the water pump and heated coil, should an emergency occur.

There are five separate displays, four for monitoring different temperatures around the rig and one digital pressure gauge. A laptop, usually located to the right of the control centre, monitors and records the data from the sensors mounted on the rig.
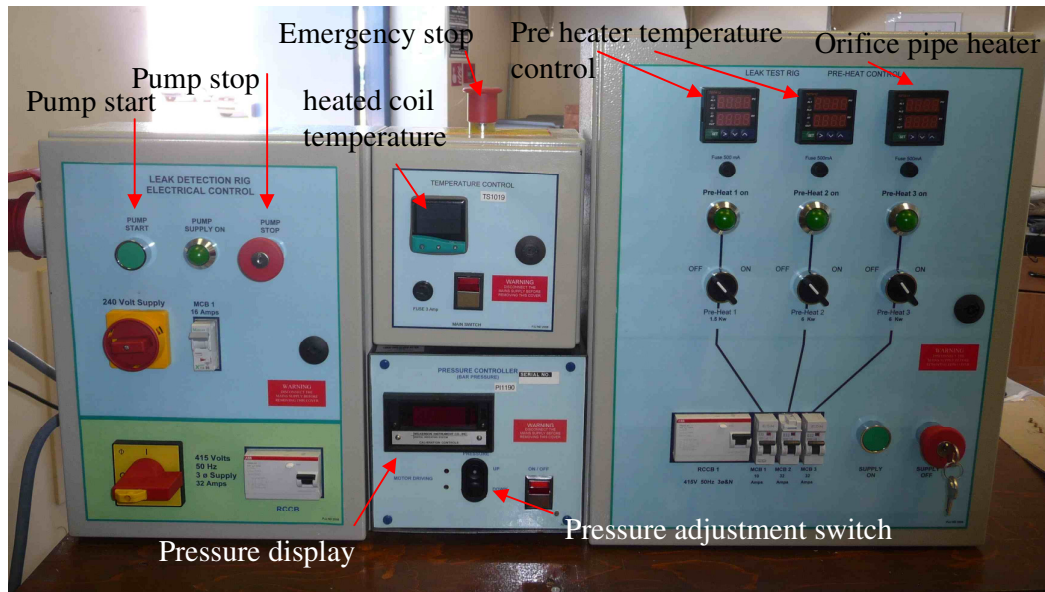
Figure 4.24 Control centre

4.17 Complete System

The rig schematic shown in Figure 4.25, illustrates the complete flow of water from the water pump through to the steam leak. The water pump starts to build up the water pressure, the accumulator then attempts to stabilise that pressure to 100 bar, which is confirmed by an analogue pressure gauge. Under normal operation the accumulator should always be used, as it allows the pressure to build slowly, but it can be disconnected by a valve, if the rig is going to be used for a different application, e.g. low pressure testing with the 2 bar pump.
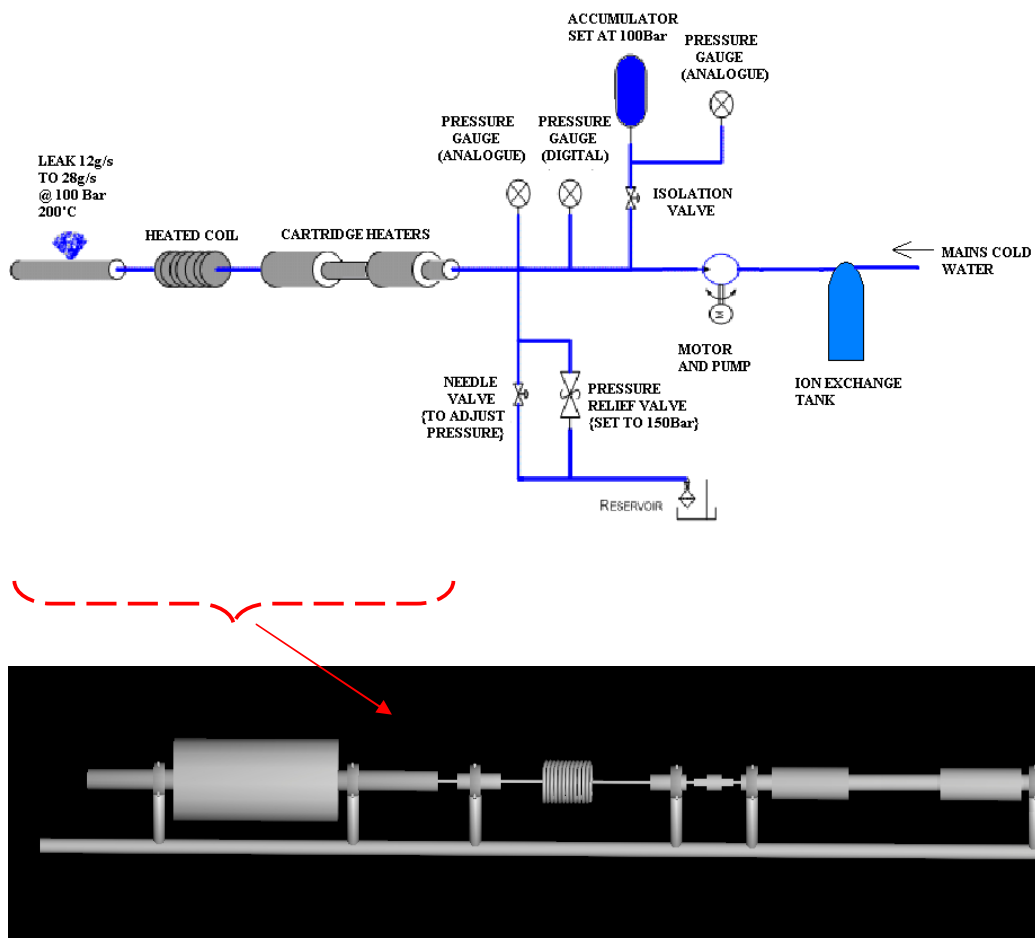
Figure 4.25 Schematic diagram of Rig

The pressure in the system is fundamentally set up using the needle valve, as this will determine the amount of flow returning back to the reservoir and consequently the pressure built up in the system. This pressure is monitored by two analogue and one

digital gauge. This firstly allows the two analogue pressure sensors to validate each other. In addition, the digital pressure gauge enables its pressure to be observed at a safe working distance from the rig. A safety release valve ensures that should the system over pressurise, i.e. above 150 bar, the water will return to the reservoir. The cartridge heaters, heated coil and orifice have all been described above.

4.18 Validation and Compromises of Rig

The rig attempts to replicate a leak from the primary circuit of a PWR. However, there are certain design limitations that could not be overcome. Because the tests are performed outdoors, the ambient temperature surrounding the lagging is considerably lower than would be expected in the RC. The following chapter discusses the results from the rig, and during the data acquisition phase the ambient temperature was about 5°C, whereas the ambient temperature in the RC is over 60°C. Despite this, when the entire rig is given sufficient time to stabilise, it is observed that the outer temperature of the lagging reaches the typical RC ambient temperature. Considerable thought was given to enclosing the entire rig in a fixed enclosure, but a small area would not be representative of the typical size of the RC. In addition, being able to view the rig and remove the lagging and jets as required would be impeded. Heating the ambient air in a larger environment was also considered, but the heating costs would be enormous and the rig already consumes over 20 kW of power just for heating the water. Therefore, these ideas were dismissed.

The pressure that is delivered from the orifice is validated by two analogue gauges and one digital gauge. These should all agree with each other, and as the gauges were brand new and calibrated by the manufacturer, the pressure was deemed accurate. The water temperature exiting the rig was monitored by a single thermocouple, mounted 50 mm away from the orifice. However, during the commissioning phase of the build, a second thermocouple was mounted adjacent to the fixed thermocouple. This was monitored by a portable meter in order to add confidence, that the fixed thermocouple was recording a temperature in agreement with the temporary thermocouple. Despite the fixed thermocouple being close to the exit point, the orifice is mounted in a potentially cold piece of solid stainless steel. Therefore, to prevent any loss of heat in this section of pipe, the orifice is heated by a cartridge heater as

described in section 4.12, thus ensuring the water maintains its 200˚C at the point it exits from the rig.

4.19 Rig Certification

Due to the high temperatures and pressures the rig is capable of achieving, it was deemed essential to have the rig design and construction certified by external third party experts. By obtaining certification, any operator using the rig has the assurance that the pipes have been tested to the maximum operating pressure of the rig and the heaters are capable of heating to the specified level. Also, from a Health and Safety (H&S) perspective, it shows a level of competence both in the design, construction and operation of the rig

Prior to the external examination of the rig, an internal review was carried out in the department to scrutinize the design mathematically and functionally. Dr Paul Chard-Tuckey was appointed the position of Lead Engineer for the rig as he has extensive knowledge of structural integrity.

A Risk Assessment document was also produced for the rig. This classifies the level of potential danger to any individual working in close proximity to it. This report also makes provisions for barriers/containment to comply with H&S.

A secondary report was also created. This outlined the procedure for safely starting up the rig, and ensures a new operator could not make any dangerous mistakes. For example the sequence of starting the water pumps, the delay required before switching on the DC generator, as well as pressure levels and valve settings, for normal operation.

When the third party experts came to certify the rig, part of the requirements were to prove the system could maintain a pressure of 210 bar for 30 minutes. (210 bar is 1.5 times maximum rig pressure). In order to prove this, a hand pumped air device was attached to the rig and the pressure slowly increased to 210 bar. If the pressure dropped by more than 1 bar during that period, the pressurised system would fail. During pressure testing, multiple leaks were found in the welds on the reservoir. They were tiny pin prick holes in the welding which provided an exit route for the air. Therefore the test was deemed a fail and the conclusion was to remove this section of pipe, and at a future date re-validate with a new section of pipe that was constructed

with threaded pipe sections. Other comments for remedial action were made, and these included:

- A protective shield was required around the heated section for H&S
- Jubilee clips on low pressure water pipes needed to be replaced for crimped items
- The accumulator in use was oil based and would need exchanging for a water type
- The two analogue pressure gauges were also out of calibration.

Following the correction of the above items, the rig was retested. This time it passed all of the hydraulic pressure tests and a plume of water was observed leaving the orifice. The subsequent test involved applying heat to the water and by slowly increasing the electrical current to the heater section, steam was observed at the jet as shown in Figure 4.26. Therefore the test was seen as a pass and the rig was safe for use.

Figure 4.26 Rig in use

4.20 Summary

This chapter has discussed the design of a rig capable of achieving high temperatures and high pressures. Initially the concept was outlined and then the requirements and architecture were discussed. A more detailed design was then carried out, and calculations were performed to determine: the material and thickness required for the pipe work, water pump, heating source and suitability of the jets for this application. Other components were detailed before being integrated into the complete rig. The system was then certified by a third party expert and signed off for use.

Chapter 5
Candidate Sensor Systems

This chapter will investigate a large array of possible solutions for measuring the evidence of a high pressure and temperature water leak. A preliminary set of sensors will be refined through experimentation or other limiting factors. The final set of sensors will be discussed at the end of this chapter along with their respective results.

The intention is to analyse data from the sensors before and after a leak, and thus establish a threshold over which a leak occurs. At this stage the assumption is that some sensors will show a clear distinction between the two states, whilst others will need more sophisticated approaches, such as complex non-linear analysis. This study differs from others discussed in the literature review, because multiple sensors are used in collaborative mode as a means of detecting the existence of a leak. One of the ambitious targets is to determine the size of the leak, this is particularly challenging as the 13 leak sizes available in the rig are only separated by 1.4 g/s (5litre/hour).

The choice of sensors have been determined by a number of criteria:

1. Suitability to the task
2. Susceptibility to neutrons, gamma and all the reactor radiation
3. Simplicity in design
4. Ease of use, including calibration
5. Type of cabling, electrical signalling, air/fluid transfer required
6. Cost
7. Degree of pre and post processing required
8. Robustness
9. Size
10. Readily available, (as opposed to specified design).

Using these criteria, the following list illustrates the range of parameters and the means by which they can be measured.

- Temperature using thermocouples, at the following positions:
    - Water in pipe before reaching orifice
    - Pipe work surrounding orifice
    - Steam plume leaving orifice
    - Outer surface of Metlag
- Humidity level surrounding the orifice using a humidity sensor
- Air pressure and air flow speed using pitot static tube or air mass meter or deflected strain gauge
- Acoustic noise emitted by steam leaving the Metlag chimney using a microphone
- Oscillations and vibrations using accelerometers, positioned on:
    - The pipe containing the leak
    - The Metlag
- Strain/stress on lagging bracket using strain gauges
- Exit temperatures from Metlag and obvious signs of a leak using thermal camera
- All visual and audio activities that occur during the running of the rig with a CCTV camera.

These devices are all shown in Figure 5.2. The thermal and CCTV camera will not be used as inputs to a leak detection system, as they would be unsuitable for the environment of the RC, but their contribution will add extra detail to the investigation, and further insight into the dispersion of the steam.

The design of the lagging area is such that the steam is encouraged, like a chimney in a house, to exit via the hole indicated by the red arrow in Figure 5.1. Immediately above this hole, a pressure monitoring device will be mounted to measure the pressure and velocity of the steam.
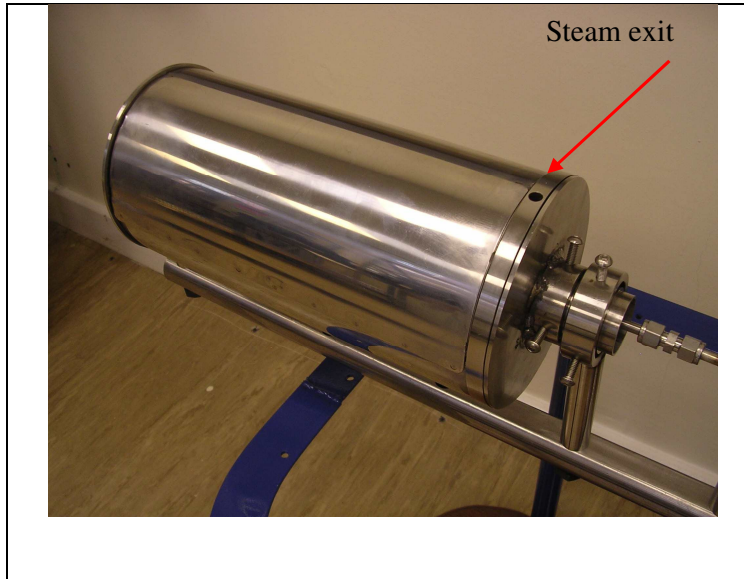
Figure 5.1 Orifice for steam to exit
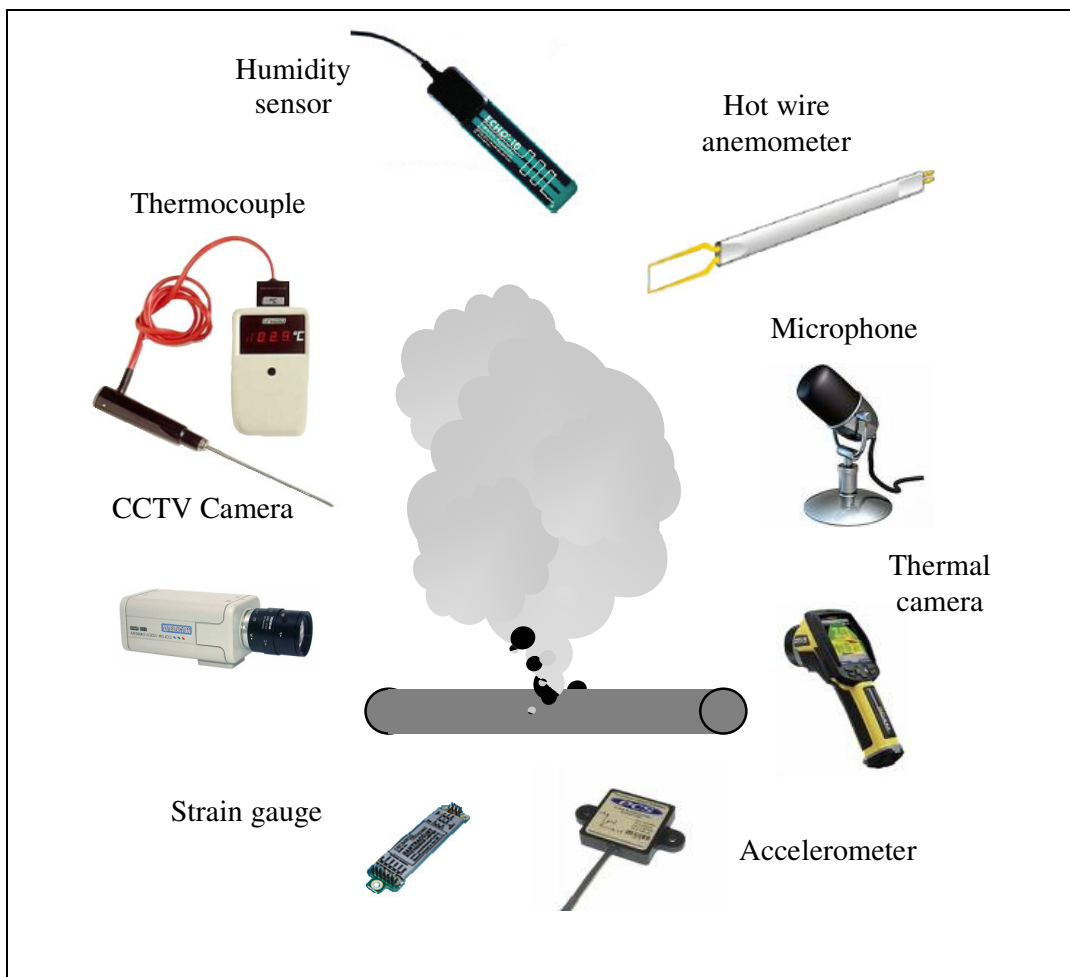
Figure 5.2 Potential measurement devices

All the sensors in Figure 5.2 (excluding CCTV camera and thermal camera) will be logged onto a data acquisition device, as explained in the following chapter.

The following sections describe all the sensors considered as appropriate for this application. A number of them will be trialled and a brief evaluation of their suitability to the task discussed.

5.1 Background Acoustic Noise

In order to prevent the implemented system giving false alarms during acoustic and vibration monitoring, it is very important to have a measured background noise characteristic of the Reactor Compartment. One realistic method to acquire these data is to place microphones and accelerometers at strategic locations around the reactor at the Vulcan Shore Test Facility, at Dounreay. However, obtaining a noise signature of an RC will always be controversial due to the security aspects of recording such data. Therefore, rather than measuring a real RC, if it is understood which elements make up the significant noise sources then an attempt can be made to reproduce them by other means.

Following a visit to a working RC, it was observed that the noisiest items were the axial flow fans that blow air around the RC and the Air Treatment Unit (ATU) which provides the effective air conditioning/cooling for the RC. This was at such a level that individuals needed to raise their voices to be heard, when stood immediately adjacent to the fan.

During the visit the reactor was inactive, consequently the rods where fully down. It is understood that the rods do contribute a very small amount of noise and vibration during their normal function which entails movement up and down on an almost minute by minute basis. The rods ensure a steady average temperature, but are not overtly noisy unless scrammed in an emergency, but this is a very rare occurrence. Another infrequent noise source is when the non-return valve in the primary circuit closes quickly. However, this would only occur when the reactor power is abruptly dropped from full power. Both of these occurrences are so infrequent that they can be discounted as a typical background noise element.

The motors in the RC are very quiet, so would only provide a low background noise contribution. The pressuriser is water sprayed several times an hour to maintain a stable pressure; this can be noisy as the water is under high pressure.

Consequently, in order to obtain the best approximation of the background noise, a recording of an axial fan is required from a non-secure facility. A potential problem could be when the water sprayer is operating in the pressuriser, as the system may misinterpret this erroneous sound as a leak, therefore providing a signal to the OAS of this occurrence, would help alleviate any false alarms.

The following sections describe a possible array of sensors to measure a leak. Some of the sensors are dismissed at the preliminary stage either due to cost, robustness, suitability to environment, but are included to demonstrate an understanding of other methods used in the industry.

5.2 Steam Velocity and Pressure

The net result of a leak from a high pressure and temperature water pipe is the production of steam. A variety of methods exists to measure the energy in the steam, some of the more common are:

- Cup anemometer using a propeller or turbine wheel
- Pitot Static tube
- Hot wire anemometer
- Doppler Lidar
- Sonic anemometer
- Deflecting strain gauge
- Air flow meter.

Each of the above methods is addressed, with regard to its design, suitability to this application and reason for its omission or use in this project. It is anticipated that having the facility to measure steam velocity and pressure will enable the system to diagnose different size leaks, as the steam velocity and pressure will increase with a larger leak, as discussed in sections 5.2.1 to 5.2.7

5.2.1 Cup Anemometer

Cup anemometers are commonly used for measuring wind speed. Typically they consist of three or four hollow cups and the variation of drag on each of the cups provides the torque for the rotational movement. This can be better illustrated in Figure 5.3 below.
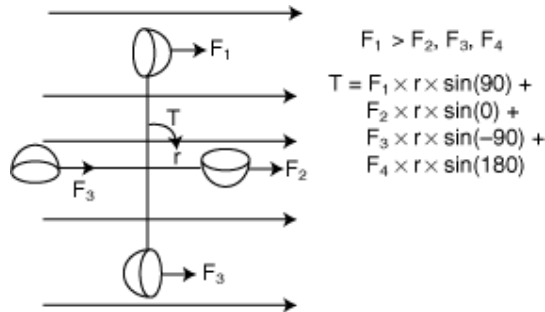
Figure 5.3 Cup anemometer (diagram courtesy of Circuit Cellar 2006)

However, this method has not been adopted for this application because:

- Detailed investigation is needed to determine the size of the cups for the force of steam being applied, otherwise it may not rotate under low velocity steam
- Moving parts
- Bulky in design
- Potentially noisy in use
- Not scaleable for this application.

5.2.2 Pitot Static Tube

The Pitot static tube is commonly used on aircraft to measure their velocity. It works by measuring and subtracting two pressures, the ambient static pressure and the dynamic pressure of the incoming wind. In order to measure the wind/steam speed, the pitot tube must be pointed directly into the wind flow. It is possible to have the pitot tube mounted several metres away from the micromanometer, used to calculate the wind speed. This is because irrespective of the length of tube the pressures in the pipes will not be affected. This is therefore ideal for remote monitoring and appears an ideal choice for this project. Also, because the design contains no moving parts and

is very basic in construction there is a low risk of failure. In order to procure the correct pitot static sensor, it is necessary to calculate the expected pressure from the orifice.

The calculation uses three pressures:

(P1) Water pressure = 100 bar

(P2) Steam pressure

(P3) Ambient pressure = 1 bar
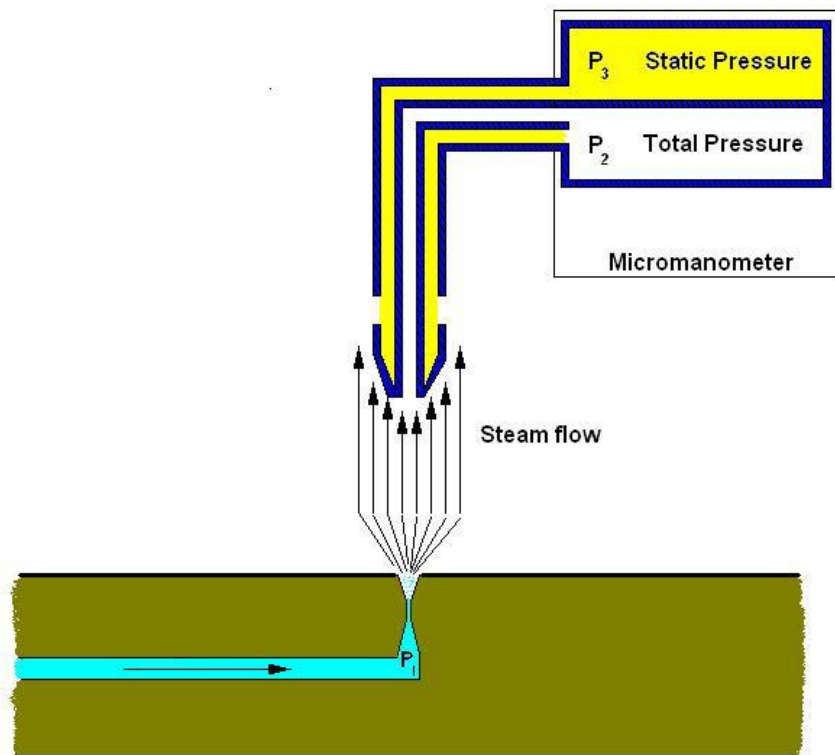
Figure 5.4 Pitot static tube with Micromanometer

$$P_1 + \frac{\rho V_2^2}{2} = P_2 + \frac{\rho V_2^2}{2}$$

When $V_2 = 0$ and $P_3 = P_1$

$$\frac{\rho V_1^2}{2} = (P_2 - P_1)$$

$$V_1 = \sqrt{\frac{2(P_2 - P_1)}{\rho}}$$

(ρ) Density of steam (or mixture)

If $\rho = 1$ kg/m^3, $V_1 \approx 10$ m/s

$$(P_2 - P_1) = \frac{\rho V_1^2}{2} = \frac{1 x 100}{2} = 50 N / m^2$$

$$(P_2 - P_1) \text{ in bar} = \frac{50}{10^5} = 5 \times 10^{-4} bar$$

The pressure drop is quite considerable. By performing an experiment with a pitot static tube immediately above the orifice, the theoretical pressure calculated above, can be compared to the measured.

5.2.3 Hot Wire Anemometer

The hot wire anemometer is typically used in the automotive industry for measuring air flow. With this information the engine calibrates the correct amount of fuel for the respective amount of air. The principle is very simple: a platinum wire (typically) is connected into an electrical circuit, the current (I) passing in the wire causes a heating effect, the cooler air passing across it causes the electrical resistance of the wire (R) to change and by understanding the relationship between resistance and air flow the system can be calibrated. For the project application, the actual air flow as a calibrated measurement is unimportant, it is the respective difference between a small and large leak that is key.

The basic mechanism for the design is shown in Figure 5.5.
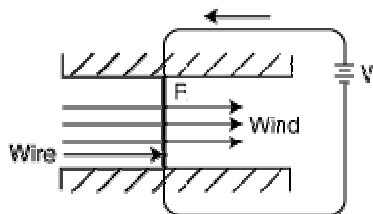
Figure 5.5 Hot wire anemometer (diagram courtesy of Circuit Cellar 2006)

This design has a number of advantages, these being, it is:

- Simple in design
- Easy to implement
- Physically small
- Scaleable, for multiple locations
- Without any moving parts.

Therefore, this method will be trialled. The hot wire anemometer intended for the project was sourced from a Ford Fiesta, as it was cheap, easily available, already mounted in a holder and should be robust.

5.2.4   Doppler Lidar

Doppler Lidar is a similar technique used by Police radar guns to measure the speed of oncoming vehicles. A laser beam is projected toward a moving object and on contact a small proportion of the original signal is reflected back to the transceiver device, but with a new frequency. By using the equation below, the target echo frequency can be calculated.

$$f_t = f_0 \pm \frac{2V_t f_0}{c}$$

f_t = target echo frequency

f_0 = radar transmit frequency

V_t = Velocity of target

c = speed of sound

If this equation is re-arranged the velocity of the target can be found.

However, the Doppler lidar principle differs slightly because the transmitted laser beam is designed to come into contact with aerosols or water. Reflections from steam and this type of medium will inherently be weaker, requiring a high specification transceiver; in particular it would need a stronger transmitter and a receiver with very high sensitivity.

Due to the extra complexity of using lasers and the associated electronics that would be required, this method will not be used.

5.2.5   Sonic Anemometer

This type of anemometer is used by weather stations and weather buoys to record wind speed and direction. This is achieved by transmitting ultrasonic sound waves from one transducer to another at a fixed distance away, typically 10 to 20cm. The speed of the prevailing wind is then added or subtracted from the ultrasonic frequency depending upon its direction. This is shown in Figure 5.6.
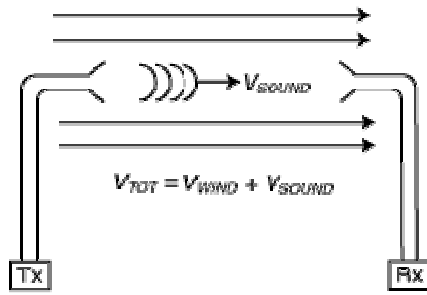
Figure 5.6 Sonic anemometer (diagram courtesy of Circuit Cellar 2006)

Even though the diagram only shows one set of transducers, by increasing the number to three and having them orientated orthogonally to each other, allows for 3-dimensional flow including turbulence to be measured.

The advantage of this system is the lack of moving parts, but also its ability to measure two parameters with effectively only one device. The design however has a flaw, this is because the wind flow is slightly affected by the physical transducers. With regard to this project the limitations are its physical size, the processing required to determine the steam speed and direction, but more importantly adding a new sound source to a sensitive environment is not acceptable.

5.2.6 Deflecting Strain Gauge

This concept was a unique approach, and so was totally experimental. Strain gauges are typically used for measuring relative motion, whether it is compression, elongation or shear. The idea was hoping to draw a relationship between pressure and deflection. It was also anticipated that there may be an oscillation associated with the different pressures, which may in turn be associated with the thicknesses and material, on which the gauges are attached. This design created for this project uses a 300 mm length of spring steel, with a thickness of 0.5 mm and width of 10 mm. The steel can take a significant deflection without distorting. This property is very important, because if the elastic limit is reached it will not behave as it did previously. The length of steel has a circular plate attached to the end, which is designed to be placed over the open steam leak. In order to measure the deflection, a full strain gauge bridge is used.

5.2.7 Air Flow Meter

The motivation behind this device was from the old type of air flow meter used by cars in the 1980s, also known as flappers. Its purpose is to measure air flow and with this knowledge, inject the correct amount of fuel. It works by the air pushing a metal flap which has a potentiometer at the pivot point, and a spring to return the flap to the closed position at idle. There is a correlation between the voltage produced by the deflection of the vane and the air flow.

5.3 Sound

Microphones are commonly used to convert sounds into electrical signals. Sound energy causes a thin membrane to vibrate rather like the human ear drum but rather than stimulating hair cells that become neurotransmitters when stimulated, the membrane excites a transducer. Not all microphones use the same type of transducer, the most common types are condenser/electrostatic, dynamic or piezoelectric. The microphone used in this report is a condensing type that requires an excitation voltage.

There is an expectation that sound will be a combination of various elements, these are as follows. On an open vented leak, the steam will produce a sound on exiting the orifice and also some resonance in the pipe; whereas on the lagged system a sound will be produced as the steam exits the chimney orifice, and the lagging vibrates with the high pressure steam deflecting off its underside.

5.4 Temperature

Thermocouples are widely used in everyday life, from monitoring the temperature in ovens to switching on the fans in a computer to prevent it over heating. The principle is that when two dissimilar metals are combined at a junction, a potential will be developed which is in relation to the temperature difference. By always using specific alloys in combination, repeatable temperatures can be recorded. This combination of alloys is known as the type of thermocouple and there are about 15 different types. The type used in this project is the K-type, as it is commonly available, inexpensive and has a good temperature range from -200˚C to +1350˚C.

Thermocouples are used for two applications; the first is to measure the temperature of the lagging, while the second is to measure the steam temperature. Two thermocouples are attached to the lagging, one in the centre of the lagging and the second 150mm away, at the end of the lagging. The other thermocouple is enclosed in the chimney with a sealed lid to prevent the steam from exiting. This ensures the outside ambient air temperature does not affect the measurement as the ambient air during these tests is considerably lower than a typical RC.

5.5 Humidity

There are two main types of electronic humidity sensors; resistive and capacitive. The resistive type detects the change in conductance on a polymer membrane due to the moisture in the air. The capacitive type uses two plates, and by applying an alternating current between them, it is possible to correlate the change in capacitance to the amount of water present. The humidity sensor used in this project uses a thermoset polymer capacitive sensing element. Even though this sensor uses a 5V supply, it has an on-chip integrated signal conditioning unit to charge the plates and output a DC voltage.

A first order fit for sensor relative humidity, with no temperature compensation is given by:

$$SensorRH = \frac{1}{0.0062}\left(\frac{V_{out}}{V_{sup\,ply}} - 0.16\right)$$

Equation 15 Relative Humidity

Allowing for temperature compensation:

$$SensorRH = \frac{V_{out} - (0.9237 - 0.0041T + 0.000040T^2)}{(0.0305 + 0.000044T - 0.0000011T^2)}$$

Where T is temperature in ˚C

Equation 16 Relative Humidity with temperature compensation

Equations 15 and 16 could be applied to the humidity output data, in order to gain an understanding of the relative humidity present. These equations are taken from the Honeywell HIH-4000 series data sheet.

5.6   Pipe Vibration

There are two fundamental vibrations expected with a leak, one is the vibration occurring on the pipe and the second is associated with the lagging material. The lagging used in the PWR is described in section 4.11. Owing to the nature of its design, the internal layers will vibrate when tapped or when bombarded with hot steam. However, the rig has its own resonances, predominantly caused by the water pump, and these vibrations cause further resonances on the face plate containing all the pressure dials, valves and the heated coil. Consequently, the wanted vibrations are only evident when the test rig pump is switched off and pressure is maintained by the accumulator. This period is marked during data collection with a trigger signal. Below are two contrasting methods of measuring vibrations on the surface of a material.

5.6.1   Laser Holography

The automotive industry has been using laser holography for over 10 years to study the vibrations on the surface of materials. The technique enables resonances on car panels to be discovered and potentially dangerous vibrations on engine components to be identified. The advantages to this system are its remoteness from the component/panel in question and ease of detection. The foreseen issues with using this system for this application are the cost of the device, and the effect of the neutron environment on the electronics within the device. For these reasons it was excluded from the trial.

5.6.2   Accelerometer

Accelerometers are used in a wide variety of functions ranging from monitoring pumps in hospitals, recording loads on bridges to determining acceleration and deceleration of a motor vehicle. An accelerometer is a piezoelectric device, typically made from either quartz crystal or ceramic. A quartz device offers a sensitivity that will not degrade over time; however it has a lower piezoelectric constant than ceramic

material. Ceramic devices offer better sensitivity at a cheaper price, but their sensitivity does not have the longevity of quartz.

Regardless of the material used, their operation is the same. The device consists of a metal shell with a seismic mass attached to the piezoelectric material. When a bending or compressive force is applied to the device, an electrostatic voltage is generated by the piezoelectric material. The voltage varies in accordance to the varying force in accordance with Newton's second law of motion, i.e. F=ma.

Accelerometers are placed at three strategic points around the leak. One is on the pipe 200 mm from the leak. This measures the resonances on the pipe caused by the exiting steam. The effect of having an open leak and lagged leak can be compared with this sensor. Two accelerometers are attached to the lagging one is immediately above the leak and the other is 150 mm away from the leak. Using the data from this sensor and the one immediately above the leak shows how distance affects the signal.

5.6.3 Other Sensors Considered

Fibre optics was also considered but due to the high neutron levels around the reactor and the potential damage to the cable, this was rejected. This same effect applies to all electronic equipment, as the neutrons damage the p-n junctions of the semiconductors. Therefore, other devices that may have been useful like a thermal camera were also discarded. A video camera was also contemplated, but considerations such as moisture in the air, limited field of view due the maze of pipes, damage to electronics and inaccuracy in minor fault detection, meant that it was abandoned.

5.6.4 Summary of Sensors

This chapter has reviewed a large amount of sensors. Due to time and cost limitations this list needs reducing to a more manageable size. Therefore, a summary of each sensor is given in Table 5.1 below.

Sensor	Function	Accepted/Rejected	Reason for rejection
Cup anemometer	Wind speed	Rejected	Too bulky & noisy
Pitot static tube	Air velocity	Accepted	
Hot wire anemometer	Air flow	Accepted	

Doppler lidar	Velocity of moving objects	Rejected	Too much electronics for a high neutron environment
Sonic anemometer	Wind speed and direction	Rejected	Addition of new signals and complexity
Deflecting strain gauge	Air pressure/velocity	Accepted	
Air flow meter	Air flow meter	Accepted	
Microphone	Sound meter	Accepted	
Thermocouple	Temperature	Accepted	
Humidity	Moisture content in air	Accepted	
Accelerometer	Vibration	Accepted	
Laser holography	Vibration	Rejected	Cost and too much electronics

Table 5.1 Preliminary sensor selection

5.7   Summary

This chapter has involved researching sensors that could be used for monitoring a steam leak. Initially, the search covered a very broad depth of sensors that had not necessarily been applied to this application. However, this initial array of sensors was reduced either because it would not fulfil all the requirements or because or it had performed badly during trials. The following chapter evaluates the final group of sensors selected, by testing them on the rig.

Chapter 6
Data Acquisition

All the sensors discussed in Chapter 5, have their respective data collected by a data acquisition device. The chosen device was a National Instruments CompactRIO™ cRIO-9024. This is a real time embedded controller on a CompactRIO™ chassis. The controller attaches to a reconfigurable embedded chassis that is designed to accommodate either four or eight unique modules. A specification for this device is available at National Instruments (2009c). Figure 6.1 shows the controller on the left with eight unique modules in the chassis. Each module is designed for a specific input or sensor. Inputs could be analogue or digital, and modules can be specifically designed for sensors; such as a strain gauge would require a Wheatstone bridge configuration to produce a meaningful output. Therefore, for this project six modules were purchased, the first four are specifically designed for their respective sensors and the last two are for future modifications to the rig. In particular the facility to have a closed loop pressure control system that takes feedback from a digital pressure sensor and controls a stepper motor to maintain a constant pressure in the system. At present the operator has to make small adjustments to a valve to maintain even pressure. The modules fitted for this project where:

1. N9211 – thermocouple
2. N9234 – Accelerometer and microphone
3. N9237 – Strain gauge
4. N9201 – Humidity, pressure, trigger voltage inputs up to 5 volts
5. N9474 –
6. N9263 –

Figure 6.1 CompactRIO™ with 8 module chassis (picture courtesy of National Instruments (2009a)

6.1.1 Data Pre-processing in Labview

The National Instruments CompactRIO™ (cRIO™) needed a considerable amount of programming in order to produce a data file with the correct format, order, scaling and size. The software used to program the cRIO™ is called Labview, a programming language designed by National Instruments (NI). Originally programs were written by writing large sections of code, but programming is now accomplished by using a graphical user interface. Despite this, creating a program to acquire data from the sensors at the required data rate and logging it to a file took nearly three months with extensive assistance from the NI technical support team. One of the main reasons for all the difficulties was because the cRIO™ had only just been released and therefore bugs were still apparent in the software. The cRIO™ offers the option of running in two modes: one is called 'Scan mode' which entails pulling the sensor information directly from the module at a default sampling speed of 1 kS/s. While the other uses a fully programmable gate array (FPGA) that resides in the cRIO™ controller, and offers the ability to sample at far higher speeds up to 51kS/s, called 'FPGA mode'. Consequently, the accelerometer/microphone module was set to run at 51 kS/s in FPGA mode. By sampling at this speed a large amount of data were captured, but more importantly a frequency resolution of 25 kHz is achievable for each sensor. As both devices are capable of measuring up to this frequency it was deemed important not to lose any potential information.

Therefore, the following sensors were run in Scan mode at 1 kS/s:

- Humidity sensor
- Thermocouple
- Strain gauges
- Pressure sensor.

The following sensors ran in FPGA mode at 51 kS/s:

- Microphone
- Accelerometer.

In order to avoid processing enormous files, the FPGA files were limited to a capacity of 20MB each. The other input captured was the trigger signal, which was associated with the scan mode inputs.

A good understanding of the cRIO™ architecture is required because Labview software must be written both for the users Windows Personal Computer (PC) and cRIO™ controller. Figure 6.2 shows two blocks defined by a blue and red border, the blue block indicates the software running on the cRIO™ whereas the red block shows software running on the Windows PC. When the software was produced for these blocks, the blue block was labelled as 'RT Host Scan' for the real time processing of data on the cRIO™, and the red block 'Windows front end' for the PC data. When the system is initiated to start recording data, the RT Host scan is started first, followed by the Windows front end. Both sets of data are able to be monitored on the windows PC.

The cRIO™ and laptop are connected via an Ethernet cable. This enables two way communications but also gives the potential for the two devices to be physically in two separate rooms or buildings. The cRIO™ also has the capability to be ganged to other cRIOs™ giving the system enormous potential to monitor an entire reactor plant.
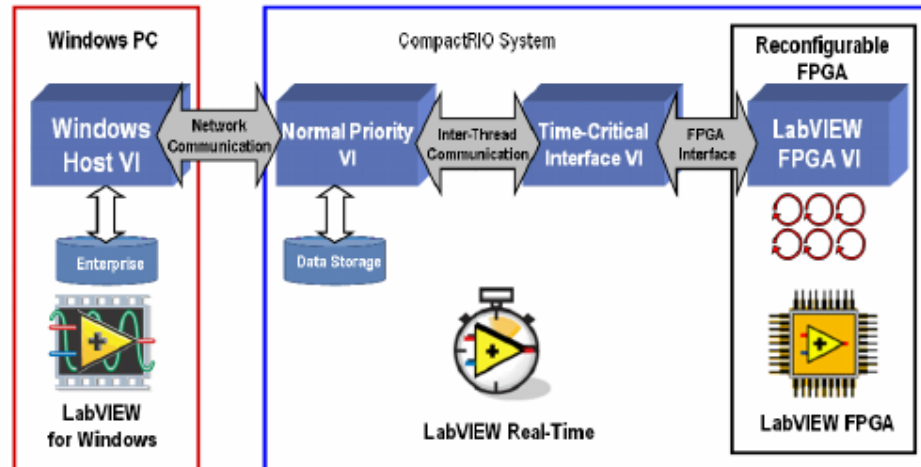
Figure 6.2 Labview block diagram for data communication, National Instruments (2009b)

The following pages show the level of programming and user interface for both the blue and red blocks highlighted in Figure 6.2.

6.1.2   RT Host Scan

As mentioned in section 6.1.1, this part of the software runs on the cRIO™. If the data did not need to be examined externally, then this section would be sufficient for data logging. However, because the data needs to stored to an external file, the windows front end software is also needed.

With reference to Figure 6.3, the diagram shows three tabs. The first tab which is the visible page, shows the calibration values for the particular sensors. The intention was to reduce the pre-processing that is necessary later on in Matlab™. However, understanding the data limits of a sensor only becomes apparent from running the tests multiple times. Therefore, in reality by the time it was understood what the values should be, the tests had been completed. If the system were to go into use as a real reactor primary circuit monitoring system, then this level of pre-processing would certainly allow the Matlab™ code to run faster.

The status blocks in the lower part of the display, would relay any problems associated with either the scan mode or FPGA modes. The loop iterations are

constantly incrementing showing the progress of the respective loop. The far right column shows the raw data in the top of the column and the scaled data in the lower portion of the column. This provides a good validation check that the system has not locked up and that the sensors are relaying back sensible results. If a sensor had become detached or broken then by experience it would be very obvious.
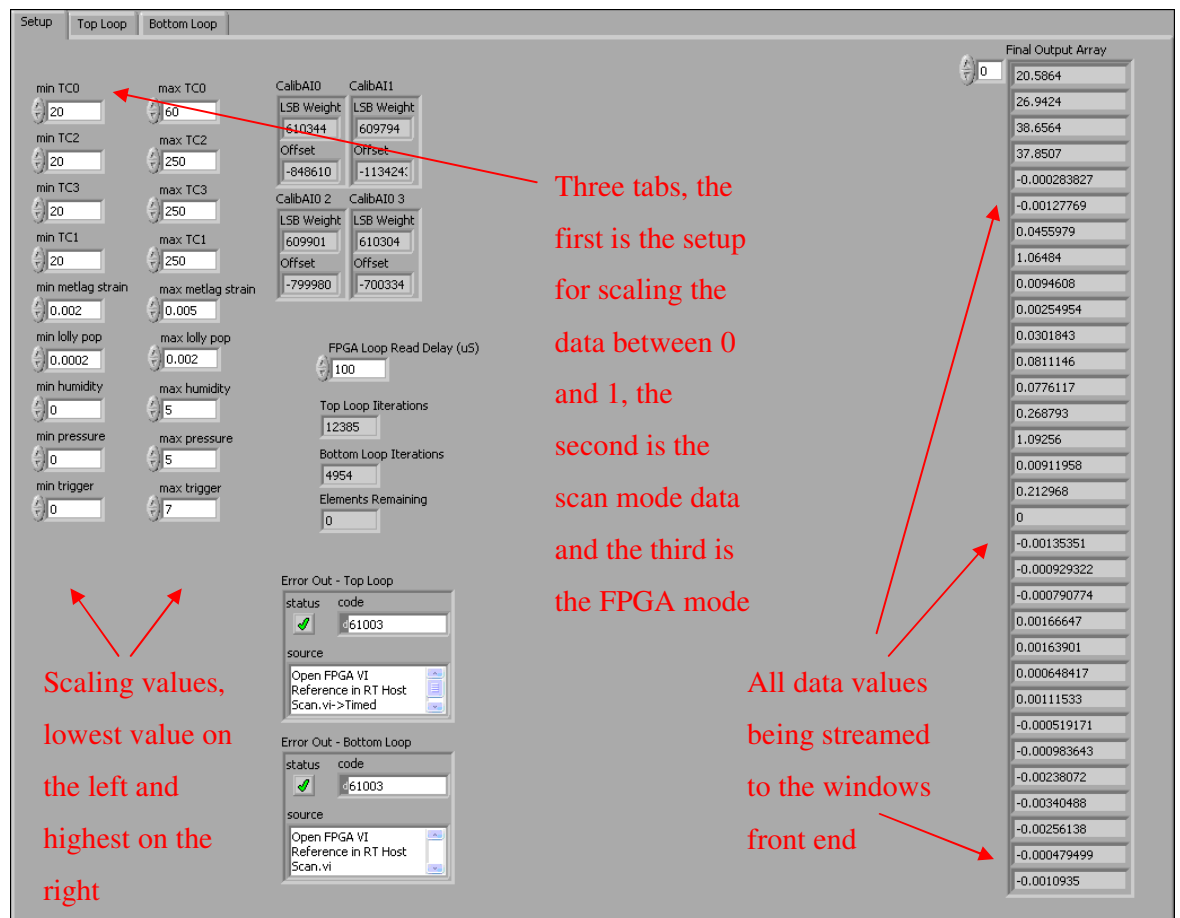
Figure 6.3 RT Host Scan front panel

Figure 6.4 shows the Labview block diagram. As explained earlier, rather then programming by creating lines of code in the usual manner, Labview builds up a block diagram of components. Within the diagram the top portion shows all the inputs from the sensors requiring the lower sampling rate of 1 kS/s. The lower block has the inputs from the three accelerometers and microphone, which need to run at the faster sampling rate of 51 kS/s.
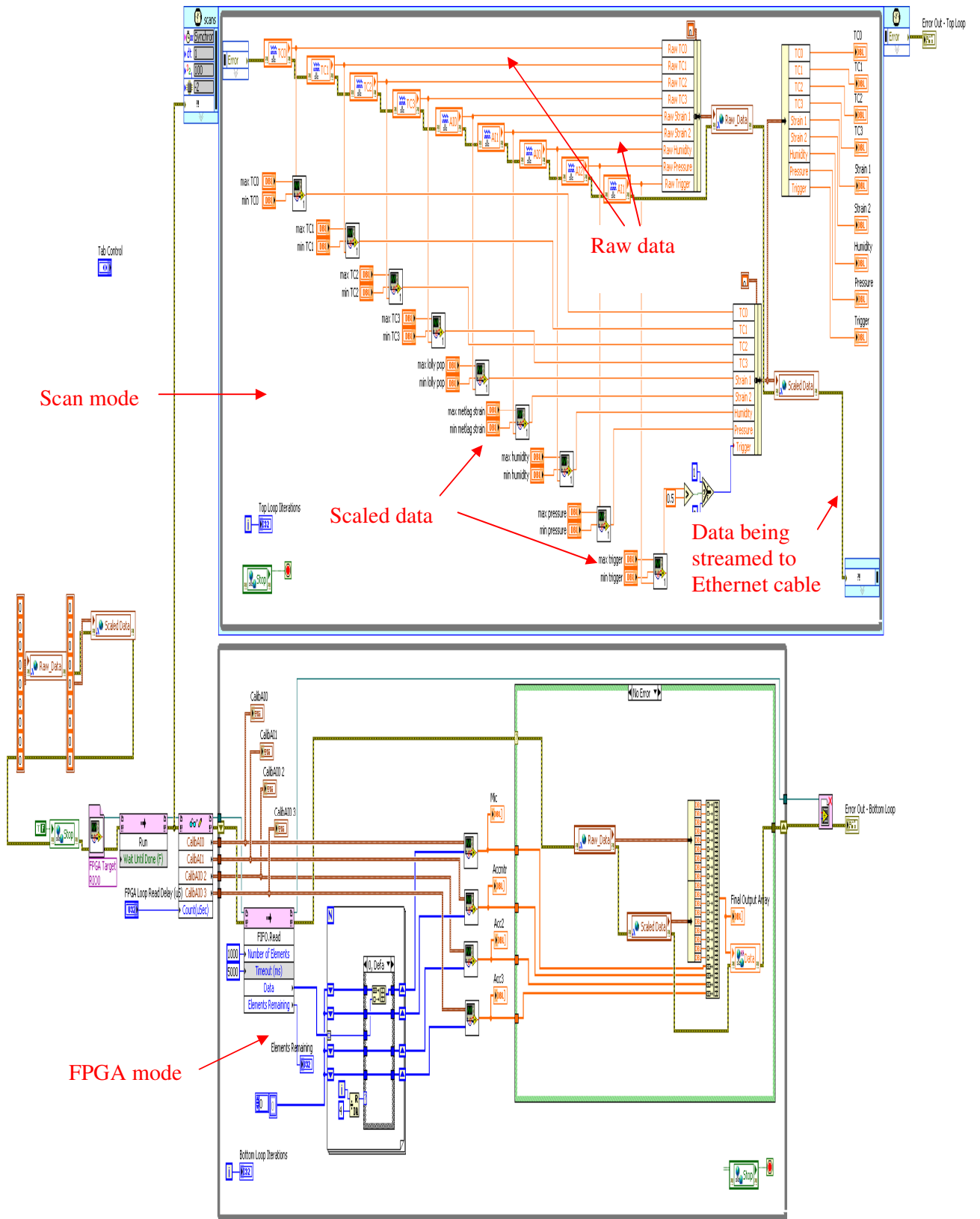
Figure 6.4 RT Host Scan Block Diagram

The labels visible in the figure include: Scan mode, Raw data, Scaled data, Data being streamed to Ethernet cable, FPGA mode, Tab Control, Top Loop Iterations, Bottom Loop Iterations.

6.1.3 Windows Front End

This part of the software is dedicated to returning the data back from the cRIO™ to the PC, in order to store it. The returning data can be viewed in real time by the operator as illustrated in Figure 6.5. Had the program been running, all of the graph areas would contain data. The first tab shows the Scan mode data in its raw form, shown in the nine graphs. The second tab (as shown below) shows the same data but scaled. The third tab comprises four graphs that demonstrate the behaviour of data from the three accelerometers and microphone respectively. The final tab contains the maximum and minimum values for the Scan mode, which it in turn uses to scale the Scan mode data.
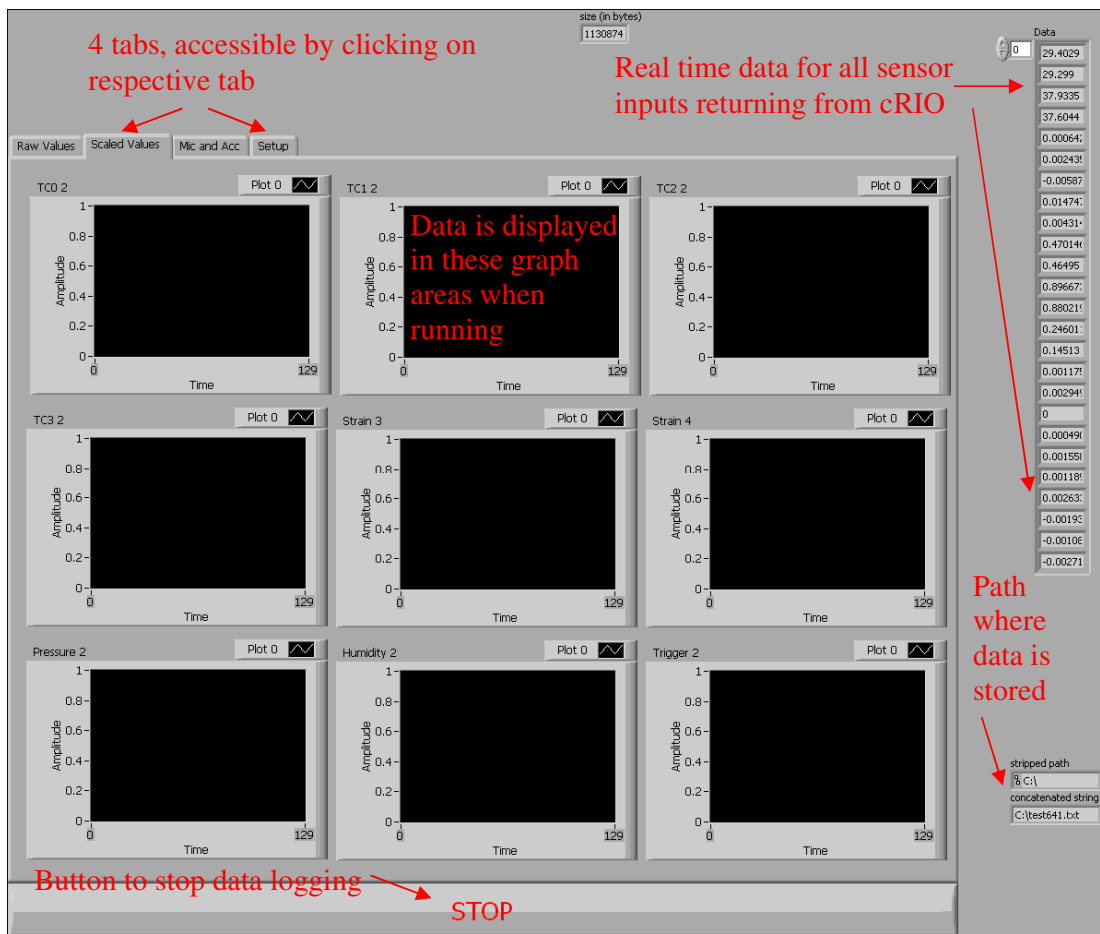
Figure 6.5 Windows front end
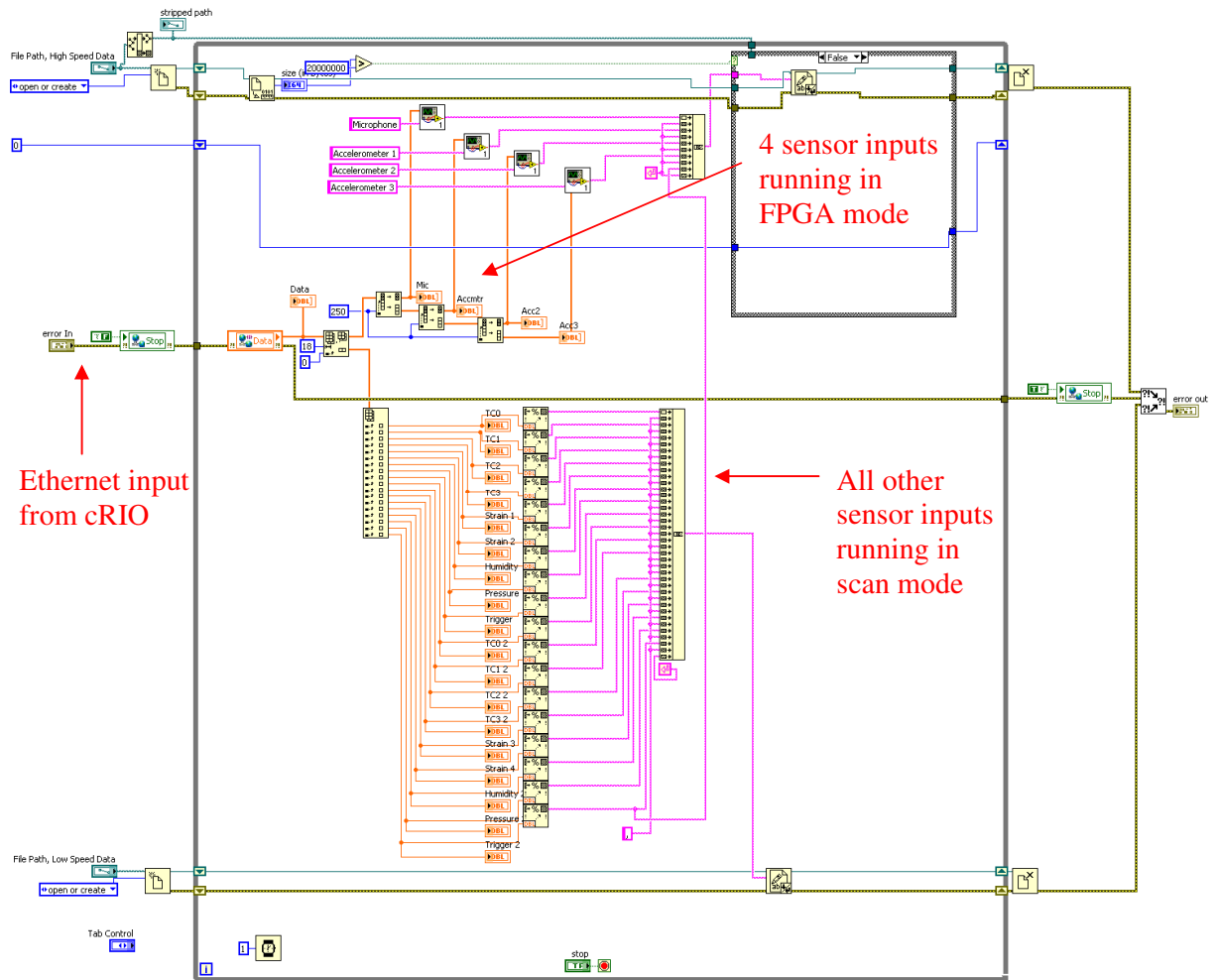
Figure 6.6 Windows front end block diagram

The diagram above, Figure 6.6, shows the Labview software that resides on the Windows PC. It can be seen from the diagram that the data from the cRIO™ enters on the left and is subsequently subdivided into the two sampling modes. The FPGA mode contains the three accelerometers and microphone, and the Scan mode contains 18 separate streams of data. These are: Thermocouple1, Thermocouple2, Thermocouple3, Thermocouple4, Strain gauge1, Strain gauge2, Humidity, Water Pressure, Trigger and then these same data items are repeated, but with their data normalised. This represents nine unique sensor inputs with their data in both raw and normalised form.

6.2   Performing an Experiment

When performing an experiment there are a number of criteria to keep in mind. This includes when to start logging as the data acquisition device stores 20MB of data in only a few seconds. It is important to observe the temperature and pressure carefully and when their values stabilise to the required level, it is good time to start logging the data. By adopting this strategy it saves logging unnecessary data that will be disregarded and also it also saves capacity on the hard disk. Due to the large amount of data stored during the runs, it was necessary to use an external hard disk with 1GB of available space. During early runs of the rig, it became apparent that the lagging material could take up to 10 minutes to reach its stable temperature. This was only evident when examining the data. Through experience it became apparent what temperature was required at the pre-heaters and how much power was needed at the coil heater in order to obtain the desired temperature at the orifice, for the given size of jet being used. In addition, through familiarity, it became apparent when the jet is becoming blocked. This only occurs when the HOH (ion exchange) tank becomes depleted, for which there are two signs. One is a bad fishy smell, and the other is limescale deposits on the rig and surface of the lagging material. The final parameter to keep in mind is the trigger signal. This is used later for data analysis. The trigger switch can be found on the front of the control console. This switch determines the three cycles of operation, which are:

1. Warming up the water and pressure to the specified value, the trigger switch is at 0 volts (illumination off)

2. Steam present from the orifice and temperatures and pressures correct, trigger set to 5 volts or digital logic 1 (illumination on)

3. Pump turned off, therefore removing any noise created by the rig, pure steam noise can be monitored, trigger back to 0 volts or digital logic 0 (illumination off).

A full set of operating instructions is given in Appendix F, detailing how to perform a test on one jet size with lagging attached.

6.3 Evaluation of Selected Sensors

Having considered all of the above sensors, the most suitable were trialled and a summary of each sensor is detailed below:

6.3.1 Steam Velocity and Pressure

During trials with the pitot static tube on an open leak, problems were encountered with the rubber pipes filling with steam which in turn, turned to water blocking the pipes and seriously affected the results. During further investigation, it was discovered that this is not unusual, and the aircraft industry address this known problem by using electrical heaters to stop this from happening. However, due to the short time span of this project and the research that would be necessary to determine a suitable type of heater and in turn a suitable temperature, this method was abandoned. The deflecting strain gauge was applied on an open jet of steam, as shown in Figure 6.7, the device worked very well. However, when a larger jet was installed the length of spring steel was deflected so far that one of the strain gauges was damaged. Consequently it was felt that the stiffness of the spring steel was too low, and in order to provide more resistance two lengths of spring steel were glued together, to increase the cross sectional area and stiffness.

Another problem that appeared to be occurring was in the recorded results, the initial strain gauge offset changed between tests. Through investigation this appeared to be due to the strain gauges becoming wet with the steam which affected their resistance. A potential remedy was to wrap cling film around the strain gauges and the wires connecting them. However, water still managed to seep under the cling film and the strain gauges kept breaking. Therefore, this method was abandoned. It had also been envisaged that the steam pressure under the lagging would force the two halves apart. This was not the case and despite attempting to measure this, as shown in Figure 6.8, this approach was abandoned as well.
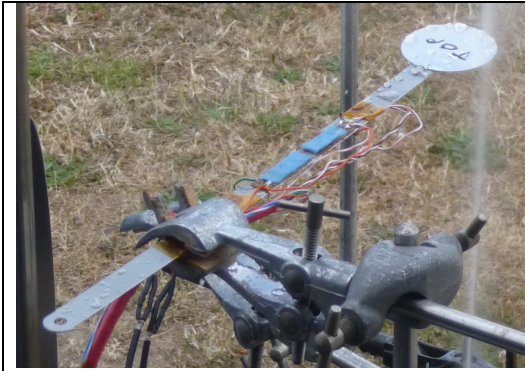
Figure 6.7 Deflecting strain gauge, directly on steam
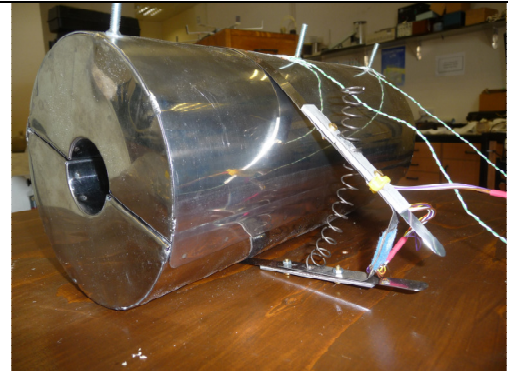
Figure 6.8 Deflecting strain gauge on lagging

A forced air flow meter design was conceived using a 150mm length of 1mm thick aluminium, 30 mm wide (Figure 6.9). The hinge and means of measurement were provided by a 10 kΩ potentiometer. This idea was tested on the lagged system, and using the chimney design the hope was the majority of the steam would exit from this area and lift the flap. However, in reality the steam exits from every available gap, specifically around the lagging joints, consequently the steam exiting the chimney had no measurable pressure. Therefore the flap did not lift and this entire concept of measuring pressure was abandoned.

Figure 6.9 Air flow meter using metal flap

In conclusion, the air velocity devices discussed in section 5.2 and the above, work successfully in their conventional applications, however when applied to this rig they proved unsuccessful. The majority of the tests were performed on an open leak. In reality this should have been the easiest means of achieving a result. Unfortunately,

each one failed for a variety of reasons. The final test using the air flow meter was performed on the lagged system. It showed that measuring steam pressure and flow on this magnitude of leak through a designated chimney is ineffective. On general observation of the chimney with no measuring device in place, the level of steam exiting is comparable to a kettle when boiling.

6.3.2 Microphone

The microphone was able to measure sound from the steam leak. The open leak has no distinct tone and to the human ear sounds like white noise. With the lagging attached, the sound is quieter. The lagging muffles the sound from the orifice and the sound of water pouring from the lagging is actually more noticeable than the sound of the steam. Even though the microphone remained a sensor during all the subsequent tests, its usefulness is very much in doubt as the RC has very loud fans that even make it difficult to have a conversation.

6.3.3 Humidity

The humidity results in reality did not produce the expected correlation between humidity level and leak size. The slightest breeze during the experiment would manifest itself as a drop in humidity. Therefore, the assumption could be made that the test setup is not representative of reality. However, in the RC there is in fact very large fans circulating the air, and so perhaps by chance the results are more valid than first thought. The humidity sensors used in this experiment did however struggle with 100% humidity, i.e. saturated steam, which was observed on leak of all sizes. It appeared that when water lay on the device, it was no longer able to function, and so the voltage output would drop from nearly 5 volts to 0 volts. From this experience a recommendation is that a more robust humidity sensor should be used in the future, as this type of device still has some merit.

6.3.4 Thermocouples

The final thermocouple arrangement was to place two thermocouples on the lagging. One was attached immediately above the leak area, and the other at the end of the lagging, above the heater cartridge section of pipe. This arrangement of thermocouples allowed measurement of the steam temperature inside the lagging and

in the chimney area. Both of these measured areas had a noticeable change in temperature from the situation with no leak, to one with different size leaks.

6.3.5   Accelerometers

The accelerometer provided the most useful measurements once the data had been processed by a FFT. During the early trials, the amplitude of the noise when the pump is running is in the order of 10^{-3} volts whereas the magnitude of just the steam is only 10^{-5} volts, 100 times lower. When observing the FFT plot during the pump running phase, there is no way of knowing what is contributed by the pump or other rig components. Therefore, it is very fortunate that the pump can be switched off, and the accumulator maintains pressure during which time a pure steam leak can be recorded. Therefore with the pump switched off, the background noise level is negligible. This is the only measurement of significance, as it represents only the leak characteristics. As a reminder, pressure is maintained when the pump is switched off, because a 20 litre accumulator has been set up to store water at 100 bar. The amount of time the pressure can be maintained varies depending upon jet size. It has been found that by closing the pressure valve after the pump has been stopped increases the measurement time quite considerably. Using a 10 cc/min jet, the pressure can be maintained for about 45 seconds whereas it is approximately 20 seconds with the 40 cc/min jet. Despite the short amount of time, when data is being collected at 51,000 samples per second, there is still sufficient time to collect enough data for analysis.

The accelerometers were by far the most useful sensor in the system. As the results will show, these devices capture an enormous amount of vibration information.

6.3.6   Summary of Selected Sensors

The purpose of the first set of tests was to determine three criteria.

1.   Does the sensor provide useful information
2.   Can the data verify a leak exists
3.   Are the data able to determine leak size.

The following Table 6.1, illustrates the results from the five sensors tested.

Sensor type	Useful sensor	Verify leak exists	Determine leak size
Strain gauge	NO (not robust enough)	-	-
Thermocouple	YES	YES	NO
Humidity	YES	YES	NO
Accelerometer	YES	YES	YES
Microphone	Uncertain	YES/NO	NO

Table 6.1 Summary of sensors

The table above indicates the effectiveness of each sensor, and illustrates whether a particular sensor has the ability to provide additional information which could enable the leak size to be determined. It was found by observing the accelerometer FFT plots that subtle differences were evident between leak sizes. Therefore, by applying the FFT data to an ANN, it is anticipated that classification will be possible between the different leak rates. The temperature graphs however, showed hysteresis occurring across the range of leaks. Consequently this data and the humidity data can only be used in a basic digital logic system. The microphone was barely able to pick up the faint background noise of the steam and water dripping when the lagging was fitted, and so its application to a reactor environment is very doubtful. However, the sound level was more prominent without the lagging fitted.

6.4 Sensor Results

The rig has two fundamental configurations; either with a leak exposed to the environment or a leak concealed by lagging. This report is only concerned with the data from the lagged leak, as this represents the typical primary circuit. Other industries may use unlagged pipes, and find these data of interest. Having verified which sensors are suitable for the task of leak detection, it is now important to examine the results and determine the best methods of data analysis. Comparisons are made between a lagged leak and an open leak, and the results discussed. All the following results were captured with the CompactRIO™, and subsequently analysed with either Excel or Matlab™. The diagram below, Figure 6.10, shows the location of the three accelerometers and three thermocouples. Accelerometer 1 is physically attached to the pipe and is therefore the sensor mentioned when the lagging is

removed. Thermocouple 3 is often referred to as the temperature sensor in the chimney. It had always been envisaged that the chimney would act an escape route for the steam. However, the reality was that the steam has negligible pressure and consequently a small flap (aluminium plate) on top of the chimney is always closed as shown in Figure 6.9. This does however help maintain a higher temperature in this area.
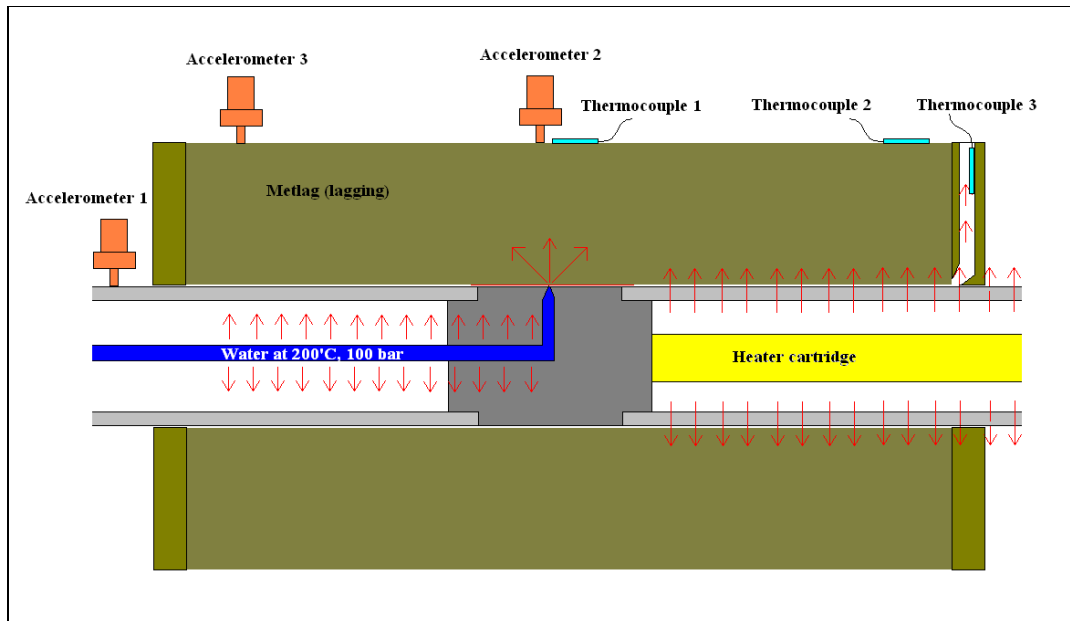
Figure 6.10 Side profile of pipe with lagging fitted and sensors attached

The red lines emanating from the heater cartridge and water pipe, show the mechanism of heat transfer. The heater cartridge is heated up to 200°C, which is representative of the temperature on the primary pipe of a PWR, and because it is encased in a brass sleeve the heat transfer is very good. The water pipe, indicated in blue, is actually insulated in a fibre glass mat (shown in Figure 6.11), to help maintain the temperature in the pipe. Consequently, the pipe that the Metlag rests on to the left of the leak, resides at a lower temperature, than that on the right. Figure 6.10 can be realised as Figure 6.11. It is interesting to note the water pouring from the base of the Metlag shown in Figure 6.11. The slight haziness evident in the photograph is due to the steam in the air.
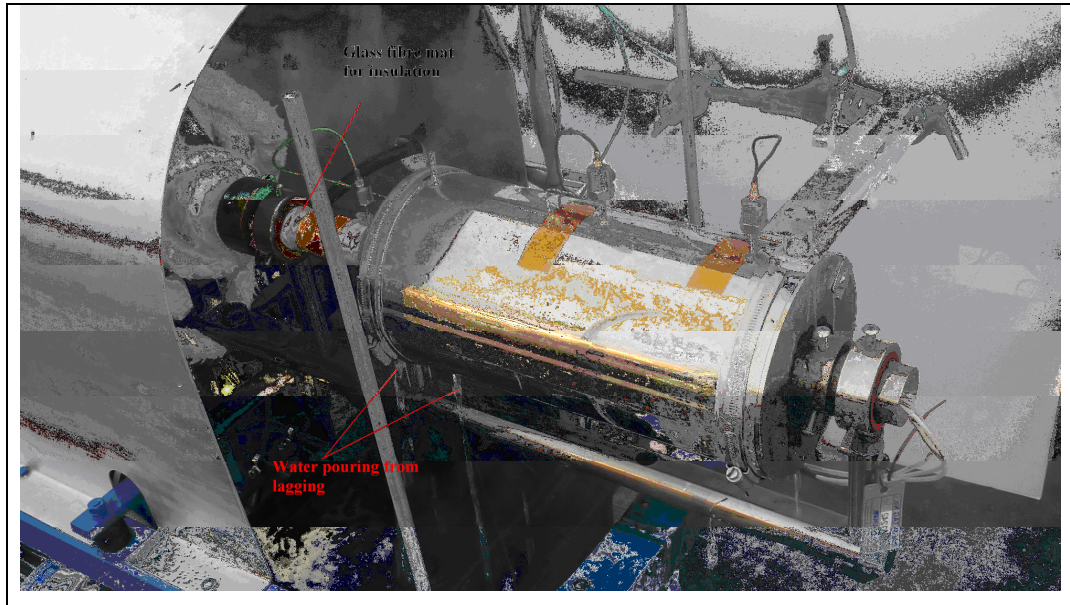
Figure 6.11 Sensors arranged on or around Metlag

6.4.1 Temperature Sensors

Figure 6.12 shows that as the leak increases in size the outside lagging temperature decreases. From observing the larger jets and the large amount of water pouring from the lagging, it is evident that this water is having a cooling effect on the surrounding area. As mentioned above, it is unfortunate that the entire pipe upon which the Metlag rests does not lie at an even 200˚C, but due to the time and cost limitations it was the best compromise. However, because of this situation it is difficult to determine whether the steam has a cooling effect on the outside of the lagging, as shown in Figure 6.12, or because the heat has failed to propagate along the Metlag. If thermocouple 2, (at end of Metlag) is taken as the more representative sensor, then when no leak occurs the temperature is at 62.5˚C and rises to between 67.5˚C and 78˚C when a leak occurs.
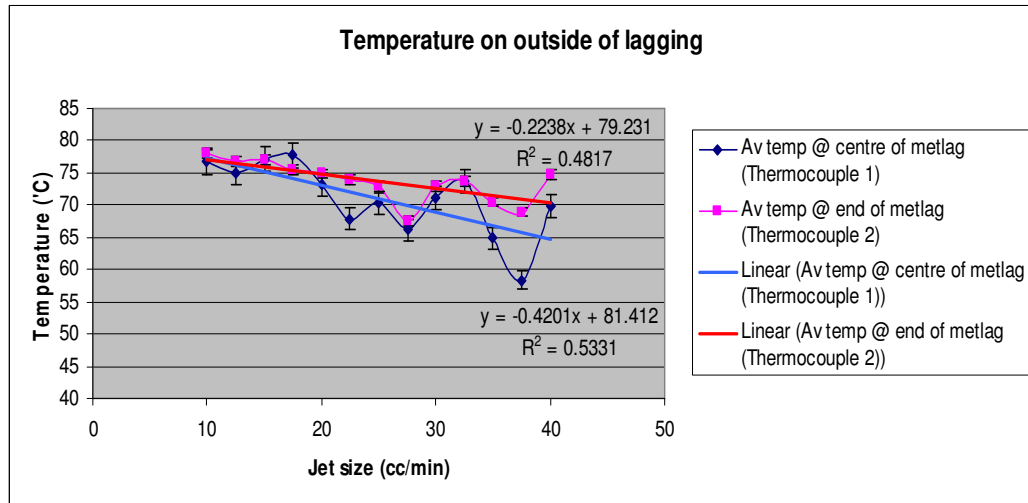
Figure 6.12 Temperature on outside of lagging

Thermocouple 1, shown in blue in Figure 6.13, shows the average temperature from three independent readings. The variation between values was about 2.5% (as shown), whereas thermocouple 2 under the same conditions only had a variation of 1%. The R^2 values show the goodness of fit. In the case of both thermocouples the best fit line (trend line) is 50% correct. Taking the square root of this value yields a Pearson coefficient of about -0.7. This shows that there is a good relationship between the size of the leak and the relative temperature.

In the real application the outside temperature of the lagging would also vary depending upon its relative distance from the nearest circulating fan. However, the reason for the undulating temperature profile shown in Figure 6.12, is possibly related to the wind and temperature fluctuations during the test. Although a variation of 20˚C seems unfeasible during normal daytime conditions the general trend is more associated with the leak size rather then background ambient temperature. This further reinforces the relatively high value for the pearson coefficient.

With regard to Figure 6.13, it can be seen that the steam temperature in the chimney area varies from 82˚C to 86˚C with a leak present, opposed to just 48˚C with no leak. This graph shows a R^2 value of about 50%, which yields a pearson value of 0.7. The general trend shows that the larger leaks have more energy and thus represent a higher steam temperature; this is also confirmed by the trend line equation.
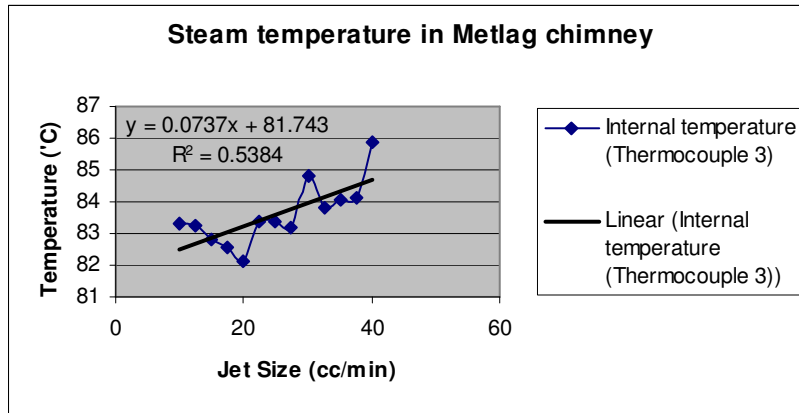
Figure 6.13 Steam temperature in Metlag chimney

6.4.2 Humidity Sensor

Humidity is one measure that would be expected to increase when a steam leak occurs. However, as Figure 6.14 shows, the plot demonstrates results that are not very logical. This is because a number of factors have affected the outcome. The experiment was conducted by testing the larger jets first and then decreasing the jet sizes. Therefore, with reference to the graph below, the data were collected from right to left. The unusual data point is at 37.5 cc/min. This seems like an incorrect value, however the reality was that because the test was conducted outside, a small breeze had developed and consequently the humidity sensor was at times picking up a very low level of moisture in the area. At this point the test may be considered invalid. However, the reality is that this is very representative of the RC, as the entire area has enormous fans re-circulating the air. Therefore, this shows that depending upon the position of the leak in relation to the re-circulating fans, the data will be more or less useful. The other strange area of the graph is at the low jet sizes from 10 to 20 cc/min, where the humidity level is nearly zero. This is due to the sensor failing, as it is unable to function with water continuously lying across the sensor surface. Despite repeatedly changing the humidity sensor, at some point in the experiment it always failed. The humidity sensor cost about £30, but a good high quality item would have been about £300, and the budget was not available. During the experiments the background humidity was about 48%, this value would need to be measured for RC when operating normally at it would probably be higher than this.

Therefore, in conclusion a good robust humidity sensor would detect the increase in humidity in the RC, but its positioning in relation to a re-circulating fan has a significant effect on its usefulness.
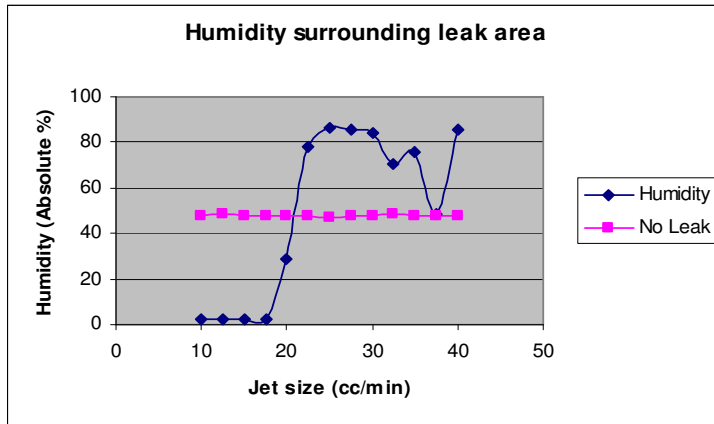
Figure 6.14 Humidty level surrounding leak area

6.4.3 Accelerometers

The accelerometers have proven in all cases to be the most sensitive to the changing leak characteristics, and thus the most effective leak identifier. However, on analysis of one leak size, the variability between plots can be quite significant. Figure 6.15, shows the variability between the peak amplitudes of each of the accelerometers as the leak size changes. It can be seen that hysteresis exists and therefore any normal mathematical methods of differentiating signals would struggle with these data.
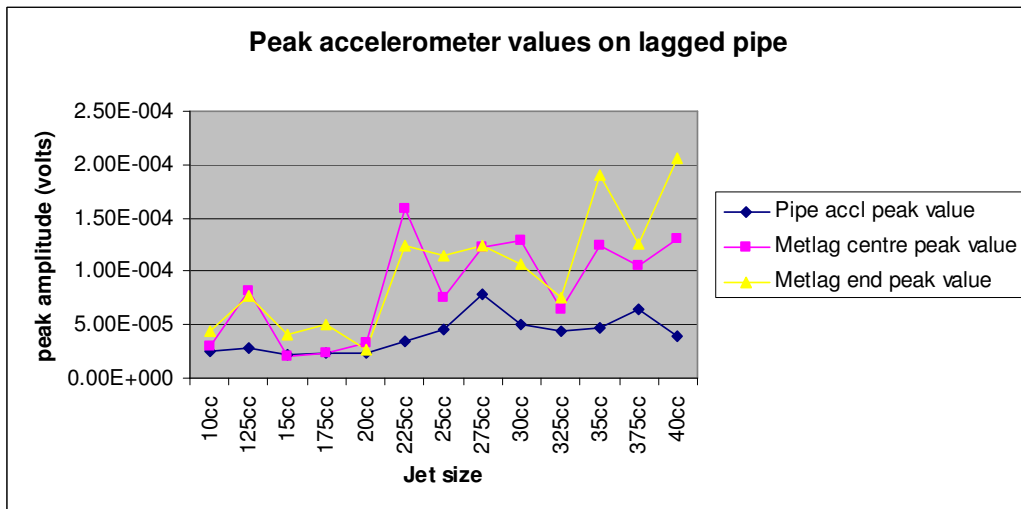
Figure 6.15 Peak accelerometer values at all three positions and leak sizes

Another interesting feature that appears during analysis is the changing fundamental frequency of each of the accelerometers. The frequency plots are created by applying

115

an FFT to the raw data in Matlab™. The interesting observations are the three accelerometers all have fundamental frequencies that increase as distance increases. The accelerometer on the lagging immediately above the leak resonates at 2.8 kHz (Figure 6.16), the accelerometer at the end of the lagging resonates at 4.7 kHz (Figure 6.17) and the accelerometer on the pipe, as shown in Figure 6.18, resonates at 10 kHz.

	Figure 6.16, Accelerometer on Metlag central position
	Figure 6.17, Accelerometer on Metlag, end position
	Figure 6.18, Accelerometer on pipe, furthest position from leak
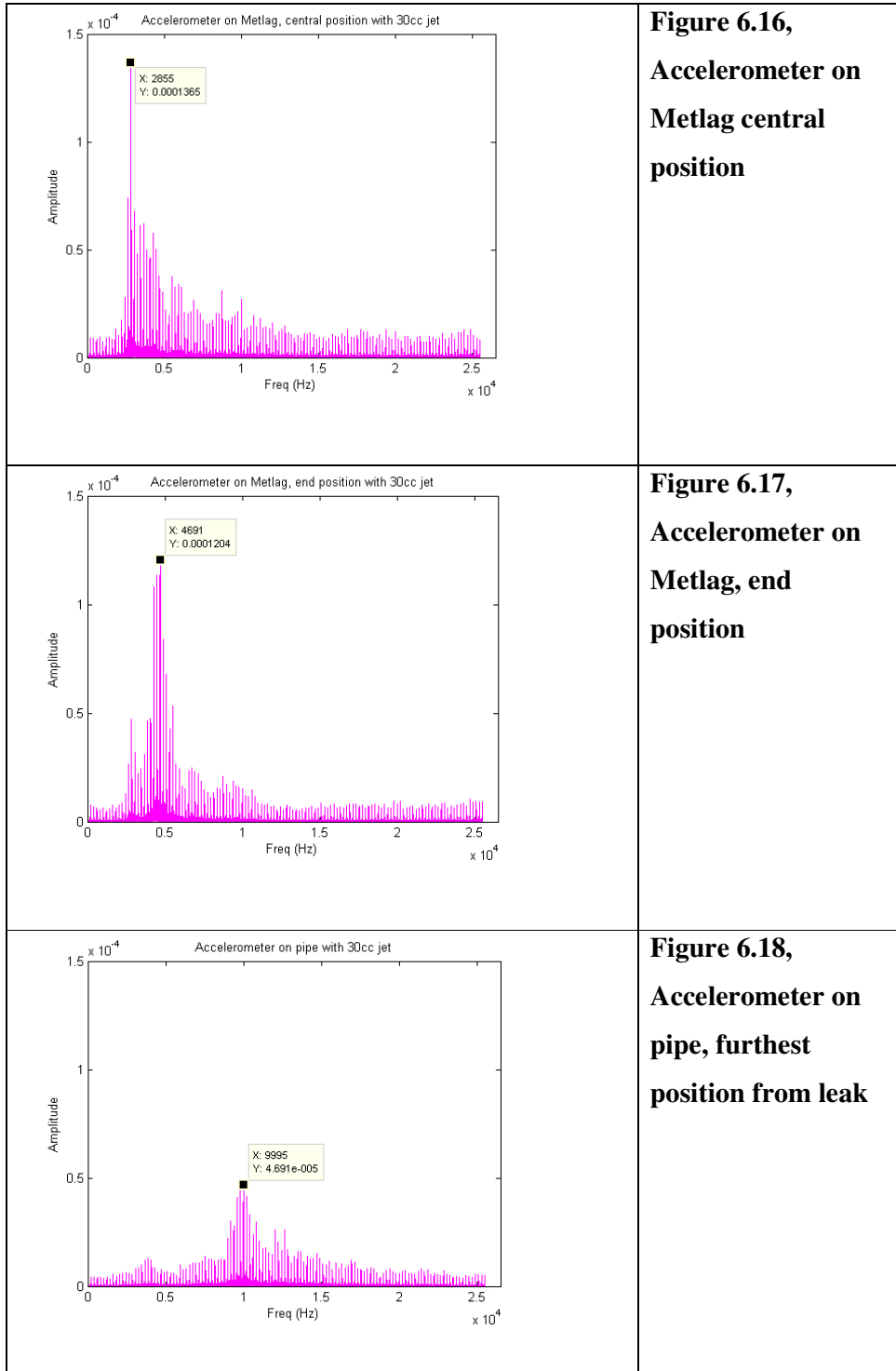
When observing the FFT graphs for each of the accelerometers, it is interesting to note that their fundamental frequency never changes and is always the highest amplitude on the plot, irrespective of the size of leak, but the energy in the side bands varies between leak sizes, as shown in Figure 6.19.
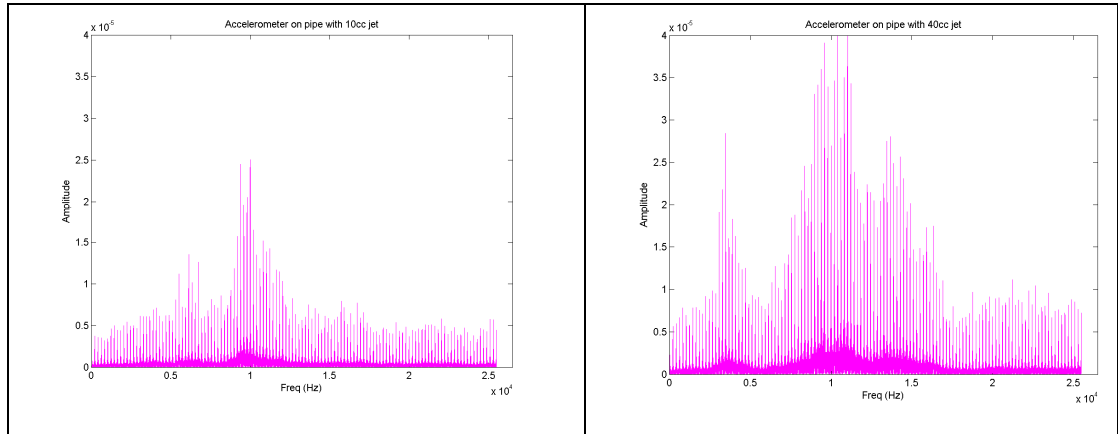
Figure 6.19 FFT of accelerometers, comparison between small and large leak

It may be assumed that the amplitude of the FFT increases in direct proportion to the leak size. This is not strictly the case, and through general observation of all 13 leak sizes, attempting to classify a leak by eye would not be possible to any degree of accuracy, as can be seen in Figure 6.20.

Figure 6.20 on the following three pages is constructed as an overview of all 13 leaks in the 3 monitored accelerometer positions. Each column refers to a different accelerometer as labelled and the first row of each column represents the no leak condition, the subsequent row shows the smallest leak 40 l/h, and each subsequent row progresses in leak size in 5 l/h steps until the last row shows the largest leak 100 l/h.

It should be noted that all the measurements were taken over a two day period, and therefore the operating conditions were as consistent as could possibly be achieved in an outdoor environment. As the tests were performed in the winter, the ambient temperature was only 5˚C.

Acc1 (accelerometer on pipe) lagging fitted to pipe	Acc2 (accelerometer in centre of lagging)	Acc3 (accelerometer at end of lagging)
Accelerometer on pipe with NO leak	Accelerometer on Metlag, central position with NO leak	Accelerometer on Metlag, end position with NO leak
Accelerometer on pipe with 10cc jet	Accelerometer on Metlag, central position with 10cc jet	Accelerometer on Metlag, end position with 10cc jet
Accelerometer on pipe with 12.5cc jet	Accelerometer on Metlag, central position with 12.5cc jet	Accelerometer on Metlag, end position with 12.5cc jet
Accelerometer on pipe with 15cc jet	Accelerometer on Metlag, central position with 15cc jet	Accelerometer on Metlag, end position with 15cc jet

119

Figure 6.20 Comparing the FFT graphs from the three accelerometers and all leak sizes

6.4.4 Microphone

Figure 6.21, shows the frequency response of the sound recorded from the leak shown in blue, versus the background noise (in red) with the lagging fitted. It shows that the there is no discernable difference between the two recordings and therefore the microphone is no use in attempting to identify a leak from a lagged pipe.
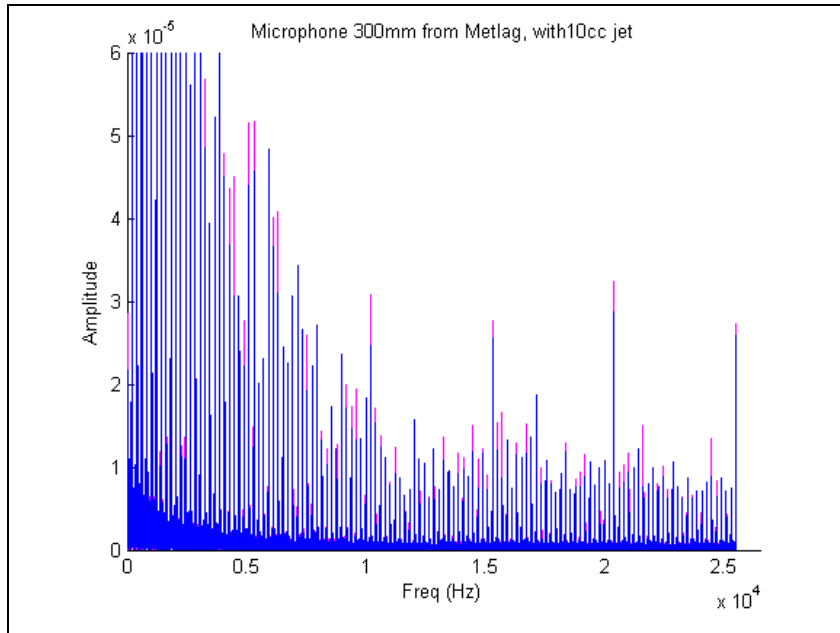
Figure 6.21 Microphone FFT with lagging fitted, leak noise and background noise

Figure 6.22, shows the same leak size but with the lagging removed. This time the blue signal is more prominent than the background noise and therefore may give an indication of a possible leak. However the primary circuit in a reactor is always lagged and even the unlagged trace is only just above the background noise level. Therefore, this method would be totally unsuitable to a RC where the background noise level is quite high due to the circulating fans.

121
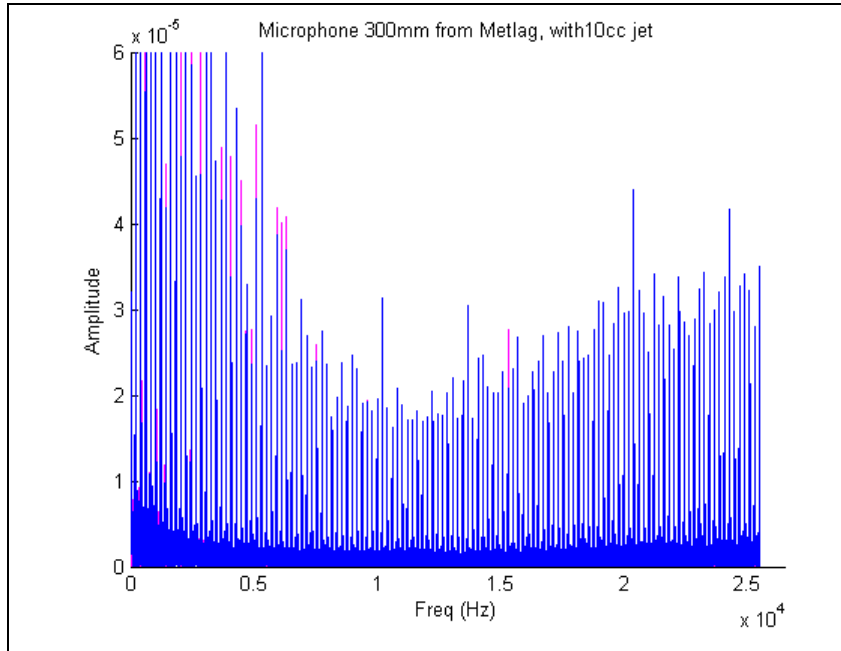
Figure 6.22 Microphone FFT without lagging, leak noise and background noise

6.5   No Lagging on an Exposed Leak at Pressure

Pipes that are unlagged exhibit different responses to lagged pipe work. Audibly the steam sound is louder, as there is no mechanism to dampen the sound. But conversely, the Metlag acts to amplify the vibrations to the accelerometers, as is illustrated in Figure 6.23. The diagram shows the effect of having the same accelerometer in the same location, roughly 300mm from the leak point. The graph shows the average peak amplitude for each jet size, in the lagged and unlagged state. The unlagged leak shows the amplitude increasing in a linear manner with increasing jet size, however the lagged plot does not. There are two interesting features of the lagged graph. The amplitude is higher than the unlagged, and the peak amplitude occurs at the 27.5 cc/min point. This may be due to a combination of the pressure and temperature at that particular flow, resulting in a turbulent flow of steam from the orifice. If time permitted it would have been interesting to alter the pressure and temperature by intervals of 10 bar and 10°C respectively and observe whether this has any effect of the peak amplitude. The other reason could be due to the internal construction of the Metlag resonating at this point. The increased overall amplitude is probably due to the mass of the lagging amplifying the signal in agreement with Newton's second law of

122

motion (F=ma). In other words the force of the steam acting upon the heavy Metlag is creating a greater acceleration, which is being directly measured by the accelerometers.
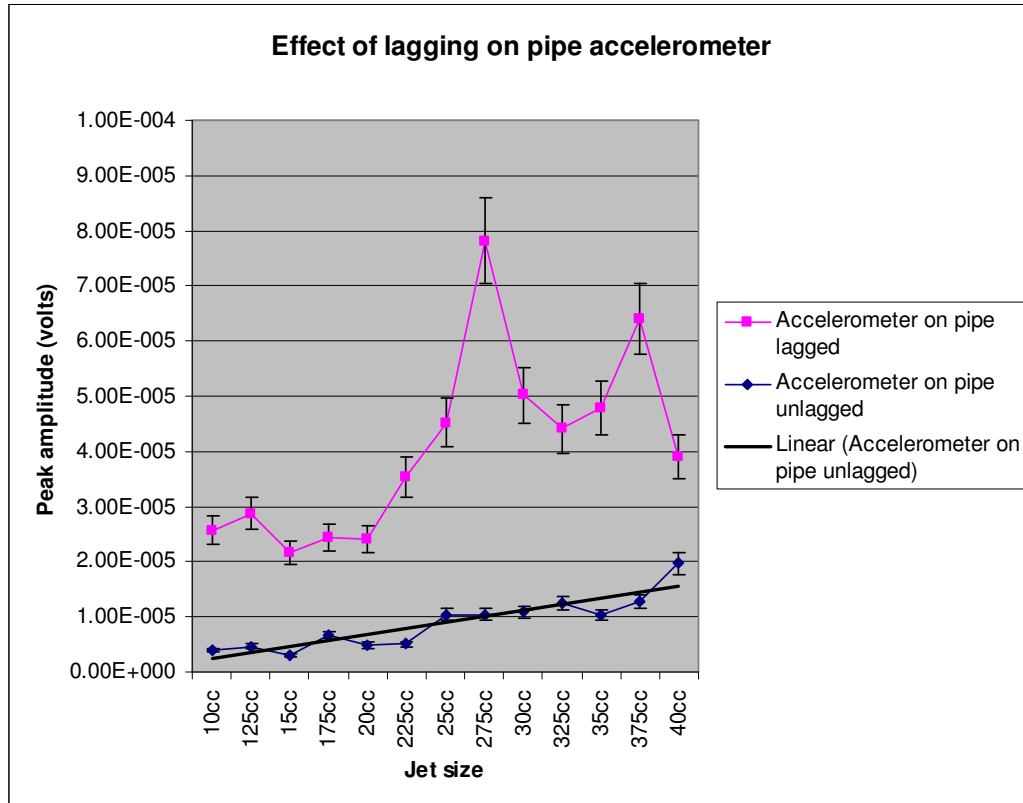
Figure 6.23 Effect of lagging on accelerometer amplitude

Figure 6.24 and Figure 6.25, both represent a jet of size 30 cc/min, however, the lagging has a dramatic effect on the characteristic shape of the plot. Also, the magnitude of the signal has roughly a factor of 10 difference between them. It should be noted that the fundamental frequency does not change. The unlagged pipe has a peak signal about 6.0×10^{-6} volts, whereas the lagged pipe has a peak amplitude of about 4.8×10^{-5} volts. The overall shape has changed dramatically and it appears the lagging amplifies the fundamental signal at about 10 kHz but completely dampens the signal at 18.5 kHz. When further investigation is carried out, it becomes apparent that every plot from every jet, has this notch at 18.5 kHz on the lagged leak section, as illustrated in Figure 6.26 and Figure 6.27.

Figure 6.24 No lagging over leak, accelerometer on pipe, 30cc/min jet

Figure 6.25 Lagged leak area, accelerometer on pipe, 30cc/min jet
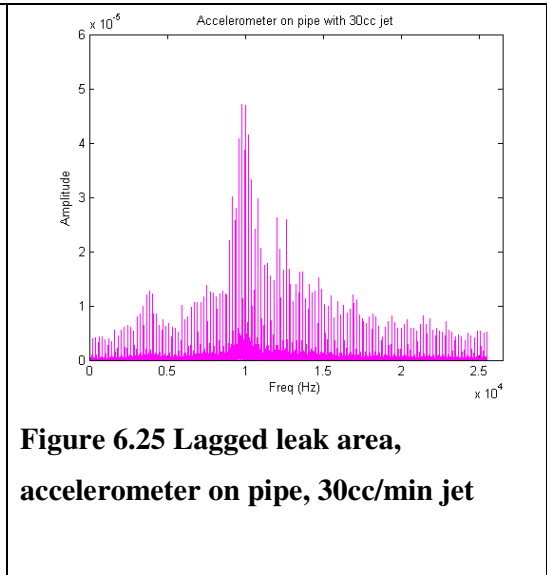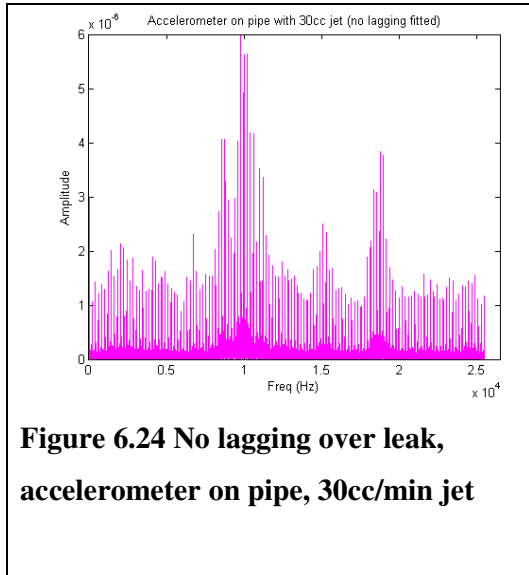
The effect of this notch is evident in all 221 plots, across all thirteen leak sizes and in each case does not exceed an amplitude of 1x10-5 volts. Although, this characteristic exists, it does not add significant weight to any of the ANN results.

Figure 6.28 makes the comparison between a pipe fitted with lagging and one without. Although the fundamental frequency is around 10 kHz, the amplitude of FFT when the lagging is fitted to the pipe is seven times higher. This parameter is important because should this technique be applied to unlagged pipes the natural background noise level would be even more critical, as it could completely drown out the steam noise.

Figure 6.26 Effect of lagging, creating a notch filter at 18.5 kHz, on jet 25 cc/min

Figure 6.27 Effect of lagging, creating a notch filter at 18.5 kHz, on jet 27.5 cc/min
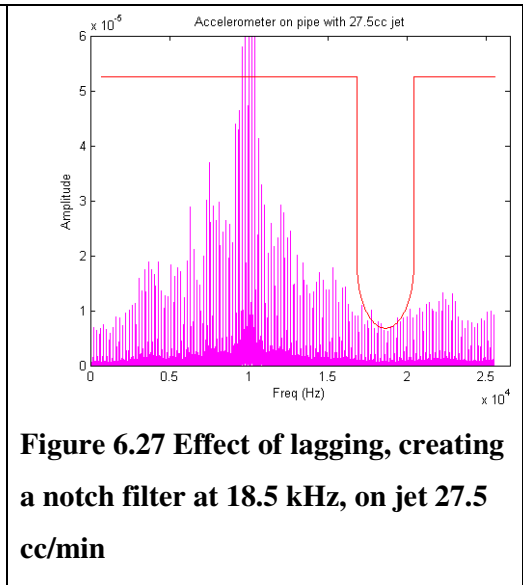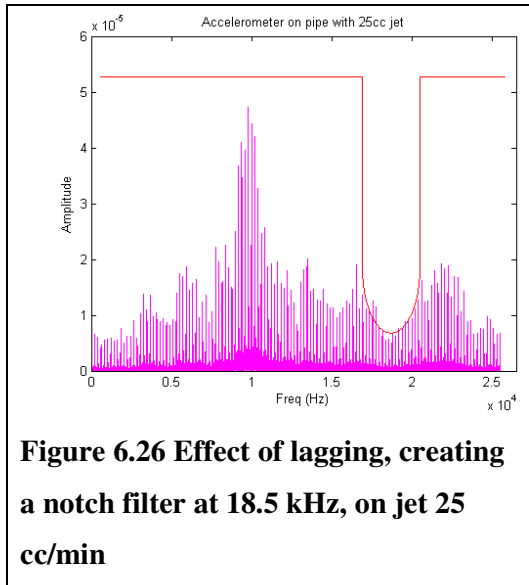
Figure 6.28 on the following four pages is constructed as an overview of all 13 leaks using only the accelerometer mounted on the pipe. However, the left hand column represents the situation when the lagging is fitted and the right when no lagging is fitted. The first row of each column represents the no leak condition, the subsequent row shows the smallest leak 40 l/h, and each subsequent row progresses in leak size in 5 l/h steps until the last row shows the largest leak 100 l/h. It must be noted that the scales for the two columns are not the same on the y axis. The left hand column is $4x10^{-5}$ volts whereas the right hand column is $6x10^{-6}$ volts.

Acc1 (accelerometer on pipe) lagging fitted to pipe *y scale max is 4x10⁻⁵ volts*	Acc1 (accelerometer on pipe) NO lagging *y scale max is 6x10⁻⁶ volts*
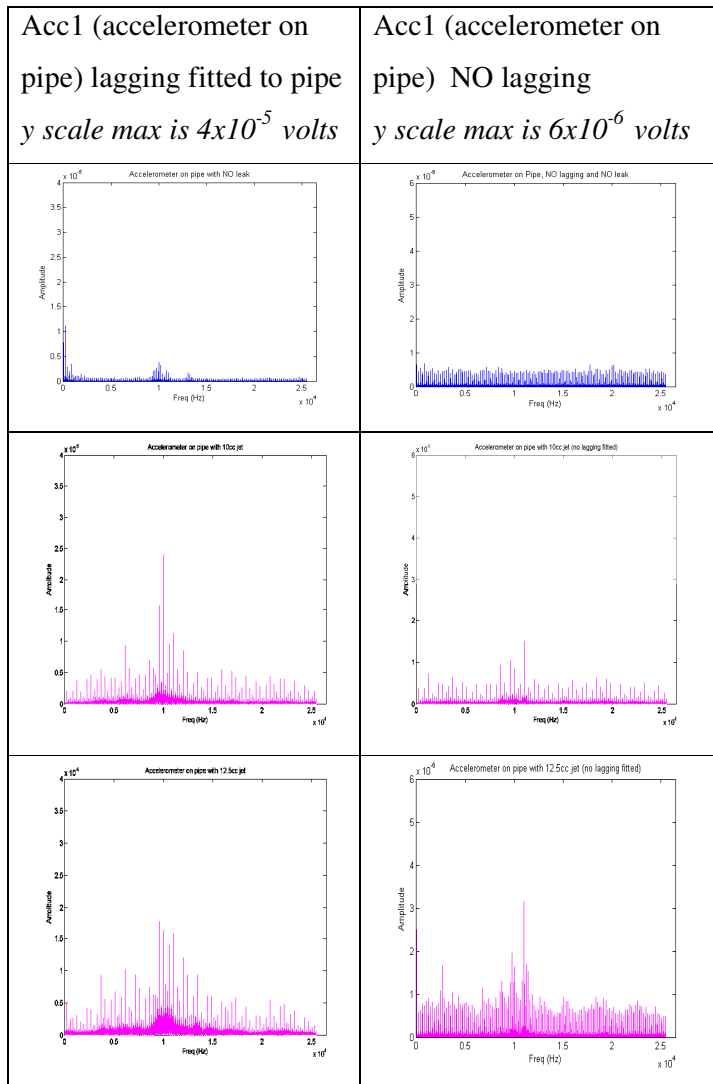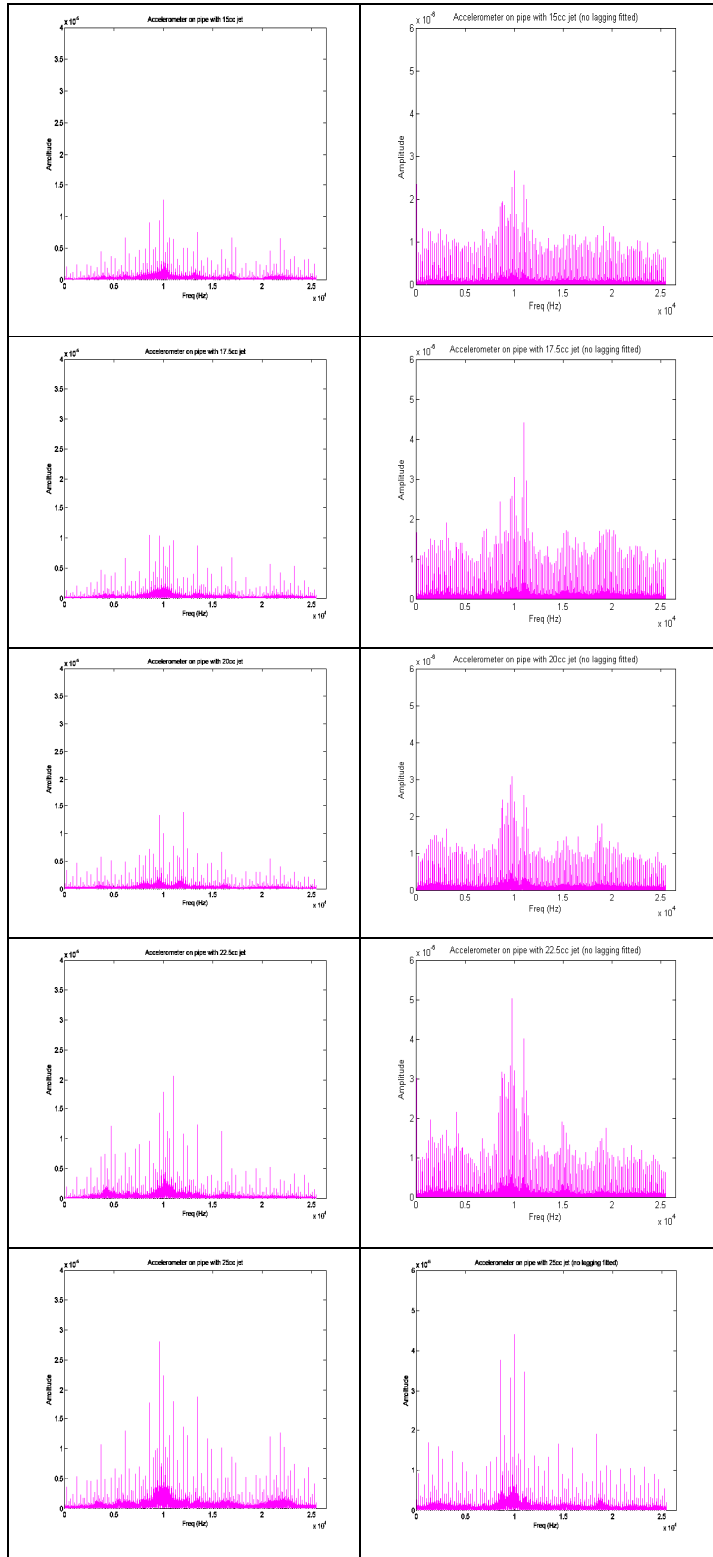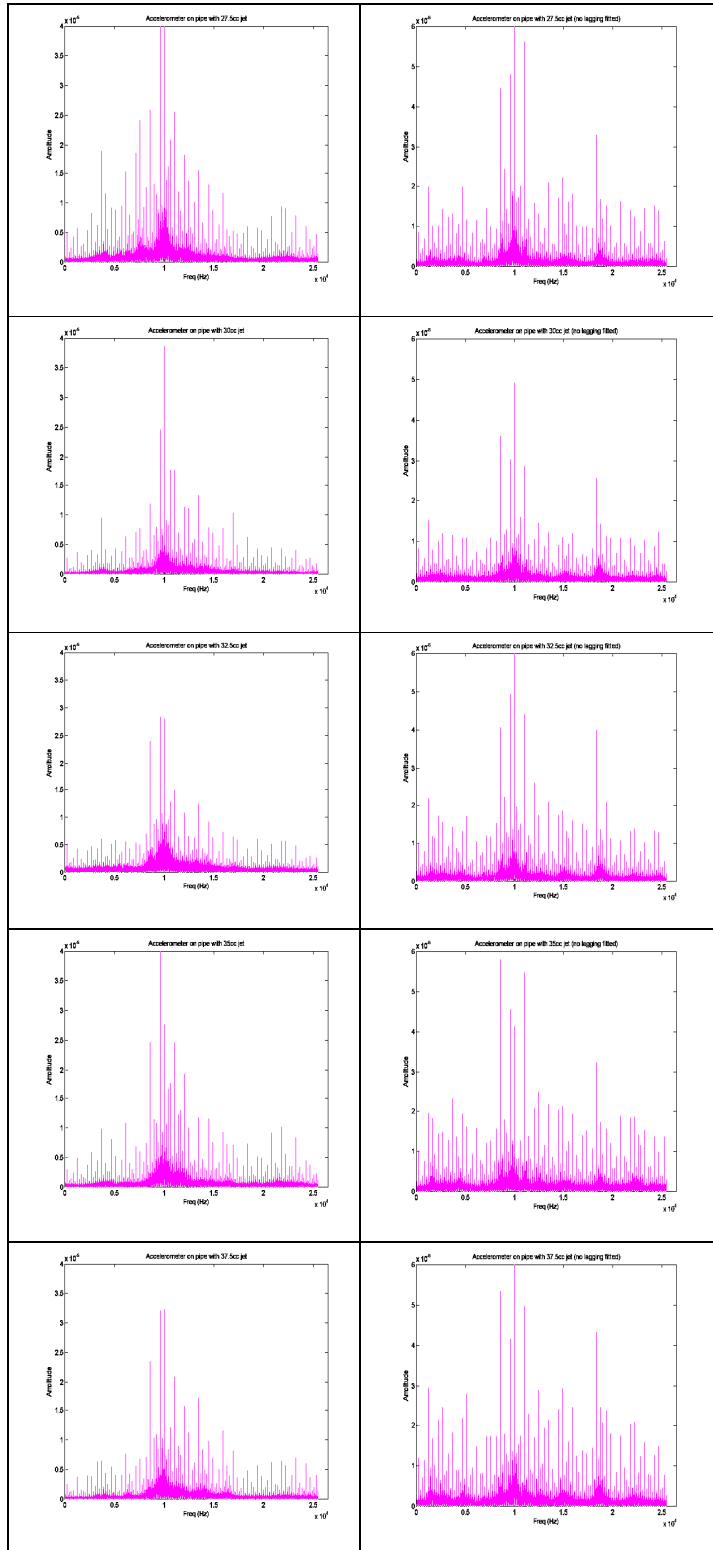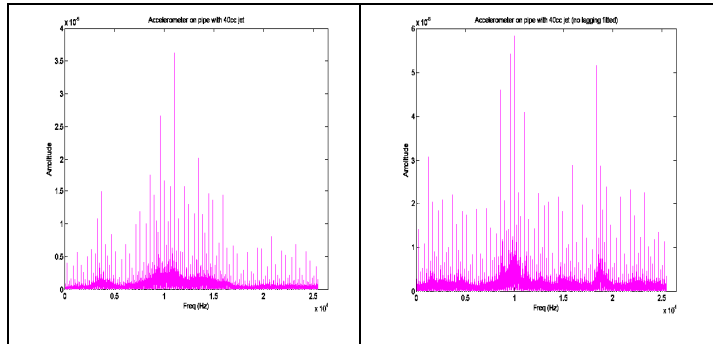
Figure 6.28 Comparing the FFT graphs from the same accelerometer on the pipe and all leak sizes, with and without lagging fitted

6.6 Summary

This chapter addressed the means to acquire sensor data using the National Instruments CompactRIO™. The graphical representation of the Labview software was presented, with screen shots of the software architecture. This demonstrated how the sensor data was acquired and transmitted to the Windows front end laptop. The CompactRIO™ was initially configured to acquire data from a wide variety of sensors, but this chapter reduces that preliminary list following experimental trials. The final set of sensors, namely: accelerometer, thermocouple and humidity sensor are measured and their results evaluated and discussed. Comparisons were also made between a lagged leak and one that is exposed to the environment from the accelerometer results. The sensor positioning around the lagging material is also presented using actual photos and a diagrammatic cross section of the lagging.

Chapter 7

Data Evaluation

Through examination of the data acquired from the sensors during the early trials, it became apparent which sensor data have the capability to be used to determine leak size and which could be only detect the presence of a leak. The thermocouple sensors showed a significant temperature change from the 'no leak' to 'leak' situation. However hysteresis was present, thus making a sensor only suitable for leak detection. The humidity sensors were nearly always operating in 100% humidity, and therefore the only obvious change was from the 'no leak' to 'leak situation'. In addition, the slightest breeze had a significant effect on the data and therefore a small change in leak size would become undetectable. However, the RC has large circulating fans and therefore this unplanned scenario makes the data more realistic. When examining the FFT plots from the accelerometers, even though the changes were sometimes small, there always appeared to be a modification in the frequency spectrum when comparing leak sizes. Consequently, the data were classified into two areas; data that could only detect the existence of a leak were used as a hard computing input and the data that could determine leak size were used in the soft computing ANN area. This technique of fusing soft and hard computing was successfully accomplished by Ovaska (2004).

7.1   Matlab™

The ANN Toolbox within Matlab™ 2008a, MathWorks™, is the tool that will be used for all the ANNs in this project. This package has become more user friendly over the last couple of years and now uses a graphical user interface to give the user a better interaction with the software. Because the success of an ANN is very much dependent on the input data, it is quite normal to use a number of different network types for evaluation purposes. The initial networks trialled were: Elman, fitting network, pattern recognition network and Self Organising Map.

Twenty three bespoke Matlab™ programs have been developed ranging from scanning the input data for the relevant portion of data, producing graphs for all the different size leaks, scaling the data, performing an ANN and building a graphical user interface. These Matlab™ programs and 110 GB of data collected by the data acquisition device, are held on the computer cluster at HMS Sultan.

7.1.1 Pre-processing Data

Pre-processing of the data is a very time consuming function. Before the data can be processed by an ANN or other method they need to be analysed by eye. This can either be achieved in MS-Excel® or Matlab™, although MS-Excel® does have difficulty with the size of some of the files. Originally, all data were analysed using MS-Excel®, but unfortunately MS-Excel® cannot accommodate the accelerometer files which are set to 20 Mb, and so it is only useful for examining the thermocouple and humidity data. MS-Excel® and MS-Notepad® could however be used at a basic level to determine the exact point in the cycle, the rig was performing at. This functionality was determined using a trigger signal.

The three cycles are explained below, and illustrated in Figure 7.1:

1. Warming up the water and pressure to the specified value, the trigger switch is at 0 volts
2. Steam present from the orifice and temperatures and pressures correct, trigger set to 5 volts or digital logic 1
3. Pump turned off, therefore removing any noise created by the rig, pure steam noise can be monitored, trigger back to 0 volts or digital logic 0.

Figure 7.1 below, does not have any scale in the x axis because the time period is variable depending upon the size of the jet. When using the smallest jet a stabilised temperature and pressure can be established in less than a minute, whereas for the largest jet it may take in excess of ten minutes to reach and maintain the 200˚C.
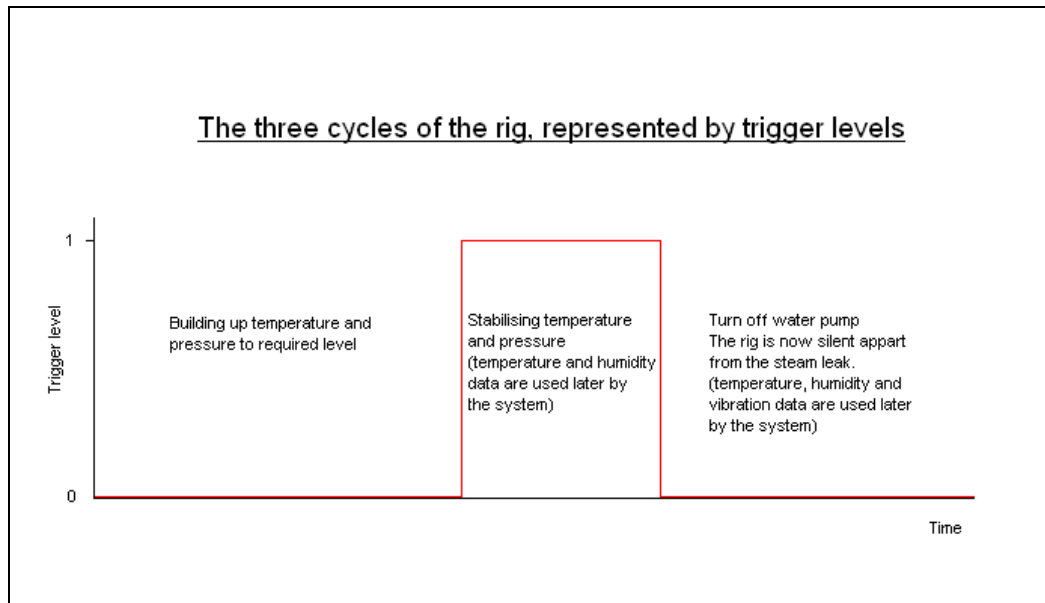
Figure 7.1 The three cycles of the rig

During pre-processing, the initial trigger 0 level is always ignored, however both the final logic 1 and 0 data levels are processed for the temperature and humidity. For the accelerometer data, only the final logic 0 level data are processed. During this period of time, only steam noise is present. This means manually scanning through the 20 MB data files watching for the transition from data logic (trigger level) change from 1 to 0.

The accelerometer data in this section are then transformed through a FFT in Matlab™, in order to observe the frequency versus amplitude as a visual plot. However, this data directly to an ANN is not possible because a single plot contains 262,625 data items, because the data has a resolution of 10 Hz. Having this number of inputs to an ANN would make the computational power of the ANN very slow, but also leading to unnecessarily long training times and poor results. Consequently, further refinement is needed to extract the parameters of importance to make the network efficient and fast.

The solution is rather than looking at individual data items, concentrate on the data sets, as these hold unique properties defining that region. Figure 7.2 shows this is achieved by subdividing the frequency plot into 5 unique areas. These areas were chosen because they represent the majority of the leak information. Figure 7.2 represents an accelerometer plot, with the accelerometer placed on the pipe. In this scenario, the peak amplitude lies around the 10 kHz area. However, when the

131

accelerometer is in the central Metlag position, it peaks at about 2.8 kHz and the accelerometer at end of the Metlag peaks at 5 kHz. Therefore, the chosen areas represent the different accelerometers positions very well. Within each of these areas four unique pieces of information are taken:

1. Peak amplitude
2. Mean amplitude
3. Standard deviation
4. Sum of all amplitudes.

These four pieces of data are taken from each of the five regions highlighted in Figure 7.2, resulting in 20 unique data items for each leak. Each leak size typically has 17 samples. Therefore, to characterise one leak size the ANN has a 17 by 20 matrix. Because there are 13 different jet sizes, vertically concatenating them produces an input network matrix 221 by 20, and an output matrix 221 by 13.
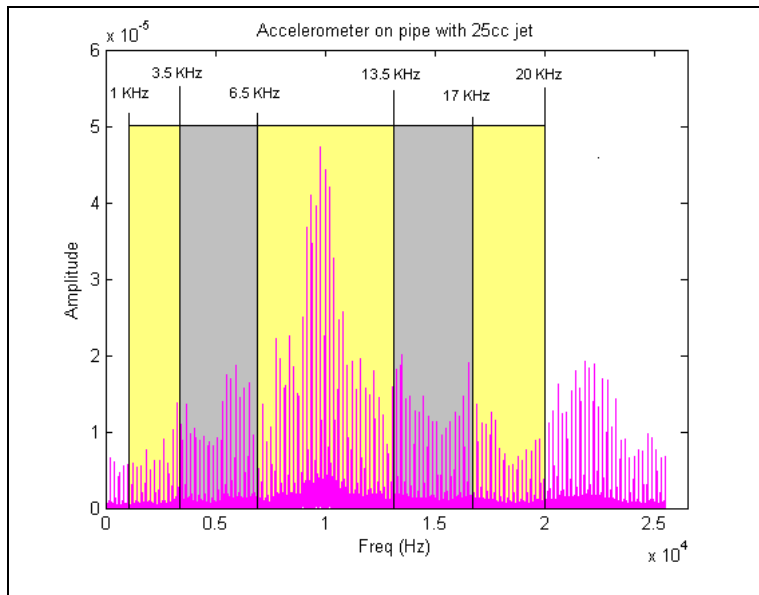
Figure 7.2 Frequency division to train ANN

In order to collect all 17 samples of data per jet size, the rig was run three times. This is because there is only a finite time to collect the data, as the accumulator can only store the water pressure for a maximum of 40 seconds, depending upon jet size. The fact that all the measurements are not taken successively is unimportant. It does

132

however, show the experiment is repeatable. The general trend is for more data to be available from the smaller jets and less from the larger, due to the flow of water. Despite this, all the jets have trained with an equal number of inputs and outputs. The network is not trained on a 'no leak' scenario because the signal resides in the noise floor. To determine the 'no leak' scenario it is sufficient to apply a simple threshold level to the input data.

The temperature and humidity data are visually straightforward to comprehend. Figure 7.3 below, shows that the temperature before the leak was about 48°C within the Metlag material, as shown by the green line, and when the leak occurs it rises to above 80°C, shown in red. As a trigger point it could be assumed that if the temperature rises above 65°C then a leak exists. Due to the design of the rig and its discrete jet sizes, it is not possible to show the transient from 'no leak' to 'leak'. If a variable size orifice was available, then this would have been interesting to study.
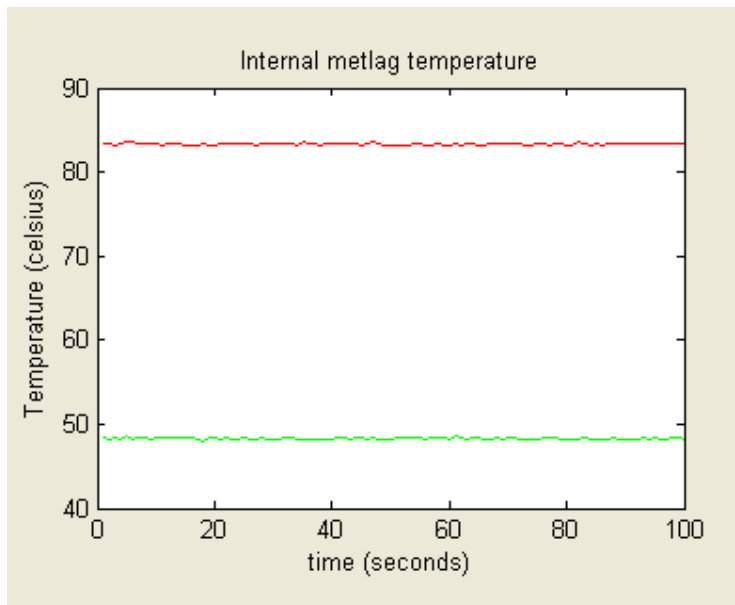
Figure 7.3 Internal Metlag temperature

Therefore, as a data item, the internal Metlag temperature will be at logic 0 until the threshold level is exceeded, when it will become a 1. The exact same principle applies to the temperature sensors on the outside of the lagging and humidity sensor.

7.1.2 Pre-processing of Data for ANN

Once the data have been acquired by the CompactRIO™, all subsequent data processing is carried out using Matlab™ (2008a). As the intention is to use a supervised network, the network needs input and target data. The target data is achieved by creating a matrix 221x13, shown in Figure 7.4. There are 13 columns, because there are 13 discrete jet sizes. As there are 17 pieces of sample data per jet, the binary target data contains one column of 17 rows of 1, and the remainder 0. This corresponds to one jet size. The next jet has the subsequent column and again has 17 rows of 1, and the remainder 0. Using this strategy the entire matrix is populated by 1's and 0's pointing at their respective jet sizes.

The flow diagram Figure 7.5, shows the steps that are necessary to convert the raw data into a data set that an ANN can use. By following the process boxes the routine is repeated by the number samples available per jet size, typically 17. Once all 17 samples are evaluated the loop exits and addresses the next jet size. Therefore, this occurs 13 times. The final deliverable is a matrix of 221x20. However, as the data are still raw and unsuitable to train an ANN, all the data are normalised, so that they lie between 0 and 1. This data set, is now the input data to an ANN.
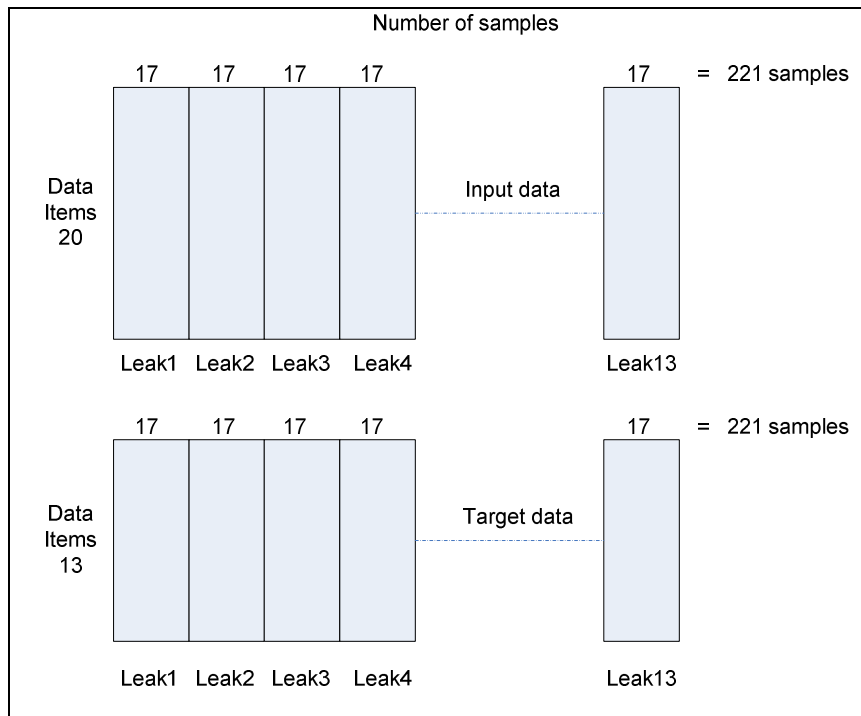
Figure 7.4 Pre-processing of data for ANN
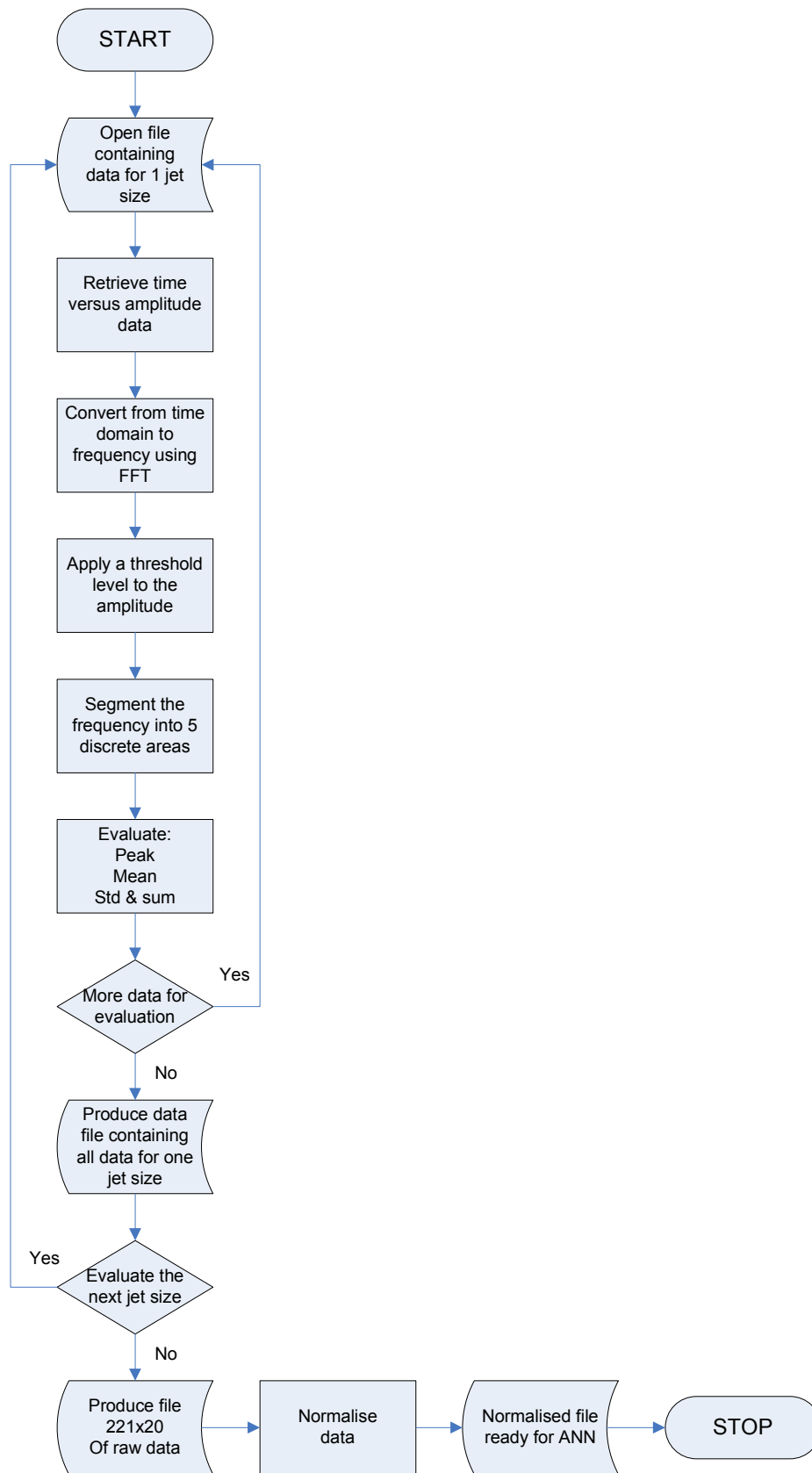
Figure 7.5 Pre-processing of data for input to ANN

To further highlight the scaling operation, Figure 7.6 shows a sample from the smallest jet in raw data form and Figure 7.7 is the scaled version. Due to space limitations only the first eight columns are shown, representing the peak, mean, standard deviation and sum of amplitudes shown in columns A to D, and repeated again in E to H. The complete MS-Excel® file contains 20 columns (A to T), in the same manner. The MS-Excel® representation of having the samples represented by the rows and data items for the columns, is easier to implement from a logistical respective. It is also the format that is accepted by the Matlab™ ANN.

	A	B	C	D	E	F	G	H
1	1.91E-006	8.39E-007	6.12E-006	0.00527716	2.32E-006	1.29E-006	1.35E-005	0.0101731
2	1.95E-006	9.88E-007	8.41E-006	0.00527071	2.25E-006	1.26E-006	1.04E-005	0.00952294
3	2.03E-006	1.03E-006	8.16E-006	0.00674693	2.37E-006	1.50E-006	1.33E-005	0.01294331
4	2.01E-006	1.04E-006	1.09E-005	0.00608402	2.41E-006	1.59E-006	1.20E-005	0.01172767
5	2.00E-006	9.95E-007	9.03E-006	0.00581173	2.35E-006	1.42E-006	1.54E-005	0.01139267
6	1.94E-006	9.03E-007	8.50E-006	0.0054545	2.33E-006	1.39E-006	1.31E-005	0.01056652
7	1.86E-006	8.59E-007	1.06E-005	0.00422961	2.22E-006	1.26E-006	1.07E-005	0.00869567
8	1.83E-006	7.77E-007	6.06E-006	0.00437129	2.17E-006	1.16E-006	1.03E-005	0.00884592
9	1.80E-006	7.44E-007	6.43E-006	0.00428359	2.18E-006	1.20E-006	9.53E-006	0.00909128
10	1.90E-006	9.28E-007	8.48E-006	0.00458851	2.19E-006	1.24E-006	1.12E-005	0.00935187
11	1.92E-006	9.20E-007	8.68E-006	0.004998	2.22E-006	1.26E-006	1.01E-005	0.0098014
12	1.98E-006	9.94E-007	8.99E-006	0.00549072	2.22E-006	1.29E-006	1.11E-005	0.01061631
13	1.91E-006	9.31E-007	7.79E-006	0.00504717	2.15E-006	1.16E-006	1.06E-005	0.00832595
14	1.92E-006	9.35E-007	8.09E-006	0.00480206	2.20E-006	1.23E-006	1.01E-005	0.00887674
15	1.94E-006	9.74E-007	8.22E-006	0.00505487	2.16E-006	1.17E-006	9.62E-006	0.00845188
16	1.95E-006	9.79E-007	8.02E-006	0.00512763	2.19E-006	1.20E-006	1.17E-005	0.00884051
17	1.91E-006	9.16E-007	7.27E-006	0.00489091	2.17E-006	1.19E-006	1.03E-005	0.00902116

Figure 7.6 Raw data, from smallest jet (screen capture from MS-Excel®)

And then by scaling the entire matrix by the columns, labelled from A to T containing 221 samples, the result is:

	A	B	C	D	E	F	G	H
1	0.246864	0.153756	0.060802	0.201821	0.487653	0.29978	0.204213	0.201865
2	0.274003	0.22012	0.14516	0.201387	0.432441	0.283959	0.126269	0.177915
3	0.331474	0.237579	0.136132	0.300719	0.530811	0.400751	0.197999	0.303914
4	0.317889	0.244779	0.235765	0.256113	0.557301	0.44249	0.166737	0.259132
5	0.312161	0.223099	0.168115	0.237791	0.515031	0.362635	0.249815	0.246791
6	0.272344	0.182323	0.148364	0.213753	0.493103	0.344989	0.194254	0.216358
7	0.217842	0.162571	0.225135	0.131333	0.409549	0.283125	0.133769	0.14744
8	0.194428	0.125874	0.058419	0.140866	0.371709	0.233754	0.124197	0.152975
9	0.172901	0.111269	0.072132	0.134965	0.378236	0.252702	0.103805	0.162013
10	0.243511	0.193145	0.147869	0.155483	0.388887	0.275026	0.145823	0.171613
11	0.25643	0.189712	0.155247	0.183037	0.406375	0.282114	0.116845	0.188172
12	0.294186	0.222575	0.166596	0.216191	0.411354	0.298962	0.143858	0.218192
13	0.247499	0.194644	0.122243	0.186345	0.352621	0.234736	0.130637	0.13382
14	0.258463	0.196566	0.133261	0.169852	0.389511	0.267684	0.118203	0.15411
15	0.266573	0.213867	0.138238	0.186863	0.362381	0.238282	0.105921	0.138459
16	0.277718	0.21577	0.130656	0.191759	0.386732	0.253974	0.158741	0.152775
17	0.25302	0.187995	0.10308	0.17583	0.368701	0.248284	0.122103	0.15943

Figure 7.7 Scaled data, from smallest jet (screen capture from MS-Excel®)

7.2   The Application of an ANN

The previous section described how the raw data were initially subject to an FFT before being subdivided into smaller regions, which were characterised by their peak, mean, standard deviation and sum of amplitudes before finally being normalised. This has all been necessary to supply an ANN with data that most significantly characterises a specific leak size. Even though this has been performed in a logical and systematic manner, it does not guarantee a successful outcome from the ANN. Section 3.5 has presented many different ANN options from network types such as feed forward or recurrent to specific network such as Self Organising Map.

This section will apply the data to a variety of different network types and review the success of each network.

In order to process data through an ANN it must first be subdivided into three categories known as training, validation and test. The percentage split is variable, but for the purposes of this report the 221 data items have been allocated; 70% for training, 15% for validation and 15% for test. Each time the network is trained the data are randomly allocated to each set. Some of the training runs have different percentage splits but the network still achieved a very close level of success. The purpose of changing the training percentage is to demonstrate the robustness of the ANN. Matlab™ has a built in facility to perform this percentage split on the input data. Assuming the data converges, the level of success is presented to the user through a confusion plot. This plot is a function of the output of the Matlab™ ANN suite. The success is calculated by applying all 221 inputs to the network, of which it has trained on 70%. Therefore, if the network had overfitted the data, then a result of 70% would be expected. However, if it is able to generalise then a figure closer to 100% would be expected. To demonstrate that the level of success is repeatable, the training runs are performed ten times and an average taken. On each subsequent training run all the weights are cleared and the starting conditions randomised. Therefore, the 70% of data chosen for training previously will not be the same set of training data for the subsequent network.

7.2.1 Preliminary Results from Different Network Types

The first data to be trained in the neural network were from the pipe accelerometer, with the lagging fitted over the leak area. This has 221 rows of data and 13 different leak sizes. All of the networks in Table 7.1 were subject to the same data, but each time the network was trained the training set had different data. The number of hidden artificial neurons was initially varied, but in all cases the best performance was achieved with 16 nodes. Each ANN type was trained and then reset ten times, and the success during training recorded. The different types of network trialled were:

"newpr" – pattern recognition network (back propagation)

"newff" – feed forward back propagation network

"newlrn" – layered recurrent network, developed from the Elman network

"newfit" – fitting network (back propagation).

ANN type	Success during training (%) (each column represents the outcome from training the network)											
	1	2	3	4	5	6	7	8	9	10	Av	Std
newpr	78.7	72.4	76.5	91.0	66.5	40.7	50.2	71.0	31.2	23.1	60.1	78.7
newff	95.9	97.7	96.8	95.5	97.7	94.6	99.5	96.8	96.8	95	96.6	1.5
newlrn	98.2	98.2	97.7	96.8	98.2	96.4	97.7	95.9	98.2	97.3	97.4	0.8
newfit	97.7	99.5	97.3	97.7	95.9	96.8	94.6	92.8	97.7	97.3	96.7	1.9

Table 7.1 Success from training data with different networks

The numbers shown in blue above (Table 7.1), represent the highest success for that particular network and those in plum the lowest, with those in red showing the average ANNs over the training runs.

From Table 7.1 it can be seen that three out of the four ANNs trained very well. Therefore, from the three most successful ANNs the "newlrn" was chosen because it has the highest overall average, and lowest standard deviation. The poorest performing ANN of the three achieved a success of 95.9%, which was higher than the other two ANNs that both achieved 94.6%. However, the difference between all three ANN averages is less than 1% and consequently both the "newff" and "newfit" ANNs

should be considered as viable alternatives in the future. As the "newlrn" achieved the highest average, this is the ANN that will be used for the remainder of this report.
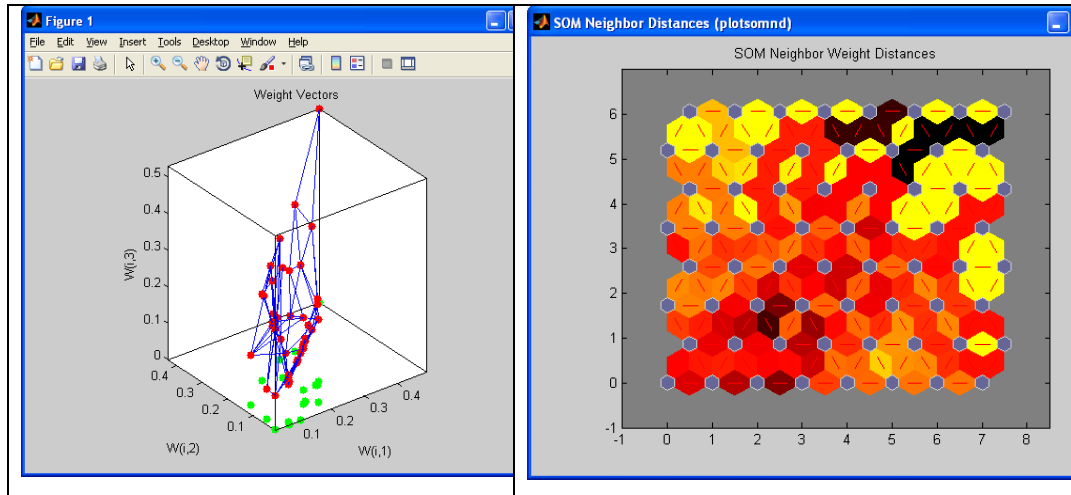
Figure 7.8 Plots from Self Organising Map network

The data were also analysed using the Self Organising Map (SOM). Figure 7.8 above shows the weight vectors and weight distances created by the network. The problem with this type of output is that it needs skilled interpretation but also there is no way of making a relationship between the size of leak and the relevant cluster.

7.2.2   Advantages of the Recurrent network

The main advantage the Elman network has over other feedforward networks is its ability to add a further degree of feature extraction. This is accomplished by taking the outputs from the hidden layer and storing these features in a context layer, which then becomes an input the hidden layer. Having this feedback path enables an Elman network to learn and recognise patterns in addition to generating temporal and spatial patterns. Temporal patterns have two components: the ordering of the component in a time series and the time duration of each component, (Wang (1996)). Recurrent networks also differ from feedforward networks because data can propagate in two directions: from input to output node and vice versa, whereas the later case cannot. Another type of recurrent network is the Jordan network, but unlike the elman network, takes the output from the output layer, as opposed to the hidden layer.

139

In general, for a feedforward network to compete with a recurrent network and its dynamic nature, it would need more input neurons, which infers more computation time and despite this would still be more susceptible to external noise, (Pham (1998)).

7.2.3   Training the Elman ANN

The following results and plots will show how successful the ANN is at training the data to achieve a high level of success. In all cases the data were trained using the Elman network with 17 sets of unique data per leak size. Of which there are 13 unique leaks separated by a flow rate of only 1.4 g/s. The number of artificial hidden neurons was set at 16. The ANN was trained with 70% training data, 15% validation and 15% test that came from the accelerometer mounted on the pipe, with lagging fitted.

The training is carried out using the Levenberg Marquardt (LM) algorithm, which applies a least squares curve fitting method, and through iterative steps modifying the damping term, the gradient and hence the error reach the goal close to zero, Kermani (2005). The LM algorithm has the advantage of being adaptive, because it is able to control its own damping. It can increase the damping if the step fails to reduce the error, otherwise the damping reduces. Therefore, when the error is far away from the minimum, the slow descent approach is used, but when the minimum is close, fast convergence is applied, Lampton (1997).

The ANN learns by calculating the weight change for a particular neuron based upon:

- The neurons input
- The neurons error
- The bias weight
- Learning rate
- Momentum constant

Figure 7.9 below shows the training screen presented by Matlab™ when the ANN is training on the input data. The training is stopped when the validation error increases for 6 epochs, and this occurred after 20 iterations. The network trained for 1.22 minutes and its training performance improved from the initial 1.02 mean square error (mse) to 0.0047 mse over this period. The damping factor (mu) finishes at 0.001. The best validation performance was achieved after 20 epochs with a resultant value of 0.01562 mse, shown in Figure 7.10.
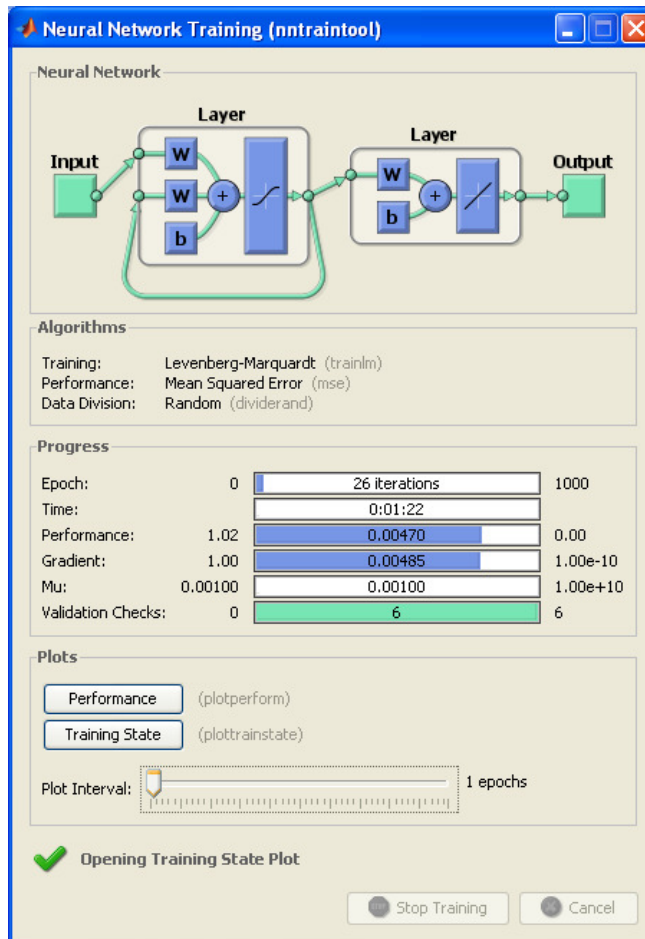
Figure 7.9 Neural Network Training
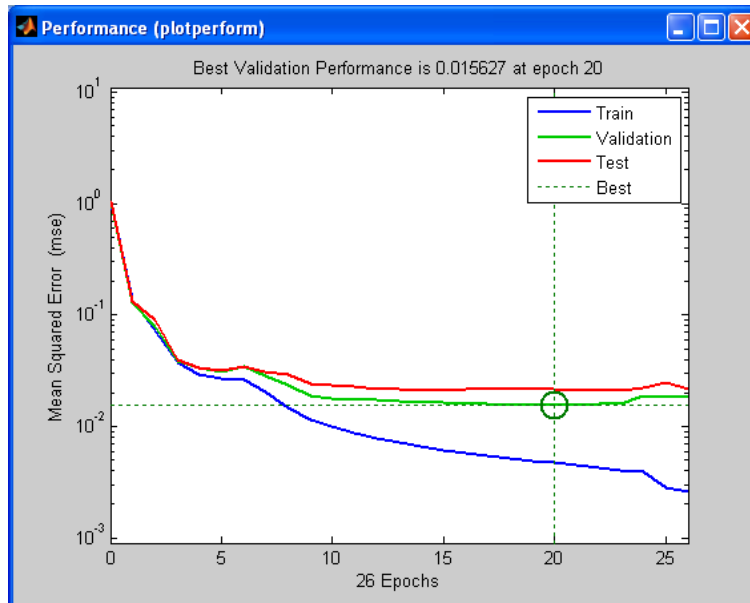
Figure 7.10 Performance plot

The success of the ANN can be assessed when all the inputs are used on the trained ANN, and the percentage output examined in the form of a confusion matrix, as shown in Figure 7.11.
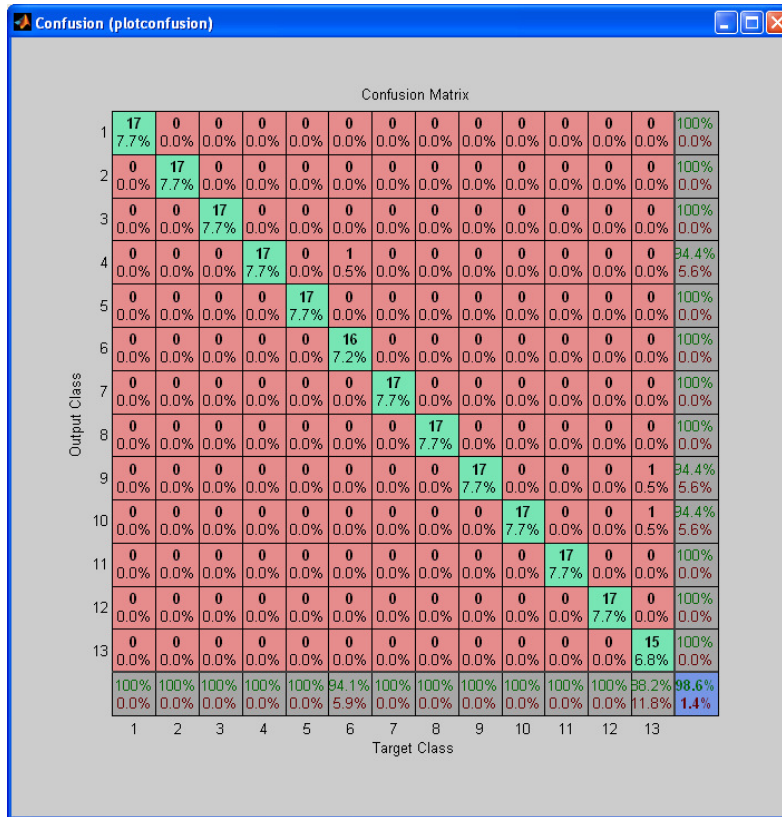
Figure 7.11 Confusion Matrix, showing the success of the ANN

The confusion plot in Figure 7.11 shows the percentage accuracy of the network when classifying each leak size. The axes show 13 output and target classes, which correspond with the 13 leak sizes, and above each leak number is the accuracy of the classification. Target class 13 is the smallest leak and 15 out the 17 inputs are correctly specified, thus giving that leak size an 88.2% accuracy. When all the errors are combined the above ANN misclassifies 1.4% of the inputs.

7.2.4 Interpretation of Confusion Matrix

The confusion matrix is a convenient and easy way to interpret the output from an ANN, as shown in Figure 7.12. It shows the target and output classes on their respective axis. The diagonal squares shown in green represent the correct prediction. Each column represents a leak size and because of the construction of the target data,

142

target class 13 refers to the smallest leak and 1 the largest. Because there are 17 inputs for each leak size, if the green square states 17 then all its predictions are correct. Each correct prediction is 0.45% and therefore if the ANN correctly predicts all 17 inputs for a particular leak size, then the final value in the green square is 7.7%. When the ANN makes an incorrect diagnosis it will either reside above or below the green diagonal. Figure 7.12 shows that on the 10th column one prediction states it is a larger leak than expected, but in addition two of the predictions are below the diagonal and consequently smaller leaks. Despite the inaccurate predictions, the ANN has still made 14 out if the 17 correct diagnosis which equates to an accuracy of 82.4%. This level is still sufficient to support the prediction made. It would be unrealistic to expect the ANN to achieve 100% accuracy at all times, when there are so many external noise factors that the accelerometers could pick up and distort the signal.
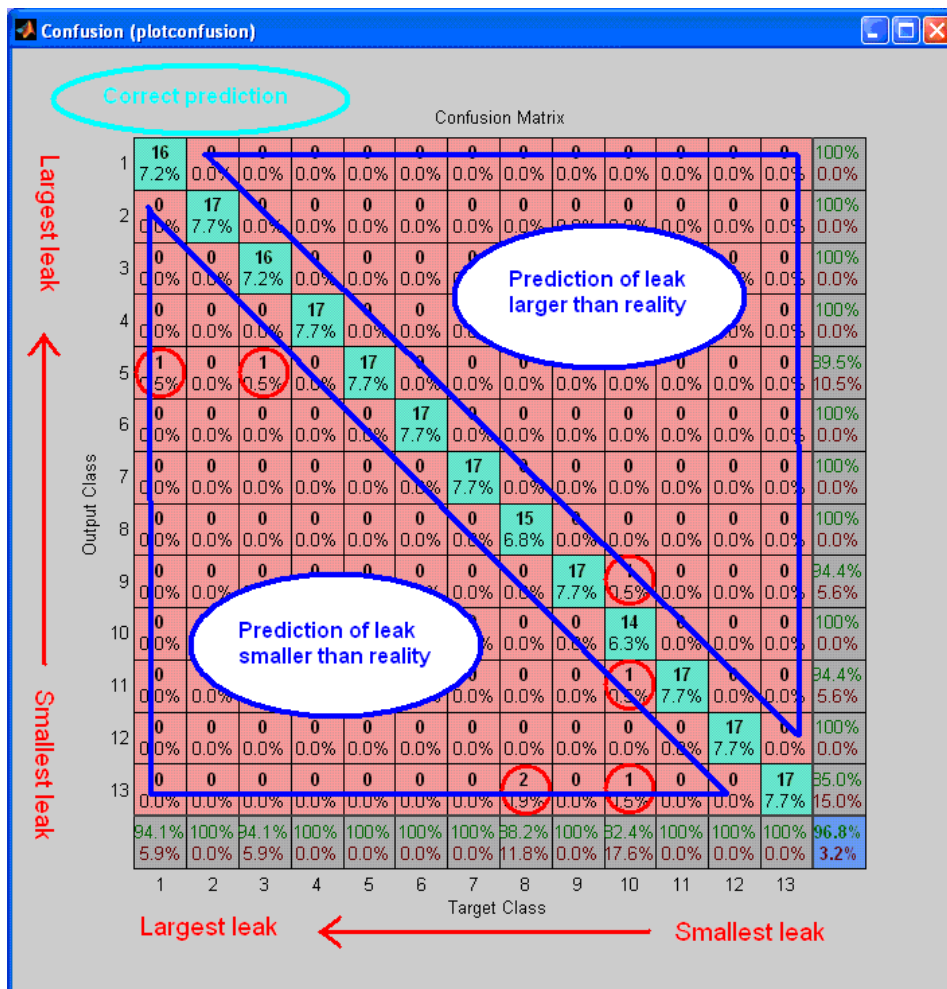
Figure 7.12 Interpretation of confusion matrix

7.2.5 Measuring the Success of an ANN

Table 7.1 showed that on average that the Elman Recurrent network could accurately classify data 97.4% of the time. The data in Table 7.2, allows the success of all three accelerometers to be examined. For clarification:

- Acc1 represents the accelerometer on the pipe
- Acc2 is the accelerometer in the centre of the lagging (immediately above the leak)
- Acc3 is the accelerometer at the end of the lagging.

ANN input	Success during training (%) (each column represents the outcome from training the network)											Train /val /test
	1	2	3	4	5	6	7	8	9	10	Av	
Acc1	93.7	95.5	94.6	93.2	96.4	96.4	95	95	87.8	95.9	94.3	60
Acc1	98.2	98.2	97.7	96.8	98.2	96.4	97.7	95.9	98.2	97.3	97.4	70
Acc1	98.6	97.7	98.2	99.5	99.5	99.1	96.8	99.5	98.6	97.3	98.5	80
Acc2	93.2	95	86.9	95.5	95.5	95.5	95	95.5	97.7	93.7	94.3	60
Acc2	97.3	97.3	96.4	97.7	95.5	95.5	94.6	98.6	95.5	95.9	96.4	70
Acc2	96.8	99.1	97.3	97.3	98.2	96.8	97.3	98.2	96.4	98.2	97.5	80
Acc3	97.7	95.5	98.2	92.8	96.4	97.3	97.7	95.9	95.5	97.7	96.4	60
Acc3	98.6	98.2	97.7	97.3	98.6	99.1	98.2	98.6	97.7	97.7	98.2	70
Acc3	98.2	99.1	97.3	99.1	99.1	99.1	99.5	99.5	97.3	99.5	98.8	80
Acc1 NL	96.4	93.7	93.2	91.9	95.5	94.6	93.7	93.7	96.8	94.1	94.3	60
Acc1 NL	95.0	97.7	96.8	98.2	97.7	89.6	94.1	95.0	98.6	96.4	95.9	70
Acc1 NL	96.8	99.5	99.5	96.8	99.1	94.1	95.5	99.1	98.2	97.3	97.6	80
Key: 60 represents: 60% of data for training, 20% for validation and 20% for testing 70 represents: 70% of data for training, 15% for validation and 15% for testing 80 represents: 80% of data for training, 10% for validation and 10% for testing NL refers to no lagging fitted												

Table 7.2 Success of ANN

The first six rows of Table 7.2 show the success of training the data when the lagging is fitted, and the final two rows show the success on an un-lagged pipe. In both cases Acc1 is in the same position and is the same sensor and the only difference is whether the lagging is fitted or not. The only other variable altered during the test was the percentage split between the training, validation and test. This percentage is split on a set of input data containing 221 rows.

The numbers shown in blue in Table 7.2 represent the highest success for that particular network and those in plum the lowest, with those in red showing the average value over the ten training runs.

It can be seen from Table 7.2 that as the amount of training data increases, the level of success also improves. However, a compromise must be met because too much training could cause overfitting, but the lack of available input data necessitates a high level of training. Therefore, using 70% for training and using the remaining for validation and test still achieves a high level of success. Table 7.2 does provide evidence that the network is robust because reducing the amount of training data by over 20% only causes a worst case deteriation of 4.2% and in the best case 2.4%.

7.2.6 Adding Outlier Data

The data used in the previous section were captured several seconds after the water pump had stopped, and before the pressure in the system had dropped below 90 bar. In order to assess the strength of the ANN, each leak size in this section has an additional 5 rows of data added, and the ANN is retrained with these new data. This new outlier data are taken closer to the point in time at which the pump was turned off and therefore they may contain residual vibrations from the rig, but conversely the pressure may have dropped slightly below 90 bar. Consequently, the ANN was previously given 221 rows of input data and it has now been extended to 286. In all cases 70% of the data was used for training.

ANN Input (286)	Success during training (%) (each column represents the outcome from training the network)											
	1	2	3	4	5	6	7	8	9	10	Av	Std
Acc1	97.2	97.9	96.2	97.6	96.5	97.2	98.3	98.6	96.9	95.5	97.2	1.0
Acc2	93.4	90.9	91.6	93.4	93.4	90.2	94.1	87.4	94.4	95.5	92.4	2.4
Acc3	94.1	89.5	91.3	89.5	94.8	90.9	90.9	92.3	90.2	90.2	91.4	1.8

Table 7.3 Success of ANN with outlier data

ANN Input	Number of inputs 221		Number of inputs 286		
	Success during training (%)				Percentage change
	Average	Std	Average	Std	
Acc1	97.4%	0.8	97.2%	1.0	0.2%
Acc2	96.4%	1.2	92.4%	2.4	4%
Acc3	98.2%	0.6	91.4%	1.8	6.8%

Table 7.4 Effect of adding outlier data on network performance

Table 7.4 shows how the addition of outlier data has an affect on the overall system performance. Accelerometer 1, fitted to the pipe has the least effect from outlier data with only 0.2% variation. However, Accelerometer 2 and 3 are most affected and this might be because the steam pressure change is directly applied onto the lagging, and as these accelerometers are fitted to the lagging the effect is more prominent.

7.2.7 Effect of Reducing Input Parameters to ANN

Figure 7.2 showed how the frequency plot for one leak at one size was broken down into five smaller sub areas, called columns. These sub areas were further investigated and four parameters extracted from each area. These being the mean, standard deviation, peak and sum. Table 7.2 showed that a set of inputs from 13 leaks ranging between 12 g/s (40 l/h) and 29 g/s (100 l/h) could be characterised and achieve an overall success in excess of 95%. Table 7.5 aims to discover which columns or data items from Figure 7.2 are the most important in achieving a good success rate. In order to do this, columns of data or data items are removed and the network retrained, the resultant success then illustrated.

Data item removed	Success during training (%) (each column represents the outcome from training the network)					Standard deviation	Average %
None	95	98.6	97.7	98.2	96.4	1.5	97.2
Column 4	96.4	95.9	98.2	96.8	97.7	0.9	97
Column 3	96.8	95.9	96.8	98.2	95.9	0.9	96.7
Column 1	96.4	96.4	95.5	96.8	94.1	1.1	95.8
Column 2	93.7	92.8	97.7	94.1	96.4	2.0	94.9
Column 5	94.1	86.9	97.7	96.4	95.9	4.3	94.2
Col 4,5	88.2	91.9	90.5	87.8	92.8	2.2	90.2
Col 1,4,5	87.3	90	88.7	92.3	90.5	1.9	89.8
Col 1,2	91	78.7	91	88.7	87.3	5.1	87.3
Col 1,2,3	90	82.8	87.3	88.7	87.3	2.7	87.2
Col 1,2,4	85.5	80.1	78.7	89.1	81	4.3	82.9
Col 1,2,3,4	81	78.7	72.4	86.4	86.9	6.0	81.1
Col 1,2,4,5	71.5	70.6	74.2	65.2	75.6	4.0	71.4
Col 1,2,3,5	60.2	70.1	73.3	68.3	51.6	8.8	64.7
Col 2,3,4,5	54.3	49.8	55.2	50.7	59.3	3.8	53.8
Col 1,3,4,5	49.3	52	56.1	50.2	43	4.8	50
Peak	97.7	98.2	93.7	96.8	95.9	1.8	96.4
Std	95.5	96.8	93.7	95.9	94.1	1.3	95.2
Sum	91.4	94.1	91.4	91	96.8	2.5	92.9
Mean	93.2	96.8	91.4	90.5	92.3	2.5	92.8

Table 7.5 Effect of removing data from ANN input (acc1 lagged)

Table 7.5 shows the effect of removing columns and individual data items to discover which sub areas define the leak characteristic, and thus ensure the ANN achieves a high level of success. To further explain, in the first column the third row is entitled 'Column 4', this means that from the five original columns in Figure 7.2, the fourth column of data is removed. This column would have contained the mean, standard deviation, peak and sum for all the 221 inputs. Therefore, the network is now training on an input matrix that is 221 x 16, opposed to the original 221 x 20. To further reiterate the principle, the first column last row is entitled 'Mean', this would have

originally held all the average values for each column. However, because this data item is removed, the network is now training on an input matrix that is 221 x 15, opposed to the original 221 x 20, and only using the standard deviation, peak and sum to train with.

When reviewing Table 7.5, the last column does not present any values that are significantly higher or lower than their neighbours. Had this been the case it would have provided an indication of which column or data item is having a more significant effect when the network is being trained. Consequently, a more in depth study is required to analyse the data. It can be seen that by removing individual or multiple columns does not make a significant difference on the final average value, illustrated in the last column. The lowest recorded percentage average shown in Table 7.5 was 50%, and this occurred when the network was only trained on column 2. Column 2 represents the frequency bandwidth that is adjacent to column 3 that has the highest amplitude and activity, and therefore this result was not expected. However, when the confusion plot is examined (Figure 7.13), it is only jet sizes 15 cc/min, 25 cc/min, 27.5 cc/min, 30 cc/min and 32.5 cc/min that have any appreciable data in the area, thus suggesting the low success.

Confusion Matrix

Output Class	1	2	3	4	5	6	7	8	9	10	11	12	13	
1	8 / 3.6%	1 / 0.5%	1 / 0.5%	0 / 0.0%	0 / 0.0%	0 / 0.0%	4 / 1.8%	4 / 1.8%	0 / 0.0%	0 / 0.0%	0 / 0.0%	1 / 0.5%	0 / 0.0%	42.1% / 57.9%
2	0 / 0.0%	7 / 3.2%	3 / 1.4%	0 / 0.0%	0 / 0.0%	0 / 0.0%	0 / 0.0%	1 / 0.5%	0 / 0.0%	0 / 0.0%	0 / 0.0%	1 / 0.5%	0 / 0.0%	58.3% / 41.7%
3	0 / 0.0%	0 / 0.0%	0 / 0.0%	0 / 0.0%	0 / 0.0%	0 / 0.0%	0 / 0.0%	0 / 0.0%	0 / 0.0%	0 / 0.0%	0 / 0.0%	1 / 0.5%	0 / 0.0%	0.0% / 100%
4	0 / 0.0%	1 / 0.5%	7 / 3.2%	16 / 7.2%	0 / 0.0%	0 / 0.0%	0 / 0.0%	0 / 0.5%	0 / 0.0%	0 / 0.0%	0 / 0.0%	4 / 1.8%	9 / 4.1%	42.1% / 57.9%
5	2 / 0.9%	5 / 2.3%	3 / 1.4%	0 / 0.0%	17 / 7.7%	0 / 0.0%	0 / 0.0%	6 / 2.7%	0 / 0.0%	5 / 2.3%	0 / 0.0%	4 / 1.8%	5 / 2.3%	36.2% / 63.8%
6	0 / 0.0%	0 / 0.0%	0 / 0.0%	0 / 0.0%	0 / 0.0%	17 / 7.7%	0 / 0.0%	0 / 0.0%	0 / 0.0%	0 / 0.0%	0 / 0.0%	0 / 0.0%	0 / 0.0%	100% / 0.0%
7	7 / 3.2%	2 / 0.9%	0 / 0.0%	0 / 0.0%	0 / 0.0%	0 / 0.0%	13 / 5.9%	3 / 1.4%	0 / 0.0%	0 / 0.0%	0 / 0.0%	2 / 0.9%	0 / 0.0%	48.1% / 51.9%
8	0 / 0.0%	1 / 0.5%	1 / 0.5%	0 / 0.0%	0 / 0.0%	0 / 0.0%	0 / 0.0%	1 / 0.5%	0 / 0.0%	0 / 0.0%	0 / 0.0%	2 / 0.9%	0 / 0.0%	20.0% / 80.0%
9	0 / 0.0%	0 / 0.0%	0 / 0.0%	0 / 0.0%	0 / 0.0%	0 / 0.0%	0 / 0.0%	0 / 0.0%	9 / 4.1%	6 / 2.7%	1 / 0.5%	0 / 0.0%	0 / 0.0%	56.3% / 43.8%
10	0 / 0.0%	0 / 0.0%	0 / 0.0%	0 / 0.0%	0 / 0.0%	0 / 0.0%	0 / 0.0%	0 / 0.0%	0 / 0.0%	2 / 0.9%	1 / 0.5%	1 / 0.5%	0 / 0.0%	50.0% / 50.0%
11	0 / 0.0%	0 / 0.0%	0 / 0.0%	0 / 0.0%	0 / 0.0%	0 / 0.0%	0 / 0.0%	0 / 0.0%	8 / 3.6%	3 / 1.4%	15 / 6.8%	0 / 0.0%	0 / 0.0%	57.7% / 42.3%
12	0 / 0.0%	0 / 0.0%	1 / 0.5%	0 / 0.0%	0 / 0.0%	0 / 0.0%	0 / 0.0%	1 / 0.5%	0 / 0.0%	0 / 0.0%	0 / 0.0%	1 / 0.5%	0 / 0.0%	33.3% / 66.7%
13	0 / 0.0%	0 / 0.0%	1 / 0.5%	1 / 0.5%	0 / 0.0%	0 / 0.0%	0 / 0.0%	0 / 0.0%	0 / 0.0%	1 / 0.5%	0 / 0.0%	0 / 0.0%	3 / 1.4%	50.0% / 50.0%
	47.1% / 52.9%	41.2% / 58.8%	0.0% / 100%	94.1% / 5.9%	100% / 0.0%	100% / 0.0%	76.5% / 23.5%	5.9% / 94.1%	52.9% / 47.1%	11.8% / 88.2%	88.2% / 11.8%	5.9% / 94.1%	17.6% / 82.4%	49.3% / 50.7%

Target Class (columns 4: 32.5cc/min, 5: 30cc/min, 6: 27.5cc/min, 7: 25cc/min, 11: 15cc/min)

Figure 7.13 Removing column 1, 3, 4 & 5 from input network

Training on single columns produced some very interesting results. In particular, by removing columns 1, 2, 3 and 4, and only training the network on the last column, the network achieved a success of 81.1% on average. However, conversely when the network was trained with only columns 1, 2 and 3 (denoted by removing columns 4 and 5), the ANN achieved a 90.2% success. This perhaps shows that all the columns across the frequency spectrum have a contribution and no one column can achieve a better result than using all available data.

Therefore, in summary despite the amount of activity shown in column 3 on Figure 7.2, all the other columns contribute in some way depending upon the size of leak. Therefore, this reinforces the decision to sub-divide the FFT plot into these five distinct areas, and as previously shown, works well with the other accelerometers that are placed at different locations from the leak.

The decision to subdivide the FFT spectrum into five discrete areas was devised because the individual accelerometers all have unique spectra and fundamental frequencies (peak amplitude signal).

Therefore, with reference to Figure 7.14 it can be seen that the predominant amplitudes of:

- Acc1 are in column 3
- Acc2 are in column 1 & 2
- Acc3 are in column 2.

This pattern is repeated throughout all the jet sizes, however the sideband frequencies of column 4 and 5 become more significant as the jet sizes change. This can be observed in Figure 6.20, which shows the frequency spectrum of all three accelerometers across the range of jet sizes.

The five column configuration used has proved to be successful, however a sixth column could conceivably be added as Figure 7.14 shows there is information also contained here. The main reasons for its exclusion were because it was nearing the maximum bandwidth that the data acquisition device could function at. Also, the frequency response of the accelerometer shows a peak above 20kHz. However, because absolute levels of amplitude are not used, a sixth column could be considered in future work. The frequency response of the accelerometer is shown in Appendix G.

Different mathematical functions could also be applied to the column data. All of these ideas should be considered for future work.
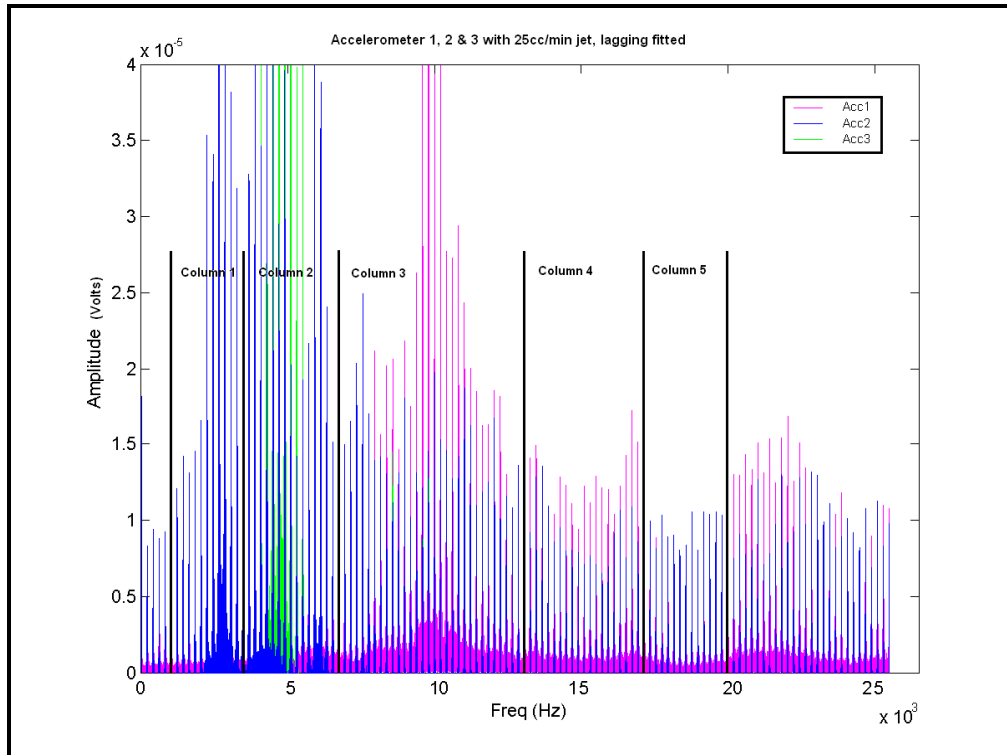
Figure 7.14 The association between column and accelerometer

7.2.8   Investigating the Training Method

Figure 7.15 shows a section of the MS-Excel® sheet used as the input data to train the ANN. The blue, pink and yellow rows represent the last three data items from column 2 with a 20 cc/min jet. This jet is compared against the light blue, plum and brown rows from the 22.5 cc/min jet. The comparison of the data values is shown in the MS-Excel® graph in Figure 7.15. The difference between the data items is how the ANN learns to differentiate between one leak size and another. The distinction is more apparent on the graph, showing the differences in amplitude for that column between adjacent jet sizes when examining the mean, std, peak and sum. All the amplitudes for the 20 cc/min jet are lower than the 22.5 cc/min jet as shown in Figure 7.2. Taking into account that there is a further four columns with similar differences and another 14 rows of data available per jet, it becomes clearer how the ANN is able to differentiate between leak sizes.

150

		Column 2				Column 3				
		Mean	STD	Peak	Sum					
0.0821	0.1204	0.148581	0.069551	0.02588	0.032944	0.290804	0.205613	0.089945	0.177022	
0.087866	0.107141	0.182513	0.085195	0.023631	0.034806	0.322561	0.230468	0.120298	0.169959	
0.07724	0.044999	0.34585	0.214817	0.080697	0.116511	0.272937	0.15868	0.049162	0.086068	
0.032435	0.04992	0.289585	0.187379	0.06458	0.114744	0.235502	0.143582	0.079798	0.100573	20 cc/min jet
0.050204	0.057293	0.325399	0.195959	0.087524	0.128872	0.270443	0.163926	0.100849	0.099985	
0.032516	0.042865	0.339354	0.214182	0.107058	0.115314	0.257073	0.16119	0.101322	0.090024	
0.122757	0.057189	0.3218	0.186172	0.098032	0.118429	0.191733	0.122326	0.082815	0.09936	
0.239916	0.286724	0.822035	0.801262	0.389572	0.579015	0.410678	0.369713	0.264883	0.233606	
0.227452	0.303399	0.839494	0.710137	0.342734	0.530756	0.416347	0.346988	0.222391	0.219999	
0.170035	0.262329	0.673203	0.64014	0.317313	0.546715	0.36357	0.332574	0.2166	0.240982	22.5 cc/min jet
0.185995	0.24483	0.680386	0.542336	0.267678	0.411223	0.380956	0.317962	0.168366	0.207863	
0.110488	0.217755	0.632837	0.554559	0.351314	0.424476	0.338097	0.29639	0.157344	0.191371	
0.125418	0.182831	0.597711	0.520198	0.294664	0.344937	0.337616	0.276834	0.169916	0.184981	
0.156043	0.188337	0.540133	0.448658	0.216337	0.325024	0.321387	0.255983	0.188187	0.187581	
0.152221	0.180624	0.536342	0.418164	0.243434	0.283742	0.341864	0.277024	0.281944	0.184082	
0.177103	0.182856	0.51179	0.414204	0.191124	0.257746	0.351756	0.290935	0.215618	0.170109	
0.158763	0.178476	0.506396	0.397824	0.182322	0.236543	0.322315	0.274555	0.161037	0.164296	
0.222507	0.193687	0.486288	0.36949							
0.100379	0.181945	0.414969	0.28814							
0.233131	0.31591	0.681286	0.60457							
0.296108	0.28231	0.722521	0.62435							
0.146709	0.256204	0.64381	0.52883							
0.215305	0.262012	0.666394	0.50210							
0.150306	0.209909	0.56949	0.39151							
0.342866	0.446835	0.691829	0.62004							

Figure 7.15 Mechanism used by ANN to determine leak size

The profile of the MS-Excel® chart in Figure 7.15 is not representative of all the columns and adjacent jet sizes. Figure 7.16 shows a very different graph profile to Figure 7.15. In this example, the comparison is between the 37.5 cc/min jet and 40 cc/min jet in column 4. The two jets show that their respective values are in close relation to each other, but this profile has a crossover point between the standard deviation and peak values. This distinct change in data values will make the training easier for the ANN as the boundary conditions will be more distinct.

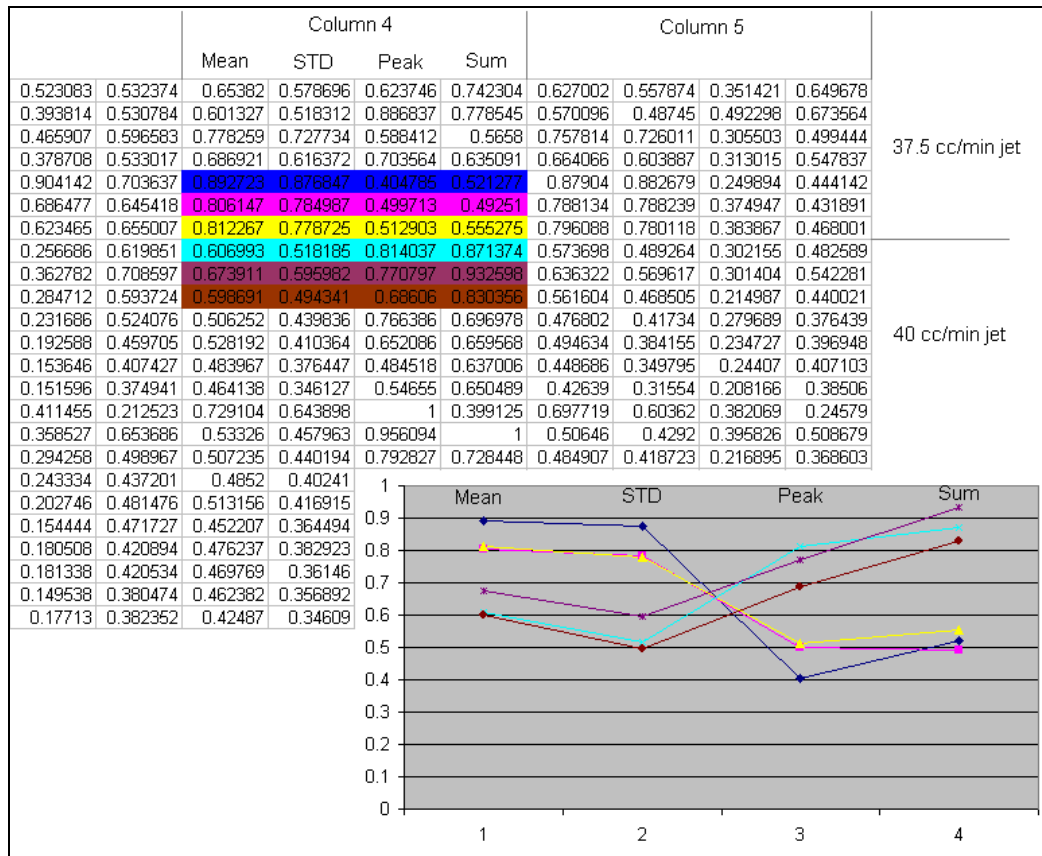|		Column 4				Column 5				
		Mean	STD	Peak	Sum					
0.523083	0.532374	0.65382	0.578696	0.623746	0.742304	0.627002	0.557874	0.351421	0.649678	
0.393814	0.530784	0.601327	0.518312	0.886837	0.778545	0.570096	0.48745	0.492298	0.673564	
0.465907	0.596583	0.778259	0.727734	0.588412	0.5658	0.757814	0.726011	0.305503	0.499444	37.5 cc/min jet
0.378708	0.533017	0.686921	0.616372	0.703564	0.635091	0.664066	0.603887	0.313015	0.547837	
0.904142	0.703637	0.692728	0.876847	0.404785	0.521277	0.87904	0.882679	0.249894	0.444142	
0.686477	0.645418	0.806147	0.784987	0.499713	0.49251	0.788134	0.788239	0.374947	0.431891	
0.623465	0.655007	0.812267	0.778725	0.512903	0.555275	0.796088	0.780118	0.383867	0.468001	
0.256686	0.619851	0.606993	0.518185	0.814037	0.871374	0.573698	0.489264	0.302155	0.482589	
0.362782	0.708597	0.673911	0.595982	0.770797	0.932598	0.636322	0.569617	0.301404	0.542281	
0.284712	0.593724	0.598691	0.494341	0.68606	0.830356	0.561604	0.468505	0.214987	0.440021	
0.231686	0.524076	0.506252	0.439836	0.766386	0.696978	0.476802	0.41734	0.279689	0.376439	40 cc/min jet
0.192588	0.459705	0.528192	0.410364	0.652086	0.659568	0.494634	0.384155	0.234727	0.396948	
0.153646	0.407427	0.483967	0.376447	0.484518	0.637006	0.448686	0.349795	0.24407	0.407103	
0.151596	0.374941	0.464138	0.346127	0.54655	0.650489	0.42639	0.31554	0.208166	0.38506	
0.411455	0.212523	0.729104	0.643898	1	0.399125	0.697719	0.60362	0.382069	0.24579	
0.358527	0.653686	0.53326	0.457963	0.956094	1	0.50646	0.4292	0.395826	0.508679	
0.294258	0.498967	0.507235	0.440194	0.792827	0.728448	0.484907	0.418723	0.216895	0.368603	
0.243334	0.437201	0.4852	0.40241							
0.202746	0.481476	0.513156	0.416915							
0.154444	0.471727	0.452207	0.364494							
0.180508	0.420894	0.476237	0.382923							
0.181338	0.420534	0.469769	0.36146							
0.149538	0.380474	0.462382	0.356892							
0.17713	0.382352	0.42487	0.34609							

Figure 7.16 The method by which the ANN trains on the input data

7.2.9 Examination of Errors in Confusion Matrix

Figure 7.17 shows the confusion matrix that is created by the ANN to review the success of the network. It does this by applying all the input data to the network it has just trained on and then presents percentages for each target item and an overall success for the network. When examining the bottom scale of the diagram, column 1 represents the largest leak (100 l/h) and column 13 (40 l/h) the smallest, and each increment is 5 l/h. Target column 10 is a 55 l/h (17.5 cc/min jet) and it has identified two leaks as being smaller (50 l/h and 40 l/h) and one larger (60 l/h). The reason target/column 13 represents the smallest leak size and 1 the largest is because of the construction of the input data matrix to the ANN.
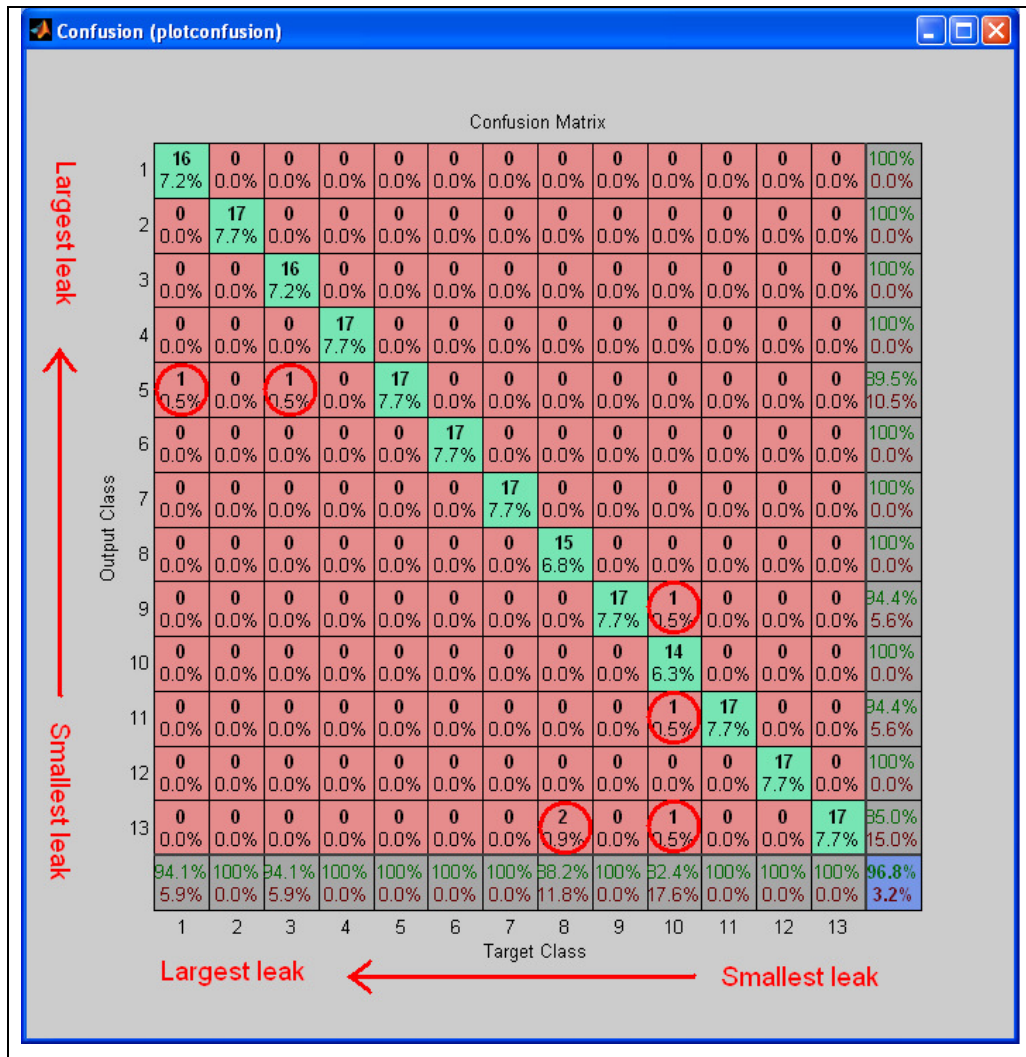
Figure 7.17 Errors in Confusion matrix

Despite the high success of the ANN, errors still exist. Figure 7.17 shows that 9 out of the 13 leaks were 100% correct (as indicated by the bottom row of numbers in green), however 4 jets had some errors. Column 10 had the highest number of errors with 3 wrong from the 17 inputs, however column 8 has two errors, both predicting a leak far smaller than reality. Therefore, column 8 could be considered far more misleading. Recording an error of 11.8% on a leak size is acceptable, however when this system is scaled up with potentially hundreds of accelerometers on the primary circuit, the number of samples taken per accelerometer will reduce. Therefore, if only five samples were taken per accelerometer, then having two incorrect predictions would result in a leak size certainty of only 60%. To resolve this problem, should a leak scenario arise, the leak detection system could focus on the set of accelerometers directly surrounding the leak area and increase the sampling rate.

153

To further understand why column 8 should be misinterpreted by the network, the FFT plots of these leak sizes need reviewing as shown in Figure 7.18.
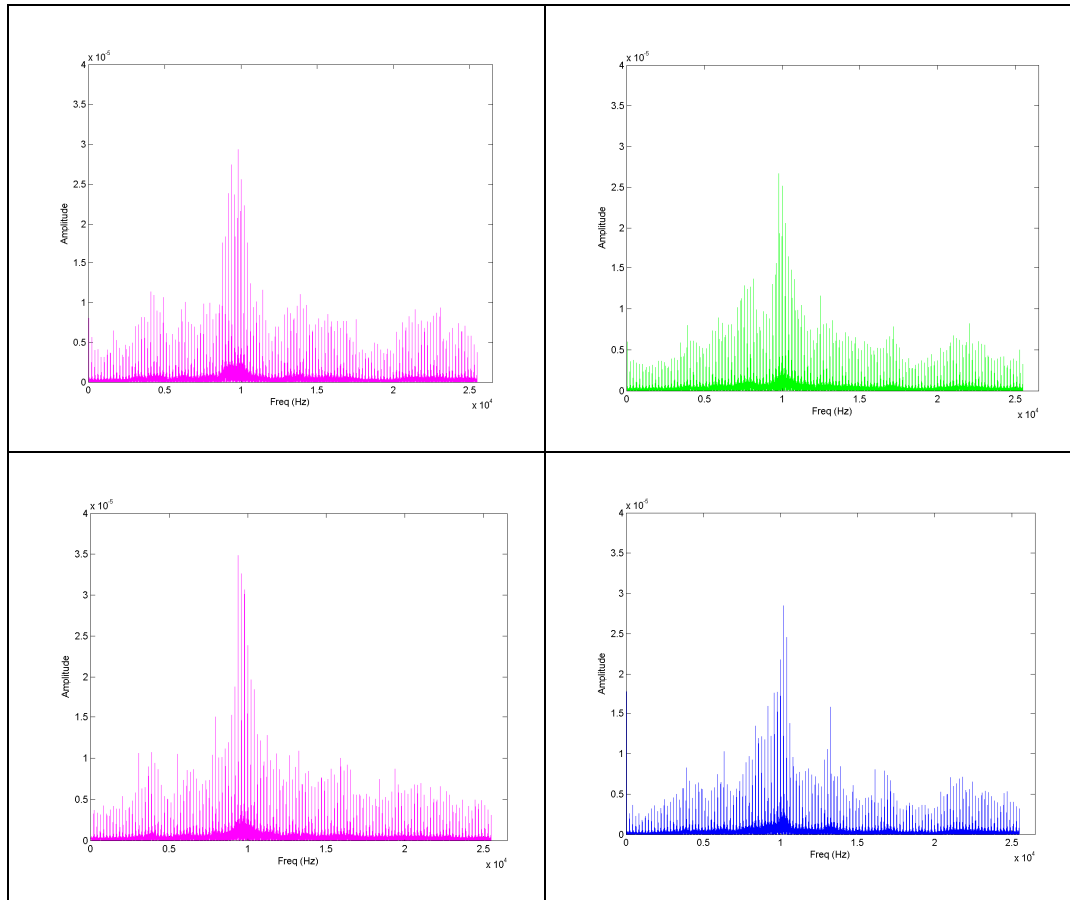

Figure 7.18 Comparison of FFT plots with similar profiles

The hand picked FFT plots in Figure 7.18 all represent profiles that have the closest resemblance to each other. Starting from the top left is the 17.5 cc/min jet, moving clockwise is the 20 cc/min, 15 cc/min and finally in the bottom left corner is the 10 cc/min jet. When the FFT plots from the 10 cc/min are examined there are occasional bursts of energy that emanate from the orifice, one of them is shown above, and this may illustrate why a much larger jet could interpret a 10 cc/min jet as being its equal. It might be that at this particular temperature and pressure combined with a very small orifice that standing waves are being produced before the orifice and this is might explain the bursts of energy that appear in some of the plots. If smaller jets had been available it would have been interesting to study the effect on a jet smaller than 10 cc/min, this would equate to a jet have an internal diameter less than 0.2 mm.

7.2.10 Addition of Noise

The input data from all three accelerometers have shown a high level of success when trained by the ANN. However, the signals recorded from the rig are purely due to the vibration from the steam leak. There is no corruption or distortion by any other signals. In the RC there will be sources of noise from the pumps, valves as well as the circulating fans. Therefore, random noise will be added to the pure signal until the network is unable to train on the data. This will give a measure of how much external noise the network can tolerate.
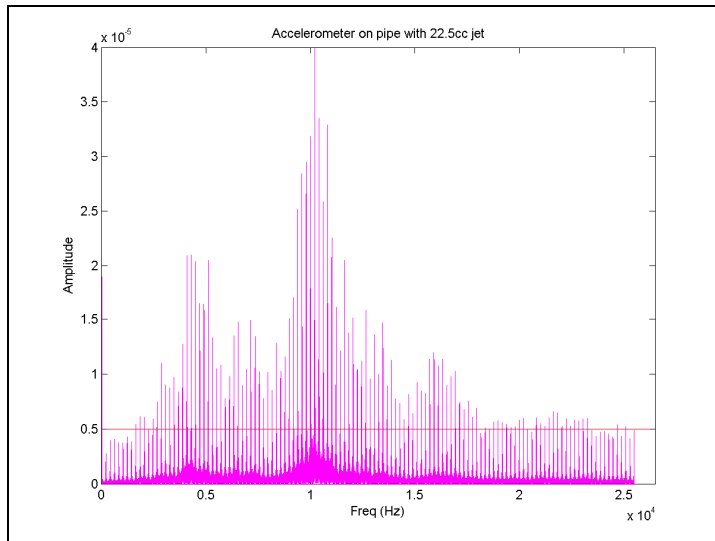

Figure 7.19 Graph to represent noise floor and maximum signal strength

If Figure 7.19 is considered a typical accelerometer plot, then it can be observed that the noise floor lies at about 0.5×10^{-5} volts (indicated by the red line), and the peak signal is at 4×10^{-5} volts. The noise floor refers to the residual level of noise in a system or the lowest usable signal level.

As a means of quantifying and computing the signal to noise (SNR) of this signal, two different methods are used:

$$SNR = \left(\frac{A_{signal}}{A_{noise}} \right)^2$$

Equation 17, computing signal to noise

Where A, denotes the amplitude of the signal or noise, in volts

155

$$SNR(dB) = 20\log\left(\frac{A_{signal}}{A_{noise}}\right) = 20\log\left(\frac{4\times10^{-5}}{0.5\times10^{-5}}\right) = 18dB$$

Alternatively:

Signal = 4×10^{-5}, which corresponds to dBV_{signal} = -88

Noise = 0.5×10^{-5}, which corresponds to dBV_{noise} = -106

SNR = Signal – Noise

    = -88 – (- 106)

    = 18dB

Therefore, 18dB signifies the signal to noise ratio measured from the rig. Adding noise to this signal will reduce this dB value. When the signal to noise equals 0, the signal and noise will be at equal amplitudes. The signal to noise levels are computed using the worst case smallest jet. Therefore, for each computed SNR level the larger jets have potentially a better SNR than the smaller ones. The following exercise will determine how much noise the ANN can accept before it can no longer train successfully.

In order to add noise to the signal, the following equation is used.

$Noise\_signal = original\_signal + var\,iance * (randn(size(original\_signal)))$

Equation 18 Adding random noise to signal

By selecting a variance of 0.003, it can be observed in Figure 7.21 that the noise floor increases to about 1×10^{-5} volts, from the original 0.5×10^{-5} volts shown in Figure 7.20. Therefore, by using Equation 18, the signal to noise is now 12dB.
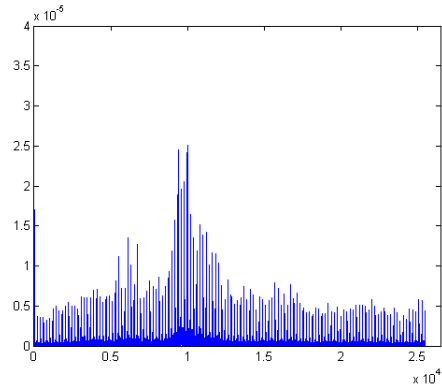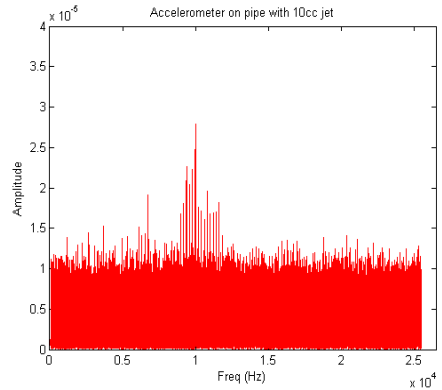
Figure 7.20 accelerometer on pipe, 10cc (SNR = 18dB)

Figure 7.21 Accelerometer on pipe with addition of noise (SNR=12dB)
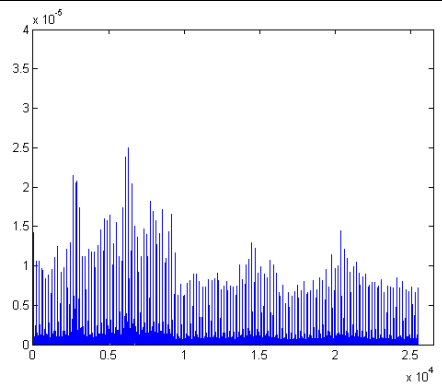

Figure 7.22 Accelerometer on Metlag, central position, 10cc (SNR = 18dB)
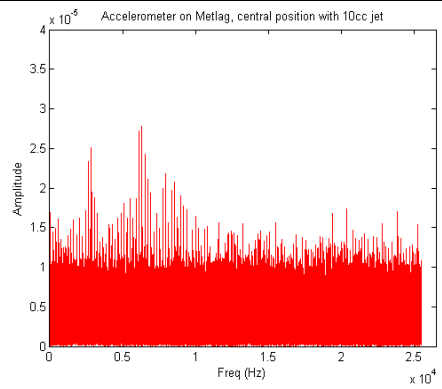

Figure 7.23 Accelerometer on Metlag, central position with added noise (SNR = 12dB)
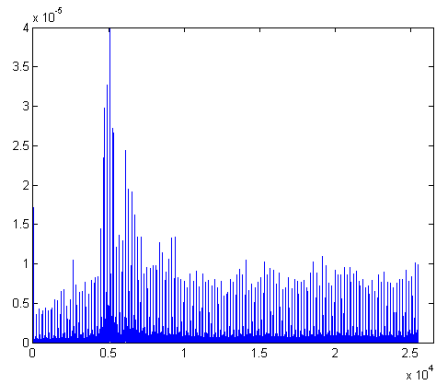

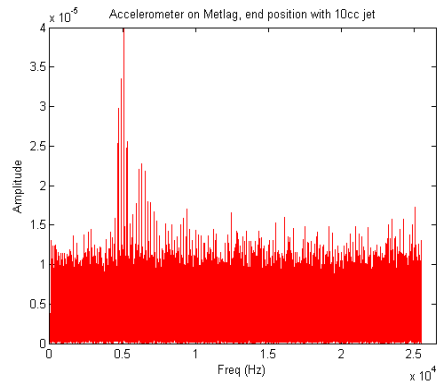**Figure 7.24 Accelerometer on Metlag, end position, 10cc (SNR = 18dB)**

Figure 7.25 Accelerometer on Metlag, end position with added noise (SNR = 12dB)

As the overall background noise level of the RC is not known, by increasing the white noise level, a threshold can be established for the ANN. There will be a point at which the lack of success of the ANN is unacceptable. If this system was going to be trialled on a working primary circuit of a nuclear reactor, then accelerometers would need to be placed on the Metlag and primary pipe and the background noise recorded. Table 7.6 shows the effect on the system by increasing the background noise level. The ANN was trained on Acc1 with lagging fitted and 70% training, 15% validation and 15% test data.

Acc1 S/N	Success during training (%) (each column represents the outcome from training the network)										
	1	2	3	4	5	6	7	8	9	10	Av
18dB	98.2	98.2	97.7	96.8	98.2	96.4	97.7	95.9	98.2	97.3	97.4
12dB	82.8	88.2	93.2	87.8	89.1	81.9	86.9	74.2	88.7	80.5	85.3
12dB	90.5	88.7	88.7	88.7	95.0	86.4	88.2	88.2	86.4	86.0	88.7
9dB	86.0	96.8	91.4	92.3	92.8	95.0	94.6	94.6	90.5	96.8	93.1
6dB	94.1	95.0	93.7	92.3	93.2	95.0	86.4	93.7	95.5	95.9	93.5
3dB	96.8	92.3	81.9	95.9	93.7	92.8	96.4	91.0	95.5	92.8	92.9
0dB	77.8	66.1	64.7	65.2	70.6	77.4	65.2	68.3	52.9	68.8	67.7

Table 7.6 Effect of adding noise on the system performance

When training with the 12dB signal to noise data, the jet sizes that the ANN performed poorly on were: the 10, 15 and 17.5 cc/min jets. This is because these jets correspond with the lowest FFT amplitudes, and increasing the noise floor completely removes any useful data that the network could train on.
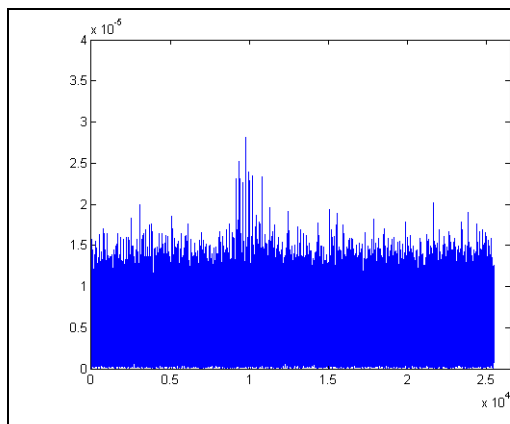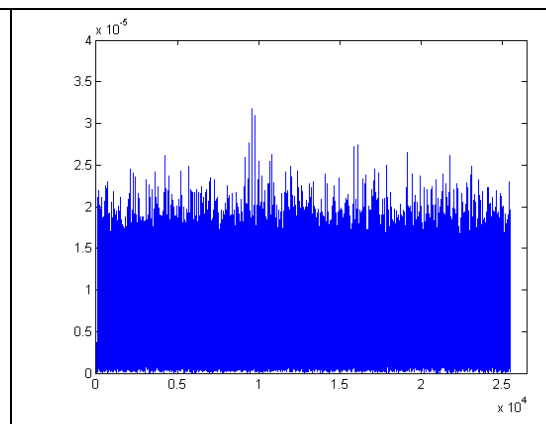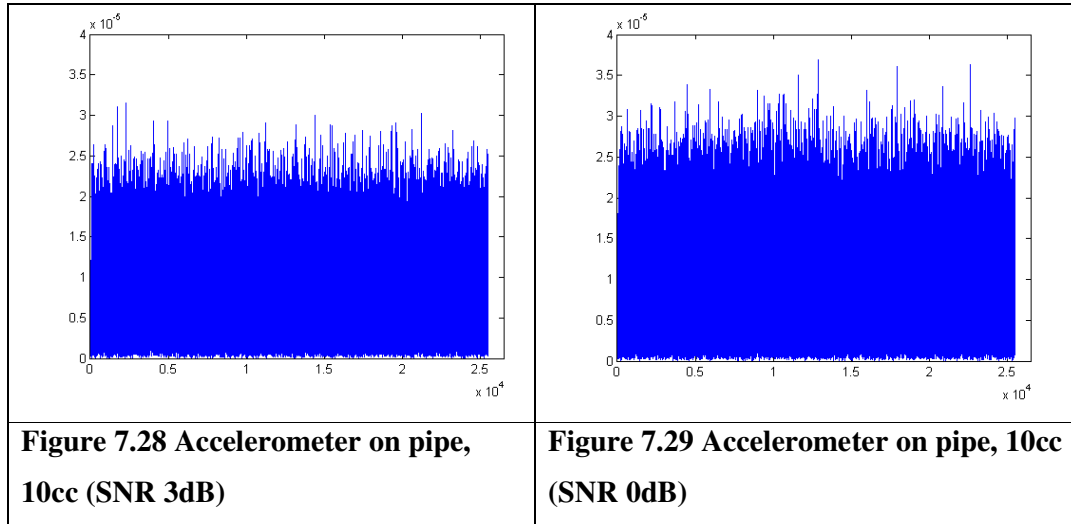

Figure 7.26 Accelerometer on pipe, 10cc (SNR 9dB)	**Figure 7.27 Accelerometer on pipe, 10cc (SNR 6dB)**

Figure 7.28 Accelerometer on pipe, 10cc (SNR 3dB)

Figure 7.29 Accelerometer on pipe, 10cc (SNR 0dB)

By increasing the variance to 0.004 in Equation 18, the noise level is increased to 1.4×10^{-5} volts (as shown in Figure 7.26), resulting in a SNR of 9dB. To achieve a SNR of 6dB the variance becomes 0.0055 and the noise level becomes 2×10^{-5} volts. By progressively increasing the background noise level, Table 7.6 shows that ANNs performance significantly degraded when the SNR was zero. Consequently, if the background level exceeds 3×10^{-5} volts or -90.4dBV then the use of accelerometers will be unsuitable for this application. The other temperature and humidity sensors could still be used, but the leak size information is not obtainable from these sensors. Assuming the RC compartment has an acceptably low background noise level, then this noise level would need to be acquired, and converted through a FFT, so that it resembled the same format as the original leak data. Then by combining the background noise for that particular accelerometer with the known leak size data, yields an expected data set for each leak size, similar to Figure 7.21. The network would then need retraining and this network saved for future reference.

7.3 Summary

Various different network types were trialled as discussed in section 7.1, but the Elman network was chosen because it maintained a consistently high level of performance. The method of pre-processing the raw data was discussed and then how the data are further processed as an input to the ANN. To test the robustness of the ANN, outlier data were added and the results reviewed. The input data to the network were examined and data items removed, the network was then retrained to gain an

159

understanding of the important input parameters. It was demonstrated how the ANN was able to train on the input data and make the distinctions between different leak sizes. Errors produced by the ANN were also examined and potential theories discussed. Finally noise was added to the signal in pre-determined steps until the ANN could no longer train successfully. This point at which the ANN fails to converge, dictates the highest threshold of background noise the network can tolerate. If the RC background noise is above this level then the accelerometers would be unusable.

Chapter 8

Operator Advisory System (GUI)

An operator advisory system (OAS) enables data to be presented to an operator conveying the state of a plant and offering advice if necessary. Complex mathematics may be used in the processing of the data, but through the use of a graphical user interface information is conveyed in a clear and concise manner. The system described in this chapter, can be navigated using simple buttons to view graphs, messages and the location of the leak in 3D. This enables a user to thoroughly interrogate the OAS. An OAS does not however, control the system which it is monitoring; it is there to provide information to a user to allow them to make an informed decision based on the evidence presented.

This OAS is the culmination of all the work to date, combining the inputs from three different types of sensor (accelerometer, thermocouple and humidity), and advising the operator of a leak detect situation.
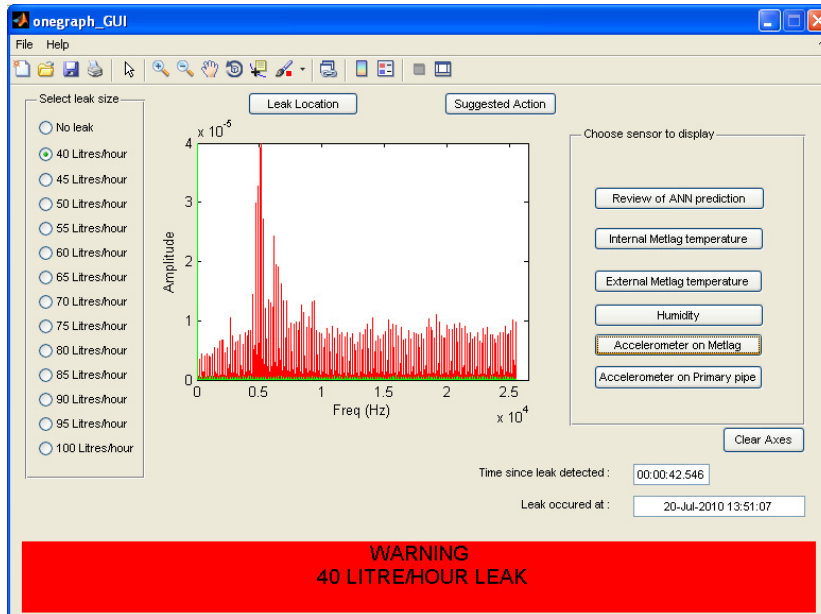

Figure 8.1 Operator Advisory system, showing accelerometer on Metlag data

The OAS simulator shown in Figure 8.1 was implemented using the Matlab™ GUI toolbox, where many different options are available to review the plant state. Following recommendations made by Alty (1995), the OAS has been designed to be as user friendly as possible, avoiding complex hierarchal structures, but using colour to represent levels of severity and button options to gain further information. The system that has been built is a simulator, because it uses the leak data captured from the rig but reproduces them using a real world scenario. Consequently, a user must select a leak size, this is achieved by selecting one of the leak sizes within the box labelled 'Select leak size' on the left hand side of Figure 8.1. The initial default when the simulator is started is 'no leak', and in this situation the lower portion of the screen is green (opposed to red, as shown above), and a message indicating NO LEAK is presented. The choice of leak sizes available are from: the 'no leak' scenario up to the largest leak at 100 litres/hour. Once the leak size is selected, the user needs to select a sensor to examine. This is possible from the box labelled 'Choose sensor to display'. The selected graph is displayed and the bottom part of the screen turns red to indicate a leak exists and the size of the leak is indicated. The screen plot in Figure 8.1, shows the FFT of an accelerometer with the normal value in green (prior to the leak) and the new level in red. This allows the user to observe the change in level. The FFT graph (Figure 8.2) will probably not have any meaning to the operator, but when a large change in amplitude occurs it will provide evidence that a problem exists. This is no different from the temperature gauge in a car, people accept it lies in the middle position, but when it starts to rise, people generally start to get concerned. As the FFT graph will be updated every couple of seconds, this will further validate that a change in state has occurred as opposed to a momentary glitch. It is very conceivable that should an operator study the data during normal operating conditions that they would become accustomed to the normal operating levels and any change in level would arouse suspicion that something was wrong.
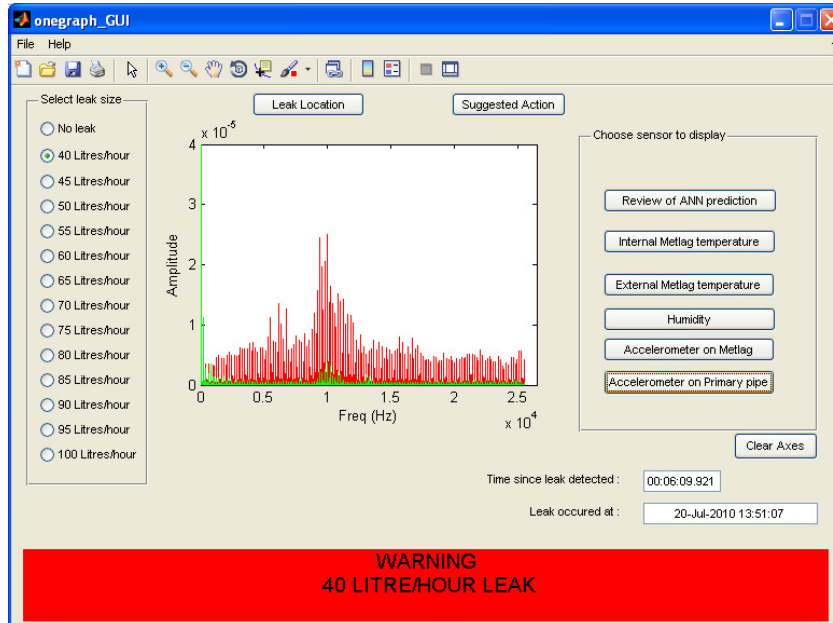
Figure 8.2 OAS, showing accelerometer on pipe

After selecting a leak size and graph, a date and time stamp is set, which shows the time and date when the leak started. A stop watch is also initiated and this runs continuously so that any personnel can quickly see how long the primary pipe has been leaking for. This information is shown in Figure 8.2 in the bottom right hand corner.

The user is also able to view a 3D diagram of the reactor leak position (Figure 8.3), by pressing the 'Leak Location' button. The leak position is denoted by the red area on the primary pipe. The simplistic diagram rotates about the reactor for two revolutions so that the leak position can be clearly understood.
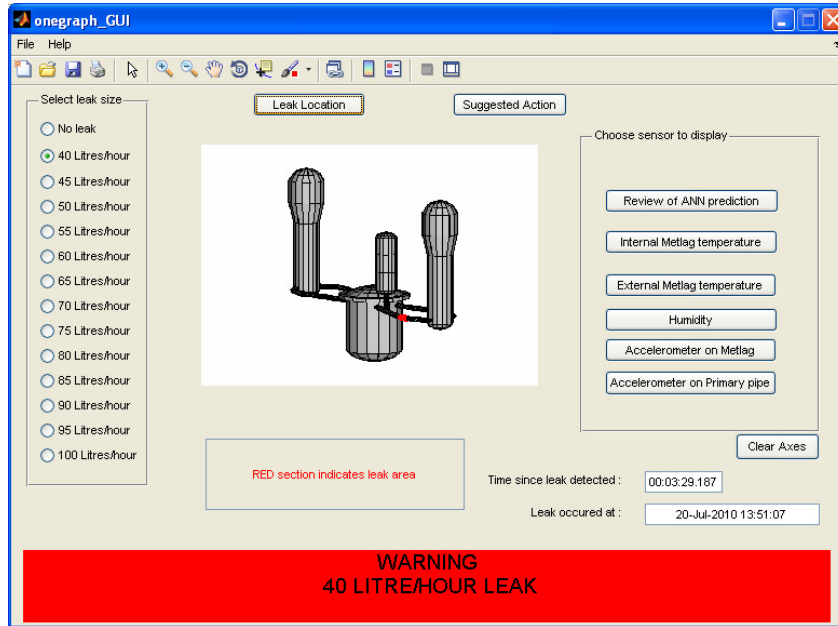
Figure 8.3 Location of leak

Figure 8.3 is very basic, but it illustrates how the system could be developed and taken further. A natural progression would be a zoom function to observe the valves, pumps and other pipe work in the vicinity, and attempt to isolate the problem. The following diagram Figure 8.4, is flow diagram of the system.
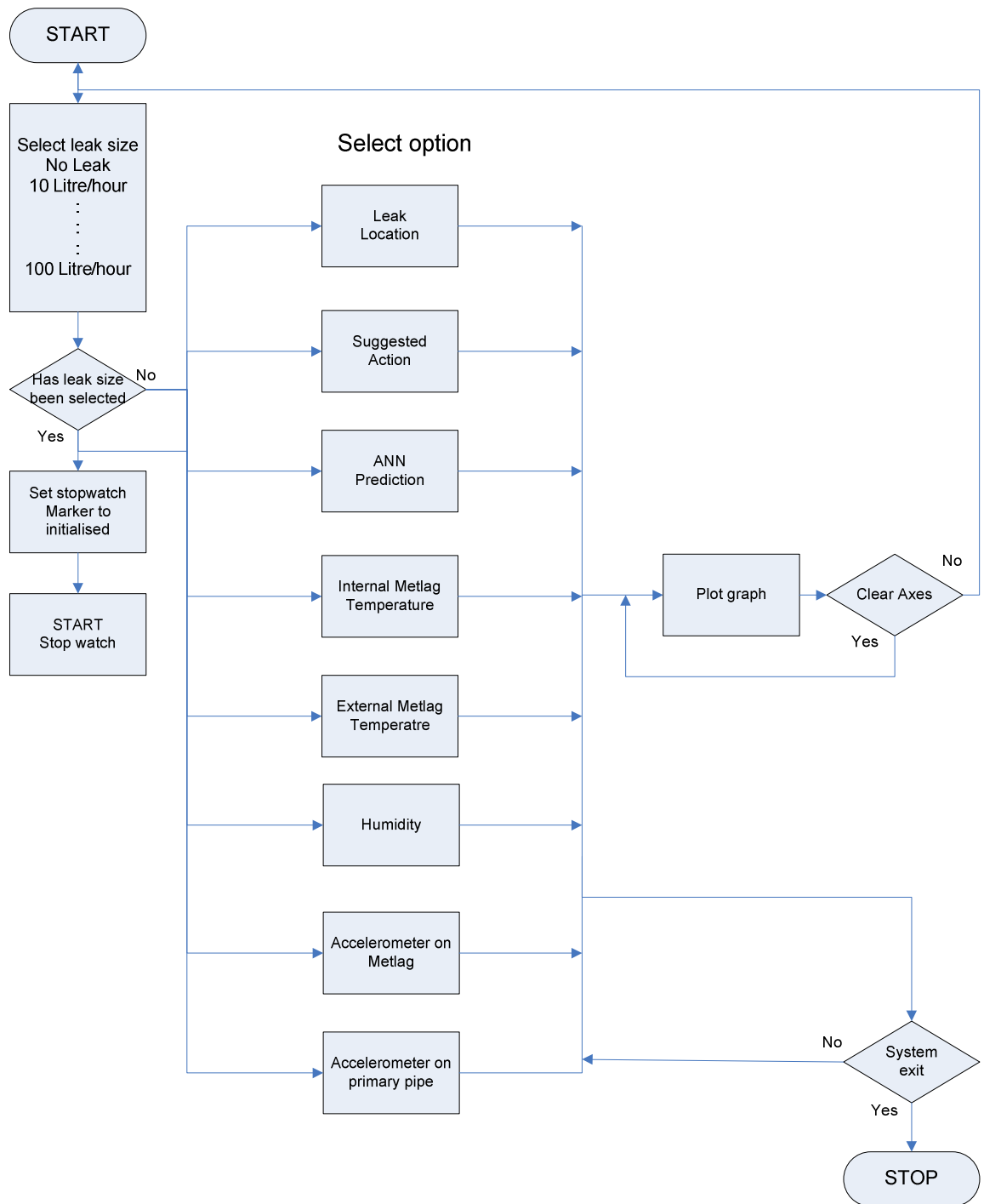
Figure 8.4 Flow Diagram of Operator Advisory System

The flow diagram shows that the simulator is designed around selecting a leak size and then observing either the graphs or information in relation to that leak size. There is an option to clear the central plot if desired and the OAS can be stopped in the usual

manner in MS-Windows®, by selecting 'File' and then 'exit' in the top left hand corner of Figure 8.3.

Figure 8.5 shows graphically the difference between the internal Metlag temperatures when running normally, shown in green and when a leak has occurred shown in red. A normal operating temperature is indicated as being 48°C, whereas this changes to 83.5°C when the leak occurs. In the real system the red line would gradually increase from its original temperature to the final temperature over a maximum period of a minute. Due to the construction of the rig using fixed jets, the exact amount of time can only be speculated.
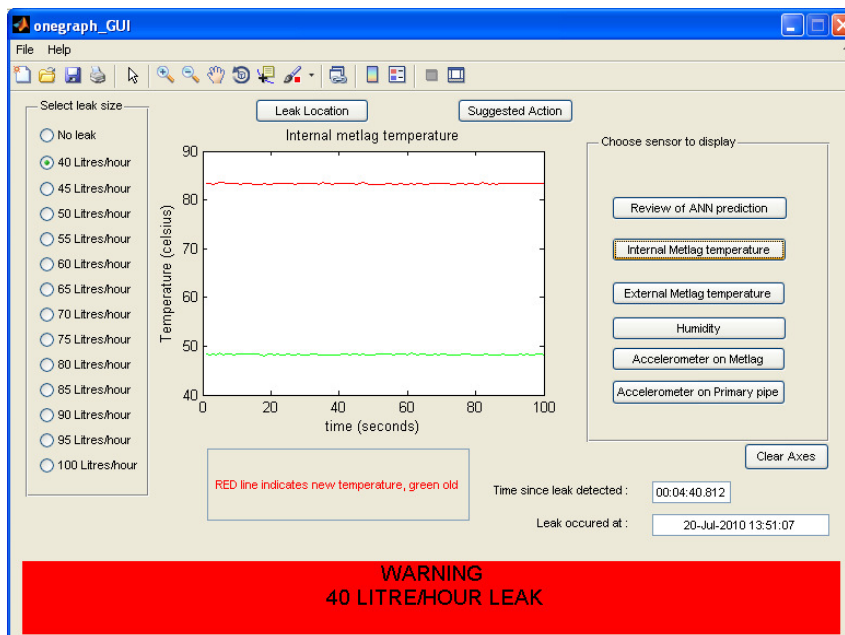
Figure 8.5 OAS, original and new internal Metlag temperature

Figure 8.6 shows graphically the difference between the external Metlag temperatures when running normally, shown in green, and when a leak has occurred shown in red. Through selecting all the various sensors to display, this system is trying to build up a weight of evidence such that any operator is able to review the information available and make their own decision based on what has been presented. The intention was never to have a system that purely ran an ANN and told the operator a leak exists. Most individuals like to look at the evidence before making a decision and due to the potential consequences of shutting down a nuclear reactor unnecessarily; therefore this system fulfils that criteria.
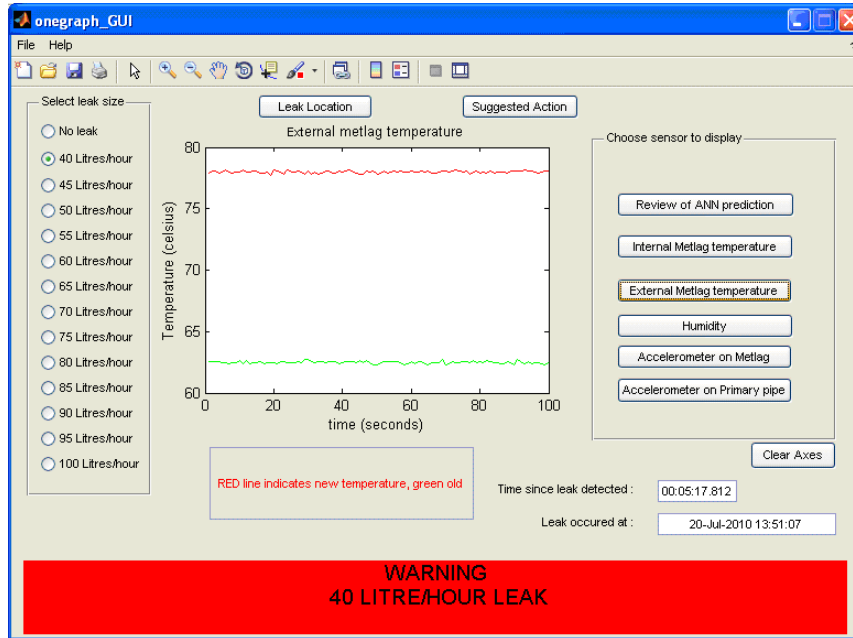
Figure 8.6 OAS, original and new external Metlag temperature

Figure 8.7 gives the operator a suggested action. The text box presents two pieces of information:

- Refer to Operating instructions for 'Loss of Coolant'
- Perform slow leak isolation drill.

These are two of the first tasks that would need to be carried out. More detailed information could be given but as this is a demonstrator, the instruction is kept very basic and avoids any confidentiality implications. The level of instruction could be designed to increase with increasing leak size. The information could also be directly tied into the location of the leak. However, due to the extensive training that all the submariners undergo, it is very unlikely that they would need advice regarding which documents to use and when to use them.
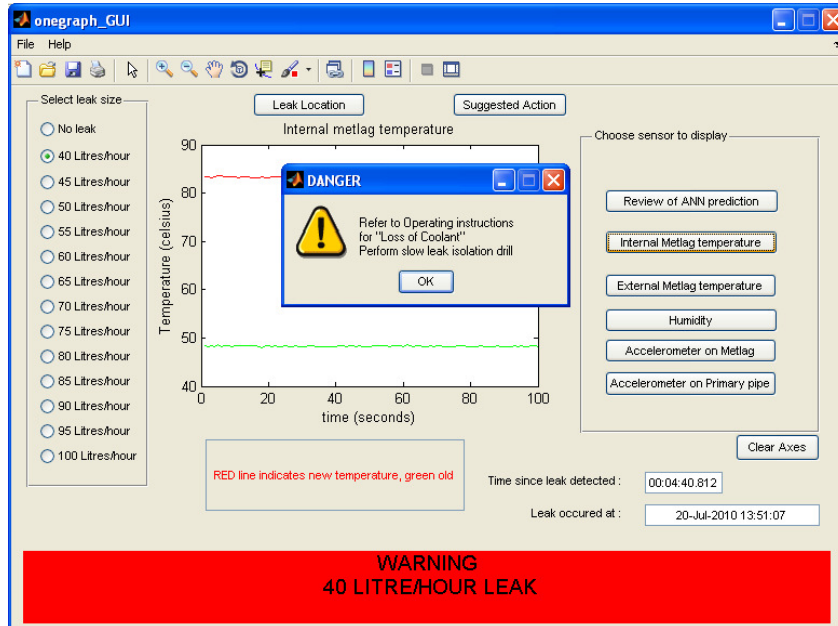
Figure 8.7 OAS, Suggested action

8.1.1 Voting Strategy

A voting strategy is required because as section 7.2.9 showed when the network is trained on one accelerometer at one particular leak size, it does not always get the result 100% correct. However, it must be remembered that there are three ANNs (one for each accelerometer) all training on different data on the same leak size. Therefore, by assessing the merits of each respective network, a vote can be taken on the most successful outcome. An argument exists that if 17 time periods of data are taken and only three data items are incorrectly classified then the overall success is still over 80%. However, if this system was implemented in a real system then the reality is that five time steps per Metlag section would be all that could be analysed. Therefore, in this scenario having 3 misdiagnosed outputs from 5 would lead to an incorrect leak size. Hence by combing all three ANN outputs into a voting strategy, would yield a more reliable success rate.
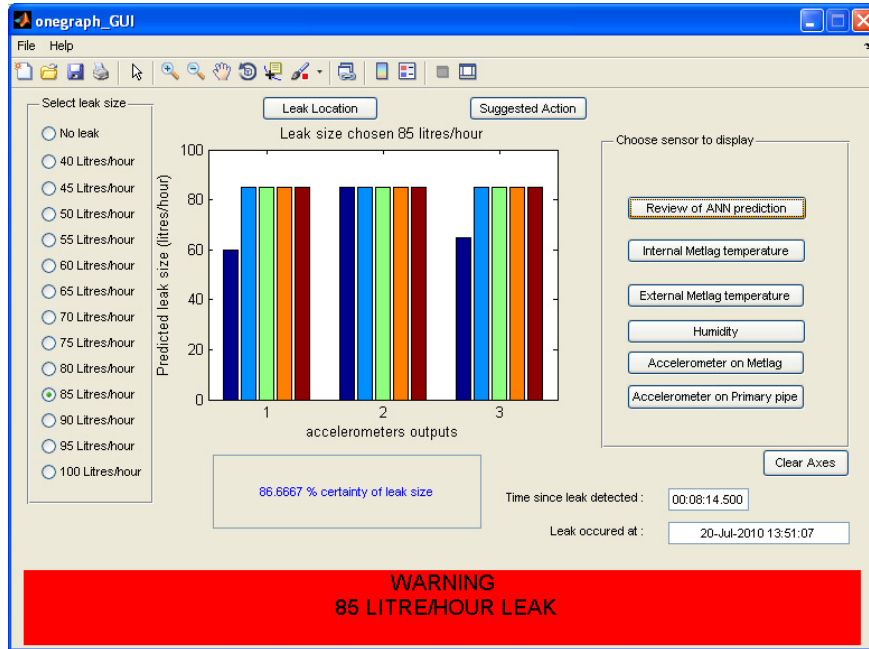
Figure 8.8 OAS, showing ANN prediction

The leak size chosen in Figure 8.8 represented the leak size with the highest error. As a natural progression to improve the reliability of the prediction it would be advisable to increase the number of samples in the leak area, once a leak has been detected. Therefore, one of the primary circuits from the reactor could either have its sampling rate drastically reduced or stopped, in order to increase the sampling rate in the leak area.

8.1.2   Evaluation

The OAS has been demonstrated to the Reactor Engineering Group at HMS Sultan. Different leak sizes where selected and the various sensors interrogated to illustrate where the comparison between 'no leak' and 'leak' situation. The system was also demonstrated to three Naval Officers and they liked the clear and concise layout of the buttons in addition to the information conveyed. One point that was suggested was to have the facility to track back in time to observe the temperature change on and around the lagging, from the point of break. Due to the design of the rig, this facility is not possible, but a real time monitoring system could facilitate this requirement.

8.2   Suggested Implementation of OAS

The simulated OAS provides a means of presenting data to an operator and should this system be implemented, various additions could be made, such as receiving inputs from other sensors already monitored in the RC, receiving a signal when motors change their operating speeds, and when a valve opens and closes. This is because they may introduce an unexpected change in the natural vibration on the pipes, confusing the OAS. However, the system produced to date does not offer an amber alert situation, shown in Figure 8.9. This situation arises because dissimilar sensors respond at different rates. Therefore, the accelerometer would be the first to detect a potential leak, followed by the internal Metlag thermocouple, then the external Metlag thermocouple followed by the humidity sensor. The leak signal for the thermocouples is triggered when the temperature passes a predetermined threshold. Consequently, these thresholds will be triggered in a staggered manner in reality. The amber alert situation will exist during this time when the sensors are not all in agreement.

The reality of placing sensors on or around the primary pipework will be logistically difficult. Therefore, the sensor spacing may change between Metlag sections, especially on corners. In addition, depending upon the position of the leak in relation to one of the RC fans, it may take a considerable build up of steam before the humidity sensor is activated. The escaping steam may also be less of a significant indicator depending upon how well the Metlag sections are joined to together.

The situation is further complicated because the ambient and background conditions that existed during the leak tests will not be the same as the RC. It can be assumed that the background temperature will be considerably higher in the RC, probably around 50°C. The humidity and moisture levels will also be higher, as the hot RC is immediately adjacent to the hull. To attempt to reproduce this background condition future rig tests could encase the Metlag area in a perspex box to heat up the immediate area around the lagging, but also enable the experiment to be viewed. This box would also need to be built in such a way that it could be removed easily between tests.

Finally, even though all the pumps and valves are designed to be quiet in operation, there will be a natural resonance emanating from them. Therefore, to setup the default conditions for the OAS it is advised that the following measurements are taken:

1. Typical humidity level in RC during operation
2. Confirmation that the external Metlag temperature agrees with the lab measured level during normal operation
3. Background vibration on the primary pipe and its associated lagging.

With these measurements taken, the thresholds on the OAS can be modified accordingly.
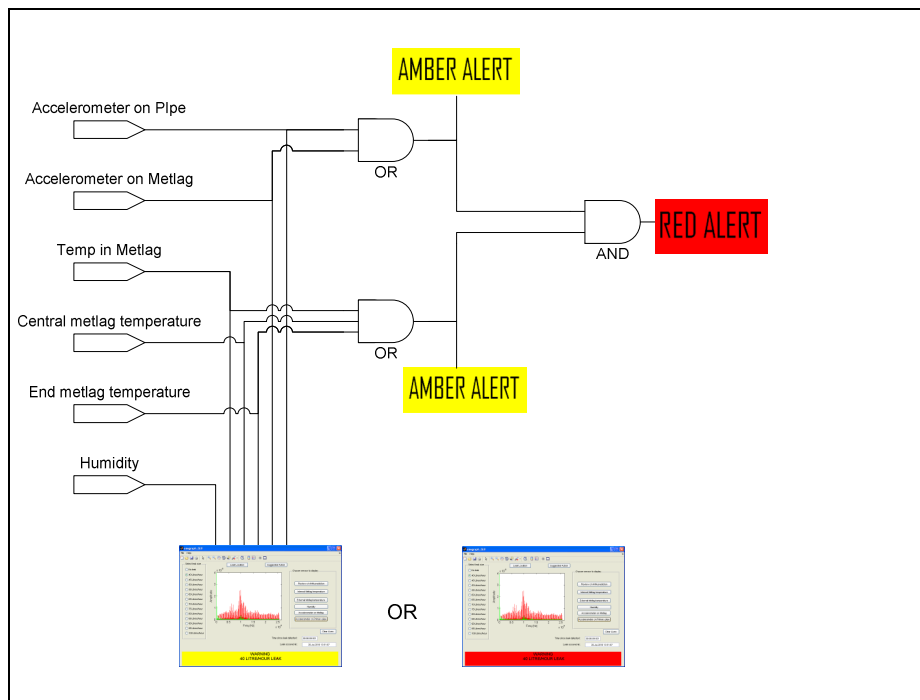
Figure 8.9 Levels of Alert, in leak detection system

The initial idea is for every section of Metlag to have up to three accelerometers, two on the outside and one on the primary pipe itself. In addition to these external accelerometers have thermocouples and within the Metlag itself create a pocket for an internal thermocouple. The humidity sensors could be positioned less frequently as they have proved to be less effective. Figure 8.9 shows two possible scenarios, where the bottom left OAS is showing an amber alert, which occurs when not all sensors were in agreement, compared to the OAS on the lower right showing the red alert.

171

Figure 8.10 shows a possible method of passing the signals from their respective sensors back to a multiplexer by effectively sweeping each set of sensors associated with a Metlag section.
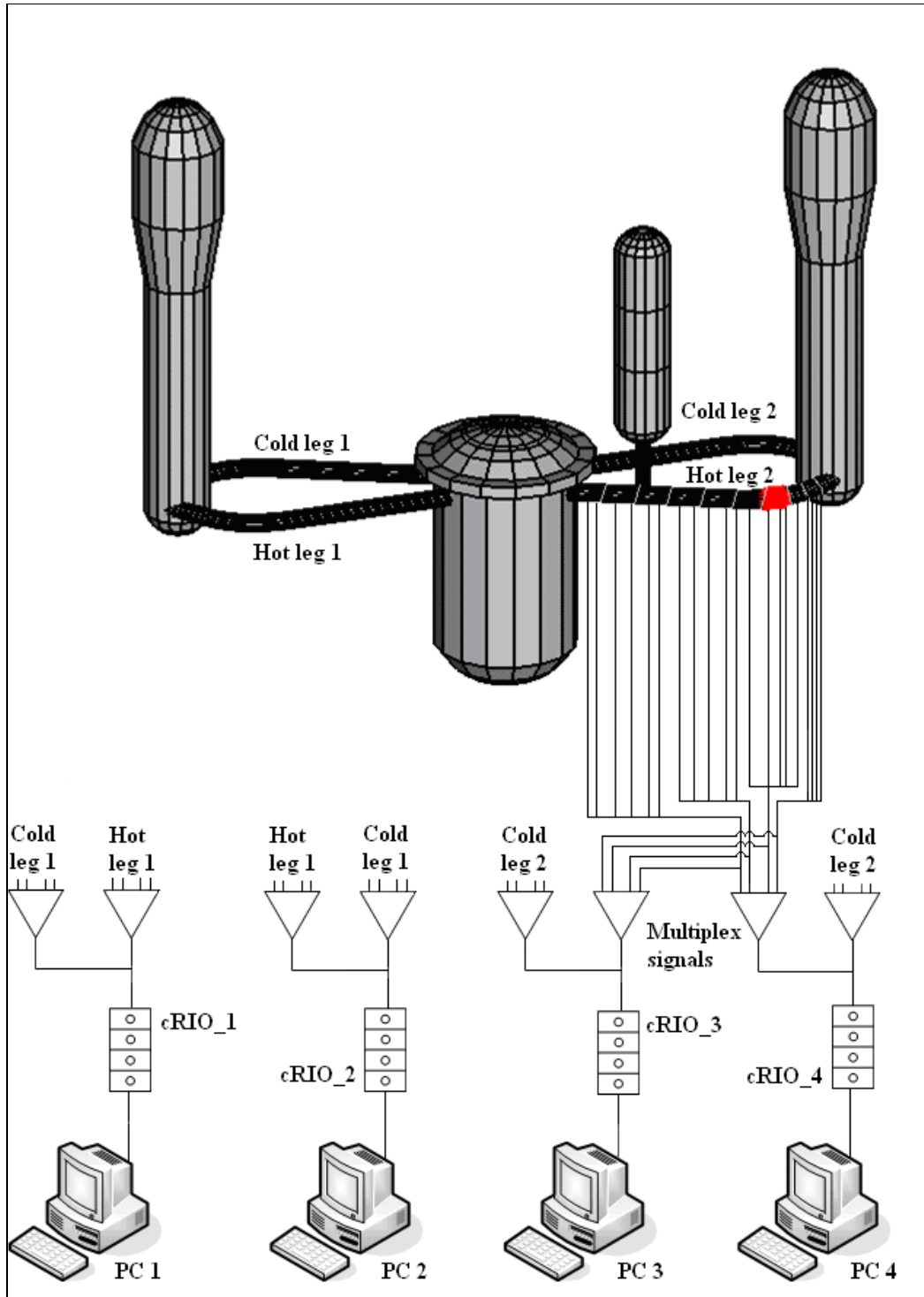
Figure 8.10 Signal cabling in Reactor Compartment

In Figure 8.10, only hot leg 2 has all of its wires connected. In that leg the concept of a set of sensors per Metlag section is illustrated. Redundancy is also built in, with the signals being distributed between two different multiplexers. Therefore, should a computer, CompactRIO™ or multiplexer fail, then another system can still analyse the data.

To implement this system, eight multiplexers would be required. Two multiplexers drive their signals into a CompactRIO™ and the output data are passed onto a computer. This computer can run on either the MS-Windows® or Linux/Unix® platform. These computers will be running a compiled version of the Matlab™ code in either C or C++, as it will run much faster. Due to the high data rates and large volumes of data emanating from the CompactRIO™ it is advised that the computers are quad core and paralleled up with another processor in order to process all the information fast enough.

8.2.1   Intelligent Lagging

The concept of intelligent lagging does not refer to lagging that contains its own processor and self diagnoses leaks, but lagging that encompasses all the sensors into one integrated unit. Ideally it would have thermocouples integrated into the accelerometers and a single plug connector that attached to an umbilical cable feeding the data back to the OAS, as illustrated in Figure 8.11.

Figure 8.11 Intelligent lagging concept

173

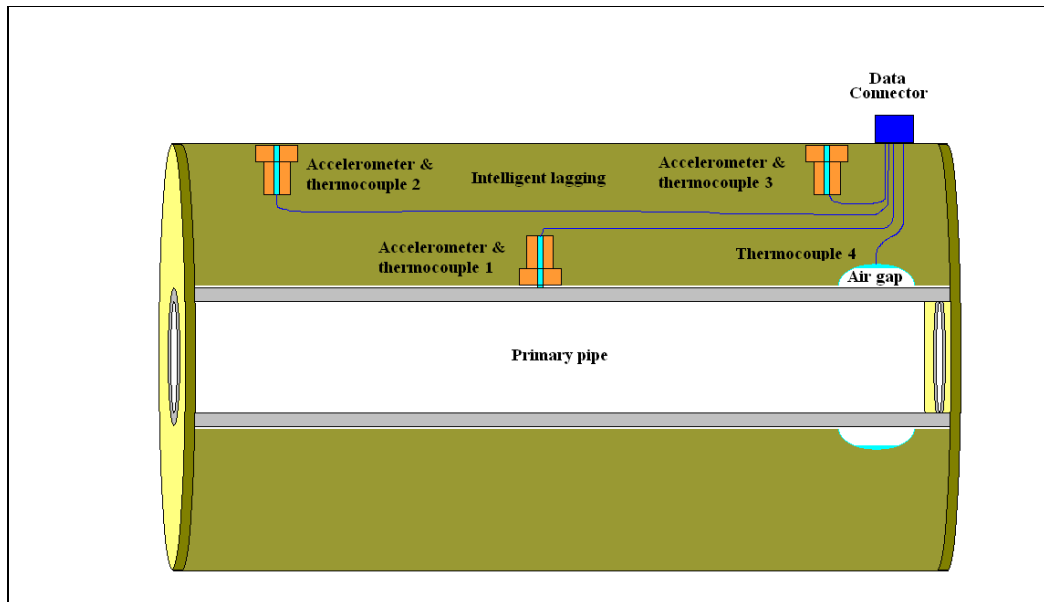The concept illustrated in Figure 8.11 integrates all the sensors inside the lagging. This helps prevent them being knocked or damaged when personnel are inside the RC. It also makes the Metlag sections far easier to assemble as the sensors will not be protruding, which could injure the engineers fitting them together during maintenance. It also avoids having a cluttered RC, as sensors on the outside of the lagging would have wires associated with them. Therefore, this design only has one connector which would be of a quick release type, to allow for ease of maintenance and should a leak occur the Metlag section/s can be easily removed from the primary pipe.

Figure 8.11 makes use of four thermocouples. Two are measuring the outside temperature of the lagging, one is measuring the primary pipe temperature and the fourth thermocouple is measuring any potential steam that would be caught in the air gap. The air gap thermocouple could measure the steam temperature around the entire perimeter, thus making orientation of the lagging unimportant. In addition the accelerometers would be integrated with the first three thermocouples. This would simplify production of the Metlag sections and potentially reduce the overall price of the system. Accelerometer and thermocouple 3 would consequently act as the accelerometer on the primary pipe as well as measuring the outside primary pipe temperature.

8.2.2   BAE Systems Wireless Communications

The biggest hurdle in implementing this leak detection system is passing the signals from the sensors back to the control room, outside the RC. This would normally involve cutting a hole in the RC wall to pass all the cables. However, Dr John Bagshaw at BAE systems has developed a technique that allows power and communication signals to be passed through several inches of steel. It has been nicknamed "Through Hull Data Link". This has applications for submarine hulls and armoured doors. The mechanism uses very high frequency acoustics, similar to a mobile phone, but selects exactly the right frequency and power to penetrate the thickness of metal. The implication of this technology is a saving of many millions of pounds, as normally each hole cut in the hull needs a special valve fitted called a penetrator, which can cost upto £750,000, and each valve needs welding into the hull, costing an additional £50,000.
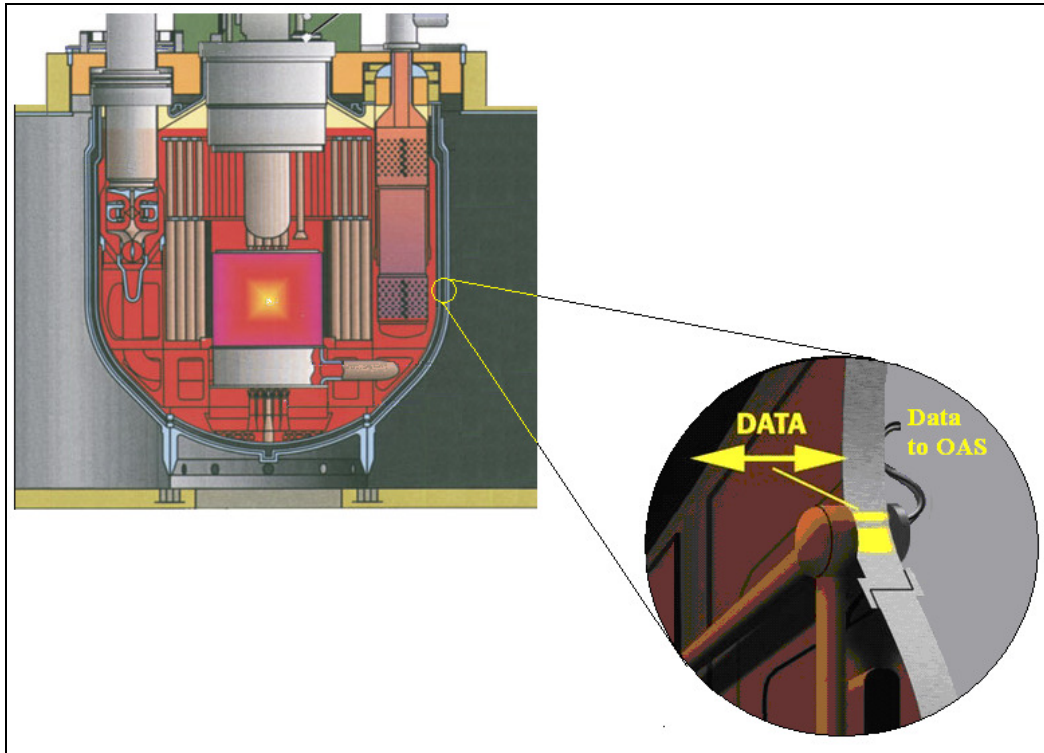
Figure 8.12 Reactor compartment with wireless communications illustrated

The diagram above, Figure 8.12 illustrates how signals could be passed from the RC back the control centre using this technology.

The system is still in the development phase but Dr John Bagshaw (2010) said that "Most recently we have demonstrated a video camera passing signals through an armoured vehicle hull. This obviously offers significant advantages in increasing the crew's situational awareness without reducing their protection". Therefore, it can be seen that this technology has many applications and would complement this project very well.

8.3 Summary

This chapter has presented screen shots of a simulated OAS in operation. Providing information regarding leak location by pinpointing the leak area on a 3D rotating reactor system, leak size through analysis by the ANN, supported by a confidence level, and graphs showing the measured sensor value before and after the leak occurred. Suggestions are made to enable the OAS to be implemented into a real system and the concept of intelligent lagging introduced.

Chapter 9
Conclusions

This project has made a number of important inroads in the detection of very small leaks from the primary circuit of a nuclear reactor. The following section will address the most significant advances from the work carried out.

A unique piece of test equipment has been produced, that can recreate a very small leak in the range 40 to 100 litres/hour, at the temperatures and pressures expected in the primary circuit of a nuclear reactor. The results produced by the rig are also unique, as the data acquired at the respective pressure, temperature and flow rates has not previously been recorded. These results are also repeatable, as the flow rates are produced by a calibrated orifice. In addition, this rig is adaptable, because it has the facility to work at temperatures and pressures above or below the typical reactor levels, should the working conditions of a PWR ever change.

Sensor selection was accomplished through a combination of a literature review, searching the internet for available sensors and past experience. Although initially the list was quite extensive, sensors were dismissed for many reasons including their frailty, intolerance to high radiation, practicality, cost or size. Sensors were then either eliminated during the feasibility study or when they were applied to a real leak situation. When the rig was in operation only three sensors were found to fulfil all the criteria, these being the accelerometer, thermocouple and humidity sensor. These would be the sensors recommended for this application, should this research be implemented on a real reactor system.

It was found that when the time series data from an accelerometer were applied to a FFT, each of the leak sizes had a unique characteristic. Small differences could be observed between the FFT graphs of the individual leak sizes. However, expecting an operator to be able to determine or even differentiate between leak sizes would be

impossible, by purely interpreting an FFT graph. Therefore, by subdividing the frequency axis into discrete regions and within these sections performing mathematical analysis, these data were now in a suitable form to train an ANN. Various different network topologies were investigated but the most successful was able to correctly differentiate and identify different leak sizes with a certainty of over 97%, over 13 different leak rates with a separation of only 1.4 g/s. This is a very significant achievement and highlights the importance of ANNs in their own right, and in the application of leak detection.

Using accelerometer data to train an ANN has proved itself to be very successful in the detection of leaks. However, relying on one sensor and one computing technique may not be regarded as enough evidence to shut down a nuclear reactor. Therefore, by combining this technique with digital logic from a number of thermocouples provides a stronger confidence that a leak exists. Consequently, these two techniques were found to complement each other well, and this approach should not be underestimated in its effectiveness.

The final deliverable from this work was an OAS. This system is unique because at this present time, an OAS for leak detection from a naval nuclear reactor does not exist. The ability also exists to run the OAS in real time, should the correct infrastructure be developed in the RC for the sensors and cabling. Through the combination of the ANN and digital logic, should all the input parameters corroborate a leak, then it can be deemed a very high likelihood that one exists. By navigating through the graphical user interface, the leak location, size and supporting data can be viewed. In addition, the system has been demonstrated and was well accepted. The primary intention was always to have a system that could alert an operator of a leak, but offer enough evidence to substantiate the claim. The OAS that has been constructed fulfils all the criteria set.

9.1 Future Work and Recommendations

This report details the design of the high pressure and temperature water rig, the data collected from the sensors monitoring the leak, the processing of the data through ANNs and other techniques, as well as the OAS. If time had been available, there are changes that could have been made to the rig, and different tests that could have been carried out with it. The recommendations for the rig are as follow.

- Add automatic pressure control to the rig, whereby the pressure can be selected and maintained by software, using Labview. The output from the CompactRIO™ could apply a varying voltage to a motorised valve and by feedback from the digital pressure sensor, maintain a pre-determined pressure. This would require removing the existing motor and valve arrangement as discussed in section 4.14, and fitting a stepper motor and additional gearing to facilitate very small changes in the valve opening. If the successor to this project does not have a very good understanding of Labview, then paying for telephone support with the National Instruments Labview Engineers would be suggested.

- Add an electrically operated solenoid valve after the control valve, to operate during the final quiet phase of data collection. Opposed to at present physically shutting a valve situated on the rig. Closing this valve allows for an extended period of measurement, when the only noise is created by the steam.

- Fit a T piece between the cartridge heaters and heated coil, with a solenoid valve on the exit T. This would serve two purposes firstly, if the jet became blocked there is a natural exit point for the hot water and secondly it would allow for faster cooling after the experiment has finished, as cold water could be passed through the pipe work.

- Add an additional sensor that monitors the water quality and sounds an alarm if the HOH tank is becoming depleted. This will ensure the pipes and jet do not become blocked with limescale build up. This can occur when the ion exchange resin becomes depleted. This is a gradual process and is easily missed. However, normally a fishy smell becomes evident and also limescale starts to build up on the metal work in the leak area.

- Extend the length of the orifice pipe, in order to study the effect on the signal with distance. Perhaps obtain a further piece of Metlag from Darchem.

- If the facility is available either modify the existing jets to reduce their internal diameter or attempt to source smaller jets. This would provide very useful data as it would be even closer to point at which the first sign of a leak is present.

- Replace the existing orifice pipe with a pipe of the same diameter but having been subjected to corrosion. There are many individuals at HMS Sultan that could assist with preparation of the pipe and apply the correct chemicals to corrode the pipe. Every piece of the rig can be unbolted and therefore removing the final orifice section would not be difficult. With this new scenario, the corroded section of pipe could be attached into the rig and its flow rate measured with cold water. This was previously carried out with all the jets, using cold water at pressure and collecting the water released from the jet in a set period of time. Thus the flow rate can be calculated. By collecting the data from this non circular leak, it would be interesting to observe the difference a round orifice at a predetermined flow rate versus a natural crack at the same flow rate. Various test pipes could be used and measured and the data could be analysed by the ANN to classify its size.

- Even though the rig has been primarily designed for use with water, it would not need much modification to apply different chemicals to the system, perhaps including oil, nitrogen and other low viscosity liquids.

Other measurements:

- It would have been interesting to alter the pressure and temperature by intervals of 10 bar and 10˚C respectively and observe the effect on the FFT with the accelerometers. This would add an insight into the relationship between pressure, temperature and the accelerometer FFT characteristic.

- The rig is capable of operating at the same temperatures and pressures as the real primary circuit and therefore, a confidential report could be produced for the Ministry of Defence with the leak results. Due to the time limitations and the confidentiality of producing such results, this was not done.

- The accelerometers could be moved to different positions on the lagging and their orientation changed. At present the leak projects vertically, which corresponds to the orientation of the accelerometers. It would however be

interesting to have accelerometers mounted orthogonally to the leak direction, to observe any differences. The distance of accelerometer could be changed, as presently they are located at the centre and ends of the lagging. From the results there appeared to be a relationship between distance and the position of the fundamental frequency on the FFT plot.

- Perform leak tests with a larger diameter pipe, a larger diameter section of Metlag has been given to Ms Sam Morris. This could be trialled in the future to study the change in FFT characteristics. A relationship could be developed between pipe diameter and FFT characteristics for a given flow rate.

This study has shown which sensors are the most appropriate for this application. However, their arrangement could be improved as follows.

- A major consideration has always been regarding maintenance of the primary circuit and not overly congesting the RC with hundreds of wires. Therefore, creating an integrated sensor array into the lagging, with minimal cabling and ease of disconnection would be a good step forward. Temperature sensors could be mounted on the underside of the lagging as well as on the outside. A dedicated cavity could be created to capture any steam in the event of a leak. This was attempted in this report, by using the chimney design. Realising this would only require a small pocket perhaps 30mm tall with a thermocouple built into it, inside the lagging. This type is configuration could be considered the first steps in constructing an intelligent lagging as shown in section 8.2.1.

- If additional heater cartridges could be inserted into the input side of Figure 6.10, i.e. where the hot water pipe is insulated, that would help gain a better understanding of the temperature variation on the outside of the lagging, which is unclear at present. This would help in two ways; it would help keep the pipe up to temperature, as it could potentially loose some of its heat in this section, but it would also then create an even 200˚C across the entire pipe length. This would make studying the temperature profile along the lagging far easier, and the effect of the steam on the lagging temperature could be correctly identified.

Data collection techniques using Labview could be improved as follows.

- Labview is the controlling software for the CompactRIO™, but producing the system required to log data from the sensors was not straight forward. The

180

software could be improved as the strain gauge inputs and microphone where not used and the software could be simplified without them. There is also a slight bug when the RT Host Scan is run. It is very minor but it does require the user to press the run button, wait for the system to temporarily start then stop, then the user presses run again, at this point it carries on running. It is a very minor fault and does not affect the running of the system, and despite talking with the National Instruments Engineers the fault was never fixed.

- A natural progression would be to take data from the CompactRIO™ to Matlab™ in real time. At the present time, Matlab™ software does not communicate with the CompactRIO™ software. However, because the CompactRIO™ is effectively a dedicated PC in its own right, it would be possible to integrate the Matlab™ software into the Labview code and have everything running as a self contained unit in the CompactRIO™. This is a very nice feature of Labview because it enables code to be developed in Matlab™ and then at a later date inserted into Labview. It would have been plausible to write all the software in Labview, but at present Labview does not support ANNs, but of course this may change over time.

Applying other ANN techniques could improve the prediction of leak size, as follows.

- At present the 'newlrn' recurrent ANN is applied to the input data, but other ANNs such the 'newff' feedforward back propagation network and 'newfit' fitting network could also be trialled, as they showed a good level of success as well.

- At present the FFT plot is subdivided into five regions. There is potential to fit a sixth region that would examine the data from 20kHz to 25kHz, as there appeared to be some varied activity in this region. Note, that the accelerometer used for the tests has gain in this region (see appendix G), and therefore the amplitude of the variation between leak sizes is over emphasised.

- The five regions could be doubled to ten and the results re-examined.

- The mathematical functions used currently, namely; peak, mean, standard deviation and sum could be complemented with other mathematical techniques or completely revised.

- Collect more data from the rig with the intention of reducing the ANN training percentage while increasing the test, and observe the results.

- In addition run the rig at the correct temperatures and pressures that the primary circuit normally operates at, and present these results to the Ministry Of Defence. This would be a confidential document.

Adding data from other sources, as follows.

- The Loss of Flow Test (LOFT) rig, is a 50 MW PWR with a nuclear core built to record thermal hydraulic measurements during large and small break loss of coolant events. A preliminary review of the database shows 15 transients with between 20 – 100 variables, measured at 50 times per second. If data can be successfully extracted from this database then it could be incorporated into an ANN, and then added to the OAS.

Upscaling this system as indicated below.

- At present the results from the leaks generated by the rig are used exclusively by the OAS. HMS Sultan has a full scale simulator that enables operators to control the reactor, but also learn to react in the event of a LOCA. Therefore, either the results or OAS could be integrated into the simulator as an aid to leak detection.
- Perform further evaluation of the OAS, from a larger group of operators' in order to obtain more detailed user feedback.
- Obtain input from a human/computer interaction expert

Additions to OAS as follows.

- The OAS could be further improved by having the facility to scroll back in time, so that the exact moment at which the leak occurred could be studied and in the case of the temperature profile, observe the temperature increasing from its natural state to its current level, with a leak.
- To prevent any false positives, by adding the current reactor sensor inputs to the OAS, would prevent a false alarm when a valve or pump may be abruptly started or stopped, which could possibly pass a harsh vibration through the primary pipe work.
- Add a zoom function to the leak location function, which is presented to the operator as a 3D model. This could help an individual pin point the leak area more easily if they have to enter the RC. In addition, the suggested action could be linked into the leak location.

9.2 Summary

The intention of this project has always been to detect leaks. However, the route to accomplishing this deliverable has involved; building and designing a high temperature and high pressure rig, selecting sensors to measure the leak, configuring and programming a data acquisition device to acquire the data, and using computational techniques to identify the leak. The combination of ANN and digital logic has been shown to complement each other well, but the accuracy of the ANN has surpassed all expectations.

The graphical OAS has provided an excellent means of presenting the results from the computational analysis both demonstrating the power of the ANN for determining leak size, but also showing how complementary techniques can in themselves offer additional supporting evidence.

References

Adah T. et al. (1997) "Modelling nuclear reactor core dynamics with recurrent neural networks", Neurocomputing, vol 15, pages 363-381, 1997

Alty J. (1995) "Operator interfaces in the nuclear environment: will multimedia help?", Nuclear Energy, vol 34, no 1, pages 47-52, Feb 1995

Antonio A. et al. (2006) "Neural and genetic-based approaches to nuclear transient identification including 'don't know' response", Progress in Nuclear Energy, vol 48, issue 3, pages 268-282, April 2006

Areva (2005), "EPR reactor notes", Framatone Anp, March 2005

Auld D. (1995) "Aerodynamics for students; integral approach to the control volume analysis of fluid flow", The University of Sydney, Australia, Available : http://www.aeromech.usyd.edu.au/aero/cvanalysis/node3.shtml#node43, last accessed on 23/08/08

Bagshaw J. (2010) "BAE Systems revolutionises submarine technology", Available: http://news.icm.ac.uk/aerospace-and-defence/bae-systems-revolutionises-submarine-technology/316/ , last accessed on 20/7/10

Basu A. et al. (1994) "Detecting faults in nuclear power plants by using dynamic node architecture artificial neural networks", Nuclear Science and Engineering, vol 116, pages 313-325, 1994

Bausch H. (1989) "Leak detection in nuclear piping outside containment", Nuclear Engineering and Design, vol 113, pages 155-162, 1989

Beaty M. et al. (2004) "The Whittaker - Kotel'nikov – Shannon theorem, spectral translates and Plancherel's formula", Journal of Fourier Analysis and Applications", vol 10, issue 2, pages 179-199, 2004

Becraft W. (1993) "An integrated neural network/expert system approach for fault diagnosis", Computers Chemical Engineering, vol 17, No. 10, pages 1001-1014, 1993

Benito R. and Dagli H. (1994) "Artificial neural networks for intelligent manufacturing", edited by Cihan H Dagli, London, Chapman and Hall, ISBN 0 412 480506

Brown T. (2004) "Surrey University lectures notes, CSM10: Backpropagation: an example of supervised learning, page 1, unpublished.

Brunet M. (1988) "Water leak detection in steam generator of super Phenix", Progress in Nuclear Energy, vol 21, pages 537-544, 1988

Circuit Cellar (2006) "Internet connected sonic anemometer" [Accessed on 04/08/09]
http://www.circuitcellar.com/library/print/0106/cyliax-186/index.htm

Claytor T. (1986) "Current practice and developmental efforts for leak detection in US reactor primary systems", Continuous Surveillance of Reactor Coolant Circuit Integrity, pp. 157-164, OECD/NEA, Paris, 1986.

Crane K. (1979) "Flow of fluids, though valves, fittings and pipe", Metric Edition – SI Units, Crane Ltd, Technical paper No 410M, 2nd print 1979

D'Souza L. (2006) "Intelligent monitoring of small transients in a complex non-linear system using artificial neural networks", PhD thesis, City University, London

Fantoni P. (1996) "A pattern recognition – artificial neural networks based model for signal validation in nuclear power plants", Annals Nuclear Energy, vol 23, no 13, pages 1069-1076, 1996

185

Evsukoffa A. (2005) "Recurrent neuro-fuzzy system for fault detection and isolation in nuclear reactors", Advanced Engineering Informatics, vol 19, pages 55–66, 2005

Folds D. (1997) "On whether to allow computers to post traffic advisory messages without operator approval", Proceedings of the Human Factors and Ergonomics society, 41st annual meeting, Albuquerque, New Mexico, USA, September 1997

Gao Y. (2005) "On the selection of acoustic/vibration sensors for leak detection in plastic pipes", Journal of Sound and Vibration, vol 283, pages 927-941, 2005

Gopal R. (1977) "Experiences with diagnostic instrumentation in nuclear power plants", Progress in Nuclear Energy, vol 1, issues 2-4, pages 759-779, 1977

Greco A. et al. (2005) "Artificial neural networks for classifying magnetic measurements in Tokamak reactors", Proceedings of World Academy Of Science, Engineering and Technology, vol 7, ISSN 1307-6884, August 2005

Hayashi K. et al. (1996) "Acoustic detection of in sodium water leaks using twice squaring method" , Ann. Nuclear Energy, vol 23, No 15, pages 1249-1259, 1996

Holland C. et al. (1995) "Noise prediction and correlation with full scale measurements in ships", Trans IMarE, vol 107, part 3, pages 195-207, 21st March 1995

Kermani B. et al. (2005) "Performance of the Levenberg–Marquardt neural network training method in electronic nose applications", Sensors and Actuators B: Chemical, vol 110, issue 1, pages 13-22, 2005

Krunze U. (1999) "Experience with the acoustic leakage monitoring system values in 17 VVER plants", Progress in Nuclear Energy, vol 34, N0 3, Pages 213-220, 1999

Kun Mo et al. (2007) "A neural network based operation guidance system for procedure presentation and operation validation in nuclear power plants", Department

of Nuclear and Quantum Engineering, Korea Advanced Institute of Science and Technology, 373-1, 14th June 2007

Lampton M. (1997) " Damping - undamping strategies for the Levenberg-Marquardt nonlinear least-squares method", Computers in Physics Journal, vol 11, issue 1, pages 110–115, 1997

Lee N. et al. (2001). "New leak detection technique using ceramic humidity sensor for water reactors", Nuclear Engineering and Design, vol 205, pages 23-33, 2001

Lombardi C. et al. (1997), "Prediction of two-phase mixture density using artificial neural networks", Annal of Nuclear Energy, vol 24, No 17, pages 1373-1387, 1997

MathWorks™ (2008), Documentation, neural network toolbox, [Accessed on 04/02/08]
http://www.mathworks.nl/access/helpdesk/help/toolbox/nnet/nnet.html

Menon S. (2004) "Piping calculations manual", Mc Graw-Hill Professional, December 10th, 2004

Mochizuki H. et al (2000), "Development of leak detection system for piping high-temperature resistant microphones (1) Development of system", In proceedings of ICONE-8, Baltimore, USA, pages 323-334, April 2nd-6th 2000.

Morishita Y. et al. (1995) "Development of a leak detection system using high-temperature resistant microphones", Journal of Nuclear Science and Technology, vol 32, No 3, pages 237-244, 1995

National Instruments (2009a) NI CompactRIO™ control and acquisition system [accessed on 12/08/09]
http://www.ni.com/compactrio/whatis.htm

National Instruments (2009b) LABVIEW FPGA and CompactRIO™. Getting started tutorial [accessed on 15/08/09]
http://www.ni.com/pdf/labview/us/fpga_compactrio_getting_started.pdf

National Instruments (2009b) Operating instructions and specifications, CompactRIO™ NI cRIO-9024
http://www.ni.com/pdf/manuals/375233a.pdf

NeuroAl (2010) Artificial neural networks [Accessed on 5/6/10]
http://www.learnartificialneuralnetworks.com/

Newman K. (2002) "Tubing limits for burst and collapse", CTES, L.C. 9870 Pozos Lane, Conroe, Texas 77303, www.ctes.com, September 25th, 2002

Ovaska S. (2004) "Computationally intelligent hybrid systems: the fusion of soft computing and hard computing", Wiley-Blackwell, IEEE press series on computational intelligence, ISBN: 978-0-471-47668-9, 410 pages, 2004

Parker (2005) "Industrial tube fittings europe" Technical Handbook, Parker Hannifin Corporation, Catalogue 4100-7/UK

Pham D. (1999) "Training elman and jordan networks for system identification using genetic algorithms", Artificial Intelligence in Engineering, vol 13, pages 107–117, 1999

Proskuryakov K. (2007) "Understanding the conditions of resonance interaction between flow pressure oscillations and mechanical vibrations", In the 12th International Topical Meeting on Nuclear Reactor Thermal Hydraulics (NURETH-12), Sheraton Station Square, Pittsburgh, Pennsylavania, USA, September 30th – October 4th, 2007

Radford N. (2003) "Classification for high dimensional problems using Bayesian neural networks and Dirichlet diffusion trees", NIPS, page 9

Seker S. et al. (2003) "Elman's recurrent neural network applications to condition monitoring in nuclear power plant and rotating machinery", Engineering Applications of Artificial Intelligence, vol 16, pages 647-656, 2003

Shepherd R. (2004) "Financial modelling with neural networks and other mathematical techniques," MSc thesis, Surrey University

Shepherd R. (2008) "Application of hard and soft computing techniques to small leak data from the primary circuit of a Pressurised Water Reactor (PWR), culminating in an Operator Advisory System", 1st year PhD report, City University, London

Shepherd R. (2009) "Application of hard and soft computing techniques to small leak data from the primary circuit of a Pressurised Water Reactor (PWR), culminating in an Operator Advisory System", 2nd year PhD report, City University, London

Shimanskii S. (2005) "Acoustic method of leak detection using high-temperature microphones", Atomic Energy, vol 98, No 2, pages 98-105, February 2005

Shimanskii S. (2004) "Development of acoustic leak detection and localisation methods for inlet piping of Fugen nuclear power plant", Journal of Nuclear Science and Technology, vol 41, No 2, pages 183-195, February 2004

Shimanskii S. (2004b) "Leak detection in the primary coolant piping of nuclear power plant by applying beam-microphone technology", Journal of Nuclear Science and Technology, vol 41, No 3, pages 359-366, March 2004

Siemens (1994) "Detecting and locating the smallest leaks early", Nuclear Engineering International, vol 39, Part 485, Pages 22-24, 1994

Streicher V. J. (1991) "Acoustic monitoring systems – system concept and field experience", Nuclear Engineering and Design, vol 129, pages 151-162, 1991

Tonolini F. (1987) "General review of developments in acoustic emission methods", International Journal of Pressure Vessels and Piping, vol 28, issues 1-5, pages 179-201, 1987

Wainwright N. (1995) "A regulators viewpoint on the use of AI in the nuclear industry", Nuclear Energy, vol 34, No 2, pages 93-97, April 1995

Wang D. (1996) "On temporal generalization of simple recurrent networks", NeuralNetworks, vol 9, No. 7, pages 1099-1118, 1996

Weller P. (1997) "Intelligent monitoring of a complex non-linear system using artificial neural networks", PhD thesis, City University, London.

Wolfgang W. (2007) "Simulation of two-phase flow in complex systems", Nuclear Technology, vol 159, pages 292-309, September 2007

Appendices

A: Nuclear Reactor System

A simplified model of a Pressurised Water Reactor (PWR) is shown below. Within the primary system highlighted in red, water is used as a moderator and a coolant because it transports heat well and is good as a neutron moderator.

The fission reaction must be carefully controlled in order to keep the reactor critical, i.e. the neutron generation constant. Control rods within the reactor are controlled by the control rod drive mechanism, as illustrated, and they allow careful adjustment of the reactivity of the core. The heat generated by the reactor core is typically in the region of 200°C, but because it is under very high pressure, it remains as a liquid. The heat extracted from the core by the water is then carried through to the steam generator, where it passes through a heat exchanger and steam is consequently developed in the secondary circuit, shown in green. The steam then turns the turbine and in turn the turbine produces electricity. The steam leaving the turbine is cooled in the condenser, returning it to water, it is then pumped back to the steam generator where the cycle begins again.
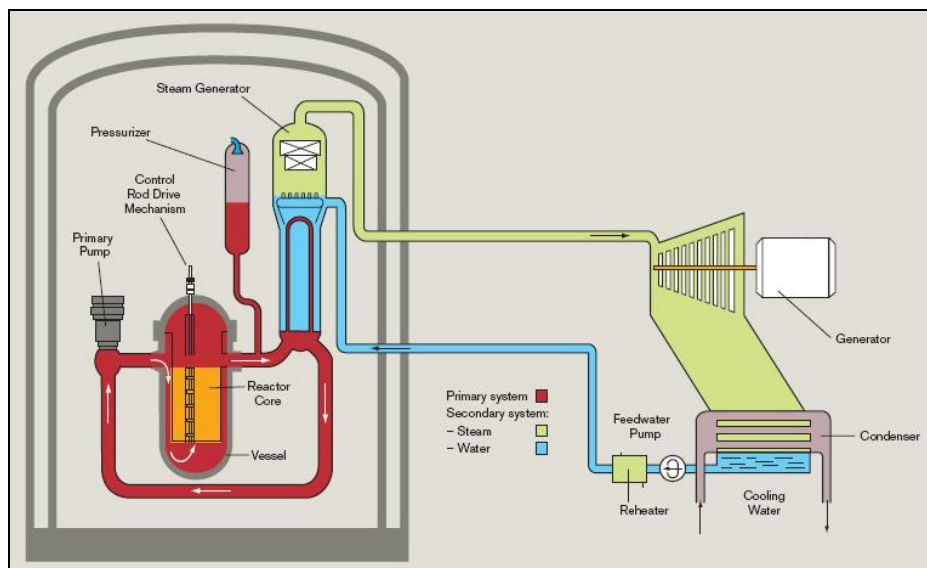
Reactor System, Areva (2005)

B: Reservoir

The purpose of the reservoir was two fold, firstly to act a pulsation damper from the water pump, and secondly to provide a reserve of water should the water pump inadvertently fail. As the system has already been calculated to flow 0.66 l/m, a suitable size for the reservoir was chosen to be one litre. Consequently the pipe is 0.63 metres long, with an internal diameter of 0.048 metres. Therefore, the internal volume is 0.00114 m^3 which equates to 1.14 litres. With one litre of water in reserve, it gives the operator over a minute to switch the heated section of coil off, in order to reduce the temperature of the water leaving the orifice, and stop internal boiling. It was later decided to add an accumulator, as this would add further pump damping but also provide a driving force in the event of pump failure. The reservoir was designed to dampen pulsations from the pump by compressing the initial one litre of air within the reservoir down to 10 cc. The water is unable to be compressed but the air pocket now acting like a sponge and expanding and contracting as the pump pressures fluctuates. The reservoir is shown below.
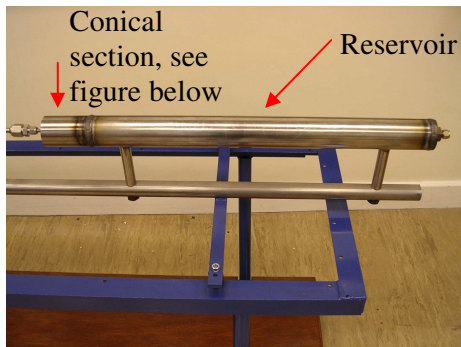
Original Reservoir

The conical shape allows the water to have a smooth transition from a large diameter down to a small one.

Machined conical shape from 50mm reservoir down to 5mm pipe

This entire reservoir section was removed from the rig because during the commissioning stage the welds joining the ends and two main pipe sections failed. This section of pipe was later replaced by a smaller bore pipe with screwed on with compression fittings and high pressure reducer couplings.

Calculations:

From the Hoop Stress equation the requirement for the reservoir which has an internal diameter of 50 mm is for the wall thickness to be in excess of 4.3 mm, for the 210 bar test.

The final pipe selection has an internal diameter of 50 mm and a wall thickness of 6mm ($\sigma_{h(m)}$ = 293 MPa).

Using Lamés equations yields:

σ_h = 98.54 MPa Maximum hoop stress

σ_r = -21 MPa   therefore P_r = 210 bar (as expected, as the internal pressure is 210 bar)

σ_a = 38.77 MPa

Pipe internal diameter	Using Hoop stress	Using Lamés for hoop stress	Maximum hoop stress for pipe
50mm	87.5 MPa	98.54 MPa	293 MPa

C: Calculating the Effect of Reservoir on Single Piston Pump

Eg if pump delivers 5 cc on upstroke and 0 cc on downstroke
and does this once per
second.

$$DV = \qquad 2.5 \quad cc$$

IF an air cushion is put into the large pipe by starting it full of air

Volume of air cushion at 1
bar   1000 cc
MAX pressure   100 bar
Min air volume V1   10 cc

Volume after smoothing V2 = V1+DV   12.5 cc

Pressure after cushioning
p2 =
p1*(V1/V2)^1.4   73.16881 bar

Water pressure change needed to achieve same smoothing
in a solid system
Bulk Modulus K =
den*Dp/Dden   2.00E+09 Pa

Initial Density, den   1000 kg/m3
Initial mass of water M1   1 kg
Initial volume V1   1.00E-03 m3
Final volume V2 = V1+DV   1.03E-03 m3

Final density = M1/V2   9.76E+02 kg/m3
Change in density Dden   -2.44E+01 kg/m3

Change in pressure Dp = K*Dden/den   -4.88E+07 Pa
                                                        -4.88E+02 bar

D: Flow Rate Conversion Table

The left hand column represents the indicated flow rate for the jet when petrol flows through the orifice at 1 bar. The second and third columns refer to the water flow rate through the orifice at 100 bar.

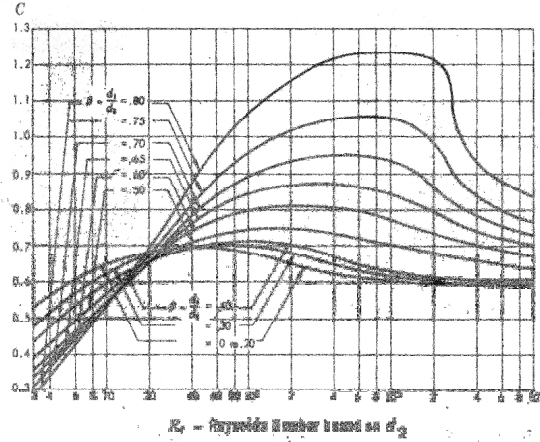| cc/m	litre/hour	g/s
10	40	12
12.5	45	13.4
15	50	14.8
17.5	55	16.2
20	60	17.6
22.5	65	19
25	70	20.4
27.5	75	21.8
30	80	23.2
32.5	85	24.6
35	90	26
37.5	95	27.4
40	100	28.8

E: Determining Flow Coefficient for Square Edge Orifice
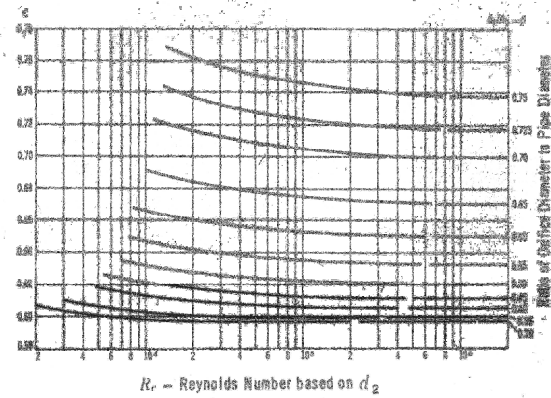
These illustrations are taken from Crane (1979)
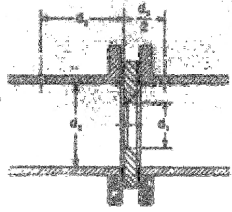
$$C = \frac{C_d}{\sqrt{1-\beta^4}}$$

$$K_{\text{orifice}} \simeq \frac{1-\beta^2}{C^2\beta^4}$$

F: Operating Instructions for Test Rig

A full set of operating instructions will now be given, detailing how to perform a test on one jet size with lagging attached.
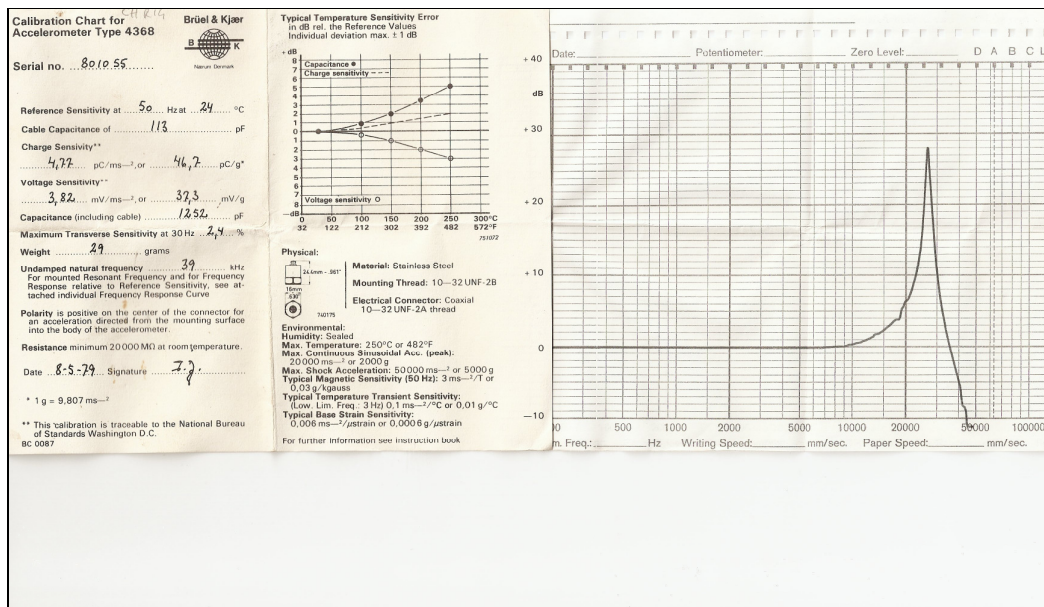
Note: All the tests were carried out in an open environment. The location was outside the general laboratory in the Nuclear Department, HMS Sultan, Gosport.

1. Attach both three phase cables to their respective sockets. Because the plugs are different it is obvious which plug is attached to which socket. Turn on the power.

2. Attach the cold water pipe to the mains water, and turn on.

3. Ensure a jet is screwed into the orifice, hand tight (do not over tighten as the brass expends when it gets hot and may be very difficult to remove for a subsequent test).

4. Attach the lagging to the pipe, at this time water should exiting the orifice under mains pressure

5. Take the metal bands and place them over the lagging at the ends. They act as fillers. Now secure the large jubilee clips over the end plate and the metal bands trying to ensure a good fit. Tighten up jubilee clips at both ends.

6. Secure temperature sensor over chimney, in its sealed chamber

7. Perform a visual Check of all the cables ensuring they are correctly attached to their respective sensors and the microphone is facing in the correct direction.

8. Turn the PC on and load up Labview. Open the Host scan window and Windows front end window.

9. Turn on the power to the control console. Check that the power to the heaters is NOT turned on, at this stage.

10. Ensure the trigger switch is not illuminated.

11. Turn on orifice heater, allow to reach 200˚C

12. Turn on the water pump and adjust pressure using valve on rig until at steady 100bar is indicated

13. Depending upon jet size; for less than 20cc use just heated coil to reach 200˚C, otherwise use pre-heaters as well, and allow temperature to reach 400˚C. Note, even though the cartridge heaters reach 400˚C, due to thermal inefficiencies, the water is probably only be heated up to about 100˚C.

14. Now that the rig is warming up and the pressure is stabilised, turn on Labview, and start logging

15. When indicated temperature is 200°C, press trigger switch to indicate correct temperature and pressure (the trigger switch will be illuminated).

16. Watch temp on lagging, allow to stabilise.

17. Once the system is stabilised, showing 100 bar and 200°C, then:
    a. Turn off the pump, using the red stop button on the rig
    b. Close pressure control valve on rig to maintain pressure for longer
    c. Press the trigger button on the console, the light should go off
    During this phase the only noise present is due to the steam leak.

18. Observe the pressure and when it has dropped by 10%, i.e. to 90 bar, stop the Labview data acquisition, using the large RED tab on the labview screen.

19. Turn off ALL the heaters, at this point there is still pressure in the system and so the water will start to cool.

20. When the pressure drops to zero:
    a. Open the control valve on the rig
    b. Reset the pump stop switch on the rig
    c. Goto the console and turn the pump back on.
    d. Observe the temperature on the console and maintain pumping until the temperature reaches 70°C. This time will be dependant upon the size of jet and the temperature the pre-heaters reached. It will sometimes take 30 minutes before the lagging can be removed.

21. If more testing is required using different jets then return to section 3 above, otherwise:

22. Keep a close monitor on all the temperatures. Due to the large amount of brass in the pre-heaters, there is a great potential for stored energy. If the temperatures start to creep up towards 80°C, then turn the pump on again and try and remove this stored heat.

23. When the temperatures are only showing a downward trend it is advisable to turn off all the power to the rig. Leave it to finally to cool down for a further 30 minutes. Now turn off the main water and disconnect from the tap. Also, remove both 3 phase cables from their respective sockets.

24. Finally pull the rig back into the lab for storage. This is a two man job.

A video of these procedures is also attached to the back of the central console.

G: Frequency Response of Accelerometer

The printout below shows the data sheet for the accelerometers used. It is important to note from the frequency response diagram, that it is linear from 0 to 10 kHz, and only has a small gain of 7 dBs from 10 to 20 kHz. The graph shows a resonant peak at 27 kHz, with a maximum gain of 28 dB. Some of the frequency responses produced in this document, show what appears to be useful information above 20 kHz, however their amplitude may be artificially high due to the extra gain in this region.

Data sheet for accelerometer